THE SELECTION AND TESTING OF COMPRESSION SEAL AND CHAMBER COATING MATERIALS FOR THE PIVOTAL ENGINE™.

A thesis

submitted in partial fulfilment

of the requirements for the Degree

of

Master of Mechanical Engineering

in the

University of Canterbury

by

D. J. Miller

University of Canterbury

2006

Abstract.

Wear and friction tests were conducted on a rotational tribometer to identify material couples for compression seals and chamber coatings to extend the service life of the Pivotal Engine™. Potential materials were identified based on reports in the literature of successful use in similar environments. From the rotational tribometer tests, the best material couple was found to be reaction bonded silicon nitride against a Sulzer Metco F4301 plasma sprayed coating followed by a Total Seal TiN coated seal against the F4301 coating. However, the performance predicted by the rotational tribometer was not realised in a fired engine, where the TiN coated seal wore almost as fast as an uncoated seal. This discrepancy was due to the large differences in operating conditions between the rotational tribometer and the fired engine, particularly the reciprocating motion of the engine. The different operating conditions mean that the results from the rotational tribometer have little or no relevance actual performance in the engine.

To overcome the limitations of the rotational tribometer a reciprocating tribometer was designed and built. The performance predicted by the reciprocating tribometer was much closer to the observed wear rates from the engine, particularly with the Total Seal TiN coated seals. Some of the results from the reciprocating tribometer were a direct-contradiction to those obtained on the rotational tribometer. When tested on the rotational tribometer the nitrided stainless steel seal wear rate was lower than that of the Mazda cast iron seal. However, on the reciprocating tribometer the Mazda cast iron seal had a lower wear rate than the nitrided stainless steel seal. From the testing conducted on the reciprocating tribometer the best material couple was found to be Total Seal TiN coated seals on the F4301 chamber coating. However, this material couple cannot be recommended to increase the seal life in the Pivotal Engine™ because at the conclusion of a twenty hour test the Total Seal TiN coating had worn through to the substrate. In addition to testing different materials, different oils were tested while keeping the wear couple constant. The oil that offered the best wear protection to both the seal and chamber coating was Castrol A747. These tests showed that different oils have as much effect as different materials.

Even with the best material combinations (Total Seal TiN seal, F4301 chamber coating) the seal wear rates in the Pivotal Engine™ are much higher than would be expected in other engines. This leads to the hypothesis that the origin of high seal wear in the Pivotal Engine™ is not due to material properties, but to design issues. The most likely problem is distortion of the chamber, which causes high localised seal loadings, and in turn causing high seal wear.

I. Introduction

Pivotal Engineering, a subsidiary of Christchurch based company Mace Engineering, was formed to develop the Pivotal Engine™. The Pivotal Engine™ was intended to overcome some of the inherent problems associated with a conventional two-cycle engine, such as high piston and piston ring wear rates and friction losses due to piston tilt and large port openings, reliability problems due to lack of control over piston temperatures and high oil consumption. The Pivotal Engine™ is an Otto cycle two-cycle engine, assembled from 500cc modules in either parallel twin or opposed four configurations with approximate power outputs of 100 hp and 200 hp respectively.

The Pivotal Engine™ utilises a piston of rectangular section that pivots on a bearing at one end with a conventional con-rod and crankshaft, similar to the concept developed by Richard James Cylindrical Motors Ltd [1]. The Pivotal Engine™ is shown in Figure 1 with a side plate removed and the piston at top and bottom dead centres (TDC and BDC respectively), showing the seal and port arrangement (note the piston shown has a modified compression seal arrangement, the actual piston and compression seal arrangement is shown in Figure 2).

The pivoting design of the piston allows coolant to be introduced through the pivot point on one side of the piston, travel through a channel under the combustion chamber, and exit through the second pivot point. The ability to entrain coolant into the piston facilitates active temperature control of the piston, all but eliminating the possibility of piston seizure due to overheating, and the cooler combustion chamber will reduce NOX emissions. Because the piston in the Pivotal Engine™ is constrained radially through the use of plain bearings, the sole function of the piston skirt is to close the transfer and exhaust ports during the compression stroke. A conventional engine relies on the piston skirt to stabilise the piston against the cylinder, which increases friction. However these properties have associated disadvantages. Any heat removed from the combustion chamber through cooling will reduce the energy available to be converted into useful work, in turn reducing the overall engine efficiency. The potentially lower temperature in the combustion chamber will also increase the amount of un-burnt hydrocarbons in the exhaust compared to a conventional engine.

For each piston in the Pivotal Engine™ there are three compression seals, two side seals and a front seal. These seals perform the same function as a piston ring in a conventional engine. The two side seals interlock with the front seal (detailed in Figure 2). Due to the piston geometry, it is necessary for the compression seals to be fitted to the piston with tight clearances. This, essentially prevents the seal from tilting in the piston and ensures normality to the side plate or exhaust block at all times. Sealing force is provided by springs and combustion pressure acting on the piston side of the seal. All three of these seals are wearing at an unacceptably high rate, limiting the life of the engine. The sealing system of the Pivotal Engine™ has similarities with both a conventional piston engine and a Wankel rotary engine. The requirement of a gas tight seal in a 90° corner is similar to the apex, side and corner seals in the Wankel engine. However, the temperature and lubrication conditions in the Wankel engine are more severe and the seals in the Wankel engine do not move in a reciprocating motion. The temperature, lubrication and dynamics (reciprocating motion) in the Pivotal Engine™ are similar to a conventional two-cycle engine.

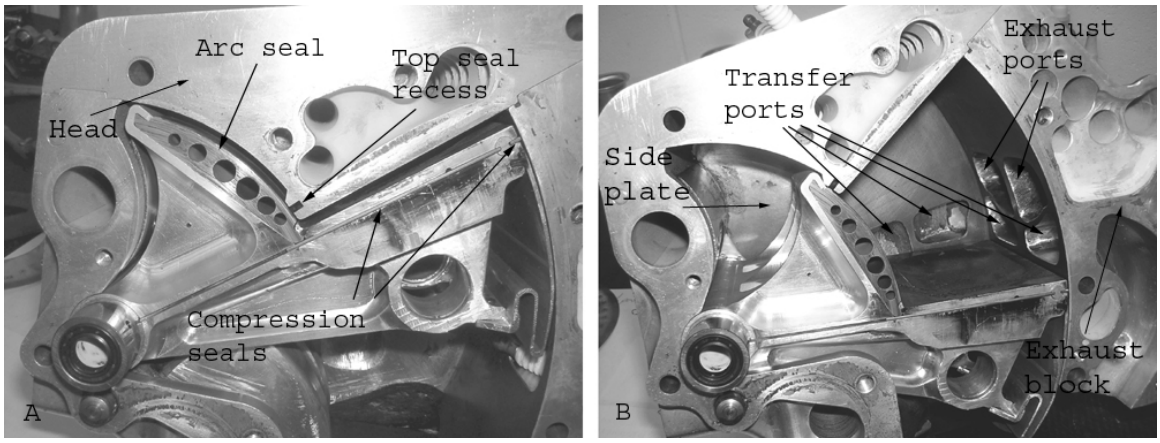

Figure 1. Pivotal™ Engine with side plate removed. (A) piston above TDC, (B) piston below BDC.

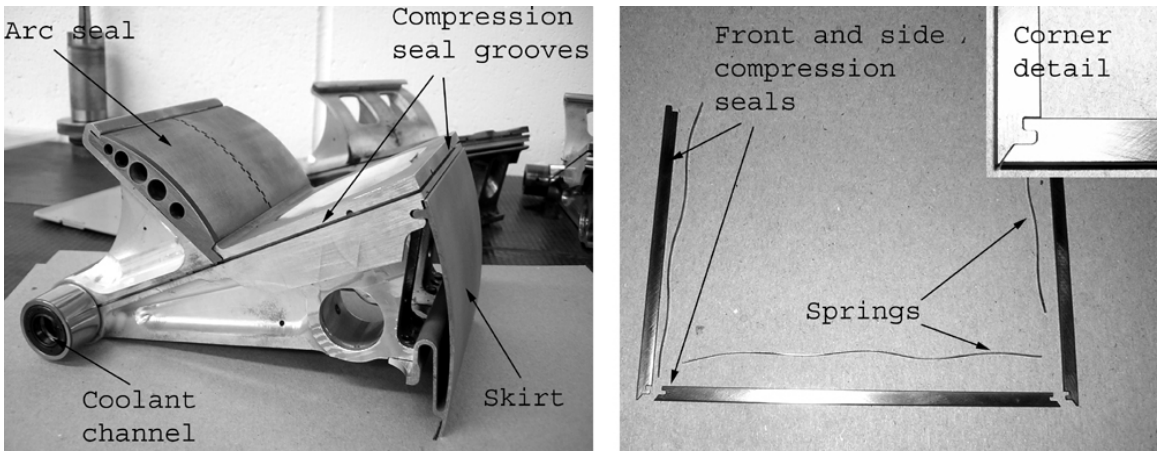

Figure 2. Piston and compression seals.

In most instances, the service life of a two-cycle engine is determined by the ability of the piston ring (compression seal) to seal combustion pressure from the crankcase. As the seal wears, its ability to seal reduces until the engine no longer produces sufficient power or fails catastrophically (i.e. broken piston ring). Therefore, it can be construed that the service life of a two-cycle engine is strongly determined by the life of the piston ring-cylinder liner system. In the case of the Pivotal Engine™ the current seal and chamber materials have a service life of less than 50 hours. Such a short life is unacceptable since for example, a service life of 600 hours is required for use as a power unit for a sports plane. It is also hoped that the Pivotal Engine™ will be utilised for a variety of other applications such as power generation and possibly automotive applications, all of which obviously require a long service life. The present research is therefore aimed at minimising the high wear rates experienced by the compression seals in the Pivotal Engine™, which lead to an unacceptably short service life.

To maximise the service life of the Pivotal Engine™, wear and friction experiments have been conducted to identify material couples that produce minimal wear. These materials include: metals, ceramics, thin film coatings, solid lubricating materials and various plasma sprayed materials. The testing of potential materials is required because wear is not a material property but a system parameter, influenced by many factors including, but not limited to: hardness, velocity, temperature, loads, lubricants and friction power intensity. All of these factors must be considered when conducting wear and friction experiments.

At the inception of this project, a rotational wear tester was made available. It was initially understood that this tester had certain drawbacks, especially that it did not simulate the actual engine conditions very well. Never the less, the rotational wear tester was used for a number of experiments (64) until it became clear that fired engine results could not be predicted from the rotational tester results. At this point, a reciprocating wear tester was designed and built. The reciprocating wear tester was built to overcome certain limitations of the rotational wear tester. Mainly, the reciprocating motion closely simulates the actual motion and ensures boundary lubrication at the turnaround points of top and bottom dead centres. In addition,

cylinder (chamber) liner material samples were small enough to be examined in the SEM and measured for weight loss.

One of the original goals of this work was to test a large number of wear couples. Severe budget constraints restricted the actual number that could be tested to six chamber coatings and nine seal materials. However, the most promising wear couple has been identified for further testing. It also became clear that the selection of oil was just as important as the seal and liner material selection. The most effective oil was therefore also identified. Finally, it became apparent that there are some possible design issues. While not specially investigated, these issues have been identified for the engine company.

II. Background.

Because of the complexity involved with piston ring and cylinder liner wear it is necessary for the reader to have some knowledge of function and design of this system. The following sections contain a brief summary of some important aspects of the piston ring-cylinder liner system.

II.A. Piston Engine Seal Design.

In a conventional internal combustion engine the top piston ring (analogous to the compression seals in the Pivotal Engine™) performs four major functions, (1) sealing combustion pressure, (2) transferring heat from the piston to the cylinder and cooling system, (3) distributing lubrication and (4) stabilising the piston [2]. While performing these functions, a piston ring and cylinder liner must have low wear rates, low friction and resistance to chemical attack from combustion products. In the case of a two-stroke engine, these parameters will ultimately determine the service life of the engine.

In recent years, as reduced emissions and increased efficiencies have become more important in the design of internal combustion engines, the requirements of the piston and ring system have become increasingly demanding. Over and above the functions outlined above, there is a further need to reduce emissions and increase efficiency through reduction of friction.

In the vicinity of top dead centre, the crevice volume created between the piston, cylinder, top ring and cylinder head influences the quantity of un-burnt hydrocarbons discharged during the exhaust cycle. The fuel-air mixture in this volume is not ignited with the bulk of the fuel-air mixture in the cylinder, leaving it to be discharged during the subsequent exhaust stroke. Positioning the top ring as close as possible to the top of the piston reduces this volume, which minimises the entrapment and consequent discharge of un-burnt hydrocarbons. The two consequences of this are that the ring is now exposed to hotter combustion gases and the top ring land of the piston is weaker due to a thinner cross section. For these reasons, thinner and therefore lighter stainless steel rings are becoming more common. Because of their lower mass, these rings reduce the inertial loading on the top ring land at the top ring reversal point (TRRP) while having better chemical resistance and strength than traditional cast iron rings.

Some oil additives can be particularly harmful to the environment. As such burning of lubricating oil can provide an appreciable contribution to exhaust emissions. The design of the ring pack, piston and cylinder liner influences the migration of oil from the crankcase into the combustion chamber. Transport mechanisms include oil travelling through the piston ring grooves, oil being scraped into the combustion chamber on the compression and exhaust stroke (up-scraping) and oil that is left on the cylinder liner during the expansion and inlet strokes. Issues such as oil travelling through the ring pack and up-scraping can be minimised through good detail design of the piston and ring pack [3].

Great reductions in oil transport may have negative trade offs with other system parameters. For instance, using oil control rings with higher tension reduces the amount of oil left on the cylinder liner but increases friction and wear. Efforts to reduce friction are somewhat limited by other system requirements, however progress has been made by using rings with low friction coatings and optimising the cylinder liner surface roughness.

To provide an adequate seal between the combustion chamber and the crank case, the piston ring is forced against the cylinder liner and the lower flank of the piston ring groove forming a labyrinth type seal arrangement. In a conventional piston engine, this force is provided through a combination of ring tension and combustion pressure. The combination of these two forces, and the capacity of the ring to conform to the cylinder liner, determines the sealing ability of a piston ring.

The force provided by ring tension is a function of ring stiffness and the degree of elastic deformation required to fit the ring into the cylinder liner (piston rings are manufactured with a larger nominal diameter than the cylinder liner). The force provided by combustion pressure acting on the inside surface of the ring during the early stages of the expansion stroke (shown schematically in Figure 3) is significantly higher than that provided by ring tension. Because the force on the piston ring is dependent on the combustion gas pressure, the high piston ring force is only maintained during part of the expansion stroke. This provides sufficient force for the piston ring to seal the high pressure gas during the expansion stroke without unnecessarily high friction during the remainder of the engine cycle. To allow the

pressure to act on the inside surface of the ring, there must be an unobstructed path from the combustion chamber to the back of the ring groove. This is usually accomplished by utilising a clearance between the ring and the ring groove. Drilling holes from the piston crown to the back of the ring groove or cut-outs in the top flank of the ring groove gives a similar effect.

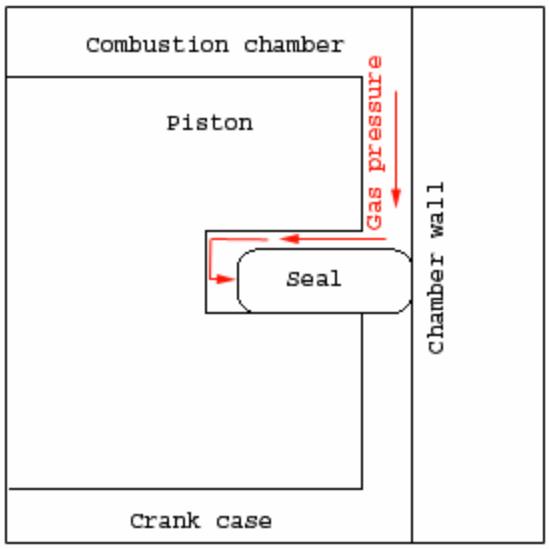

Figure 3. Combustion pressure acting on piston ring.

The two latter methods are more common in racing or high performance engines. They allow the use of low tension piston rings to minimise friction through most of the engine cycle, and still maintain sufficient force between the piston ring and the cylinder during the combustion process. However, low tension piston rings compromise the ability to control oil distribution on the cylinder liner leading to high oil consumption, and the holes or cut-outs can become blocked with carbon deposits. These are not generally issues for racing engines but prevent the use of these designs in automotive type applications.

II.A.1. Piston Ring Profiles.

Several common ring profiles are shown in Figure 4. The dyke ring (Figure 4 A) requires that part of the top ring land is machined off to accommodate the raised area of the ring. This type of piston ring generally has a low ring tension to reduce friction during the intake, compression and exhaust strokes. Relying on gas pressure acting on the inside surface to force the piston ring against the cylinder liner during the combustion stroke. Dyke rings tend to have low wear rates due to the large surface

area and low force. As a result of the low force, friction losses are low through the inlet, exhaust and compression strokes. The increased mass of the piston ring means that care must be taken to ensure the top ring land has sufficient strength at the TRRP.

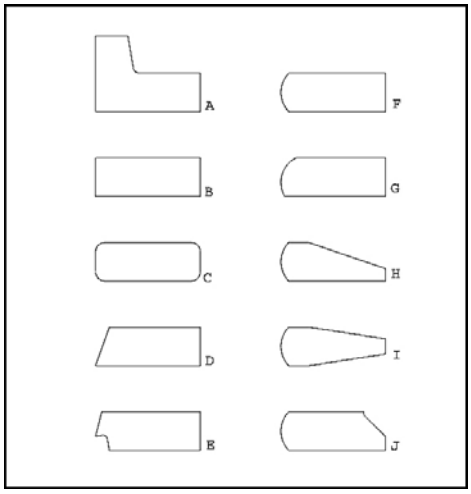

Figure 4 Piston ring profiles. The left side of the profile is in contact with the cylinder liner. (A) dyke. (B) square face. (C) modified square face. (D) taper face. (E) Napier. (F) barrel face. (G) offset barrel face. (H) barrel face with half keystone. (I) barrel face with keystone. (J) barrel face with bevel.

The flat face ring (Figure 4 B) has in most automotive applications been superseded by a flat face ring with small radii on the corners (Figure 4 C) or a barrel face ring (Figure 4 F). The radii and the barrel face profiles help promote the formation of hydrodynamic lubrication during the mid-stroke of the engine. The seal profile currently used Pivotal Engine™ is similar to that shown in Figure 4 C.

The taper face (Figure 4 D) and Napier (Figure 4 E) profile are most commonly used as a second compression ring in four-cycle or externally scavenged two-cycle engines where the control of oil distribution is important. Due to the profile of the ring, oil is scraped off the cylinder liner during the expansion and inlet cycles in an effort to reduce oil consumption. Because of the more balanced distribution of gas pressure over the inside and outside surfaces of the ring, these profiles exhibit less wear during the running-in process. However, the more balanced gas pressure also means that these profiles can be susceptible to ring collapse (as explained in section

II.A.2. Piston Ring Dynamics.) if the gas pressure in the second ring land becomes too high.

Like the taper face and Napier profiles, the offset barrel (Figure 4 G) will have a lower contact force from gas pressure than the flat face or flat face with radii. The offset barrel is used to minimise the up-scraping of oil into the combustion chamber on the compression and exhaust strokes in a similar fashion to the taper and Napier rings, however the resultant forces from the pressure distribution can cause it to collapse near TDC if used as a top compression ring.

The half (Figure 4 H) and full keystone (Figure 4 I) profiles locate in a piston groove of the same shape. The purpose of this profile is to prevent the ring from sticking in the ring groove, which would result in the loss of the ability of the ring to seal. This occurs when oil in the ring groove is heated to the point that it burns, forming carbon deposits in the ring grooves. For this reason these, two profiles are common in diesel engines.

The use of a bevel on the inside edge (Figure 4 J) is used to provide a static twist to the ring, usually with the outside of the ring towards the top of the piston (positive static twist). The static twist of the ring helps to control the dynamic movement of the ring through the engine cycle, allowing some degree of control over up-scraping and oil consumption while maintaining good dynamic sealing abilities.

II.A.2. Piston Ring Dynamics.

There are several ways that the top compression ring can form a seal between the piston and the chamber wall. Figure 5 A shows the ideal position of the top compression ring just after the cylinder has fired. The compression ring is flat on the ring groove and normal to the chamber wall. This arrangement has the lowest specific force on both the cylinder liner and the lower flank of the piston groove, giving the least wear as well as providing the best gas seal between the piston and the cylinder liner. This type of sealing arrangement can be achieved either through the use of low clearances between the ring and the groove, utilising a ring which is very stiff or by having a positive static twist on the ring.

Implementing low clearances between the ring and the groove will provide adequate sealing until the wear of the ring produces a flat face with no radii (or barrel face). Once this condition is met the ring will wear rapidly, as its ability to form a

lubricating film is greatly diminished. If the ring has sufficient movement in the ring groove it is possible for the radii (or barrel face) to be regenerating with wear. Figure 5 D illustrates how the ring regenerates the radii as it wears, by showing two rings superimposed on each other, one on the top flank and the other on the bottom, as would be possible during the inlet and compression cycles respectively.

During the early stages of the compression stroke, the inside edge (ISE) of a ring with positive static twist will seal against the lower flank of the piston groove, as shown in Figure 5 C. As gas pressure increases the ring will be forced flat against the lower flank of the piston groove, as shown in Figure 5 A. As well as being able to seal in this manner the positive twist also reduces up-scraping during the compression and exhaust strokes. With an ISE sealing configuration it is however possible for the ring to 'collapse' into the seal groove if the combustion pressure acting on the outside of the seal can overcome the ring tension before the ring is forced onto the lower flank, as shown in Figure 5 F.

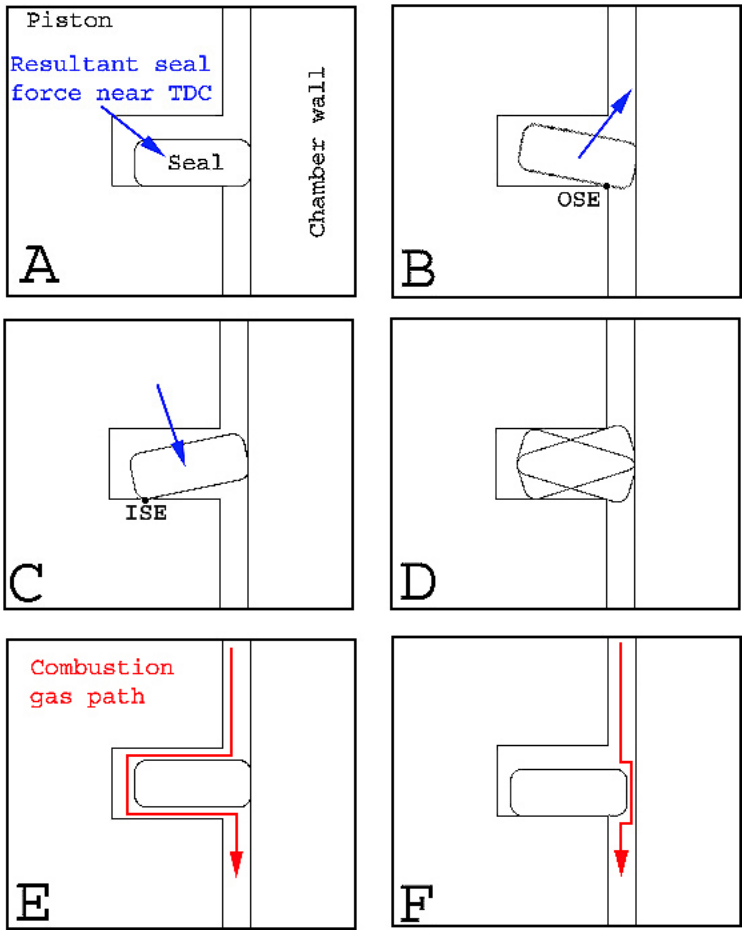

Figure 5. Compression seal, piston and liner cross sections (not to scale)

If the piston ring is not sufficiently stiff or does not have adequate positive twist, the seal can wrap around the lower flank and seal on the outside edge (OSE) as illustrated in Figure 5 B. This can lead to a phenomenon known as float or flutter. This occurs when the pressure differential across the ring (top to bottom) is not sufficient to overcome the inertial forces at the TRRP [3], allowing the ring to lift off the lower flank as illustrated in Figure 5 E. Ring float will not only reduce the engine efficiency but cause severe damage to the flanks of the ring groove as the lubricating oil is removed/burnt off the ring groove by the hot combustion gases, creating a more severe metal-to-metal contact between the ring and the piston during the ensuing engine cycles.

II.A.3. Piston Ring Tribology.

In the piston ring-cylinder liner system there are several possible wear mechanisms including two and three body abrasive wear, adhesive wear and corrosive wear. Abrasive wear is a cutting type action and is characterised by plastic deformation in the sliding direction. The cutting action is due to either hard asperities or hard particles that are trapped between the contact surfaces. Abrasive wear is the most common wear mechanism in the piston ring-cylinder liner system. To minimise abrasive wear of the piston ring-cylinder liner system, piston rings are generally manufactured from a material that is harder than the cylinder liner. Manufacturing the piston ring from a harder material reduces the rate at which abrasive wear removes material from the piston ring. This is important, as it is the wear rate of the piston ring that usually dictates the life of the piston ring-cylinder liner system.

Adhesive wear occurs when asperities on one surface weld to asperities on the opposing surface, and are subsequently broken off. Adhesive wear is more likely to occur under high load and high temperature conditions. Under these conditions, the protective oxide layer can be removed from the wear surfaces, which exposes a reactive surface that can easily weld to the opposing surface. It is common for adhesive wear to lead to severe scuffing. Corrosive wear occurs when chemically aggressive compounds form from the breakdown of lubricants and combustion by-products. These compounds react with the wear surfaces, thus removing material.

II.A.4. Lubrication and Lubricants.

In a two-cycle internal combustion engine, the lubricant performs three main functions: (1) transferring heat from the piston to the cylinder liner, (2) providing a film to separate metal components, and (3) as a medium to transport extreme pressure anti-wear additives to the metal-to-metal contact zones. An important aspect of the piston ring-cylinder liner wear system is the thickness of the oil film that separates the piston ring from the cylinder liner. The oil film thickness is dependent on the instantaneous relative velocity, applied load and the oil viscosity, which is in turn dependent on temperature.

In lubricated wear, there are three basic lubrication regimes, which are determined by the thickness of the oil film. If the composite surface roughness is greater than the oil film thickness and most of the load is being supported by the surface asperities, the system is operating in a boundary lubrication regime. In a mixed lubrication regime most of the load is supported by the oil film between the two surfaces, but there is still some contact between the surface asperities. In the hydrodynamic lubrication regime, the load is carried solely by the oil film and there is no metal-to-metal contact. Therefore, the most severe wear occurs in the boundary lubrication regime followed by the mixed lubrication regime. In the hydrodynamic lubrication regime there is generally no wear because the surfaces are not in contact. The lubrication regime can be predicted from a Stribeck diagram. A Stribeck diagram relates friction force to velocity, viscosity and load. Figure 6 shows a Stribeck diagram that has been constructed to represent the piston ring-cylinder liner system at mid-stroke. This diagram implies that the system wear will be lower if the velocity or oil viscosity are increased, or if the load is decreased (by increasing the oil film thickness).

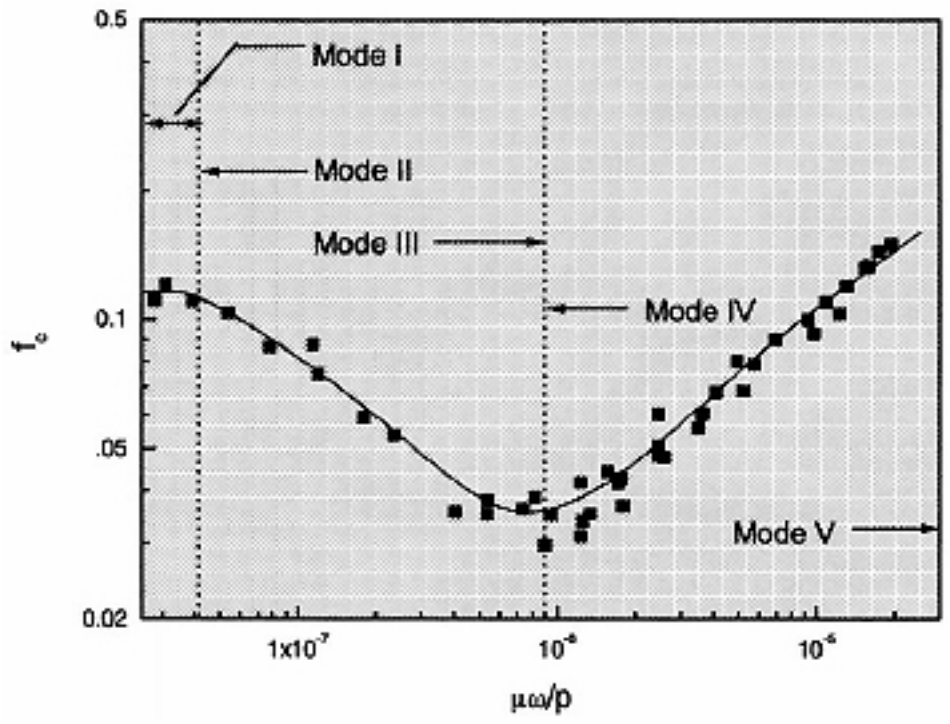

Figure 6 Modified Stribeck diagram (f_c coefficient of friction v.s $\mu\omega/P$ dimensionless bearing parameter) representing a piston ring near mid stroke. Mode I to II is boundary lubrication, mode II to III is mixed lubrication and mode IV to V is hydrodynamic lubrication [4].

In conjunction with separating the rubbing surfaces, oil contains anti-wear additives such as zinc dialkyldithophosphate (ZDDP). In the contact zone, it is common for the protective oxide layers to be removed from the rubbing surfaces. This leaves a very reactive surface that reacts with the EP additives, aiding in the formation of protective films. The films can prevent wear through a number of methods. For example the film has to be worn away before any of the bulk material can be removed, and thus acts sacrificially. A relatively soft film can also embed abrasive wear particles, effectively removing them from the wear system.

II.B. Mazda 13BT Rotary Seal Design (Wankel engine).

The compression seals in the Mazda rotary engines do not operate in a reciprocating motion like the seals in the Pivotal Engine™. However the seal arrangements between the two engine designs are similar. Both the 13BT and Pivotal Engine™ must be able to form a gas tight seal in a 90° corner, for this reason the design and materials used in the successful Mazda system were investigated.

The seals in a Wankel engine (shown in Figure 7) have the same functionality and requirements as piston rings in a conventional engine. However, a different approach was taken with the selection of seal and chamber materials in the Mazda 13B series of engines. The apex seal is made of electron beam chilled cast iron, which runs on a porous chromium plated steel insert that is cast into the aluminium rotor housing. The side and corner seals are manufactured from a soft iron and these seals run on a nitrided cast iron surface [5]. So, in effect, the apex seal system has two relatively hard materials in contact while the side and corner seal system have soft seals in contact with a hard surface. This is in contrast to most piston engines which utilise relatively hard piston rings on soft cylinder liners.

The side seals in the 13BT engine are not designed to form hydrodynamic oil films between themselves and the side plates. The side seal has a thickness of 0.686mm, a height of 3.15mm and a clearance of 0.028mm with the side seal groove, which are similar to the dimensions of oil control rings in a four stroke piston engine. The small clearance between the side seal and the rotor prevents combustion pressure from acting on the back of the seal, allowing the contact force to be controlled solely by the wave spring behind the seal. This arrangement allows the seal to still operate satisfactorily with over 0.3mm of wear (limited by the loss of force applied from the spring), significantly more wear than can be tolerated by a piston ring.

Like the side seal, the apex seal has a tight fit into the rotor with a nominal clearance of 0.054mm. Because of the motion of the rotor, the apex seal profile is self regenerating accommodating up to 1.5mm of wear. This sealing arrangement is shown in Figure 7. The corner seal in the rotor is the junction point between the two side seals and apex seal. The corner seal has a rubber insert to dampen the vibrations of the apex seal, which can cause ‘chatter’ marks on the rotor housings.

The 13BT has a similar total loss lubrication system to most two-cycle engines, an oil metering pump injects a small amount of oil onto the trochoid surface to provide lubrication to the apex, corner and side seals. Although the rotational motion of the Wankel engine should allow the formation of hydrodynamic lubrication between the apex seal and the trochoid surface the high temperatures in the combustion process tend to burn the oil off the trochoid surface, in this way the conditions encountered by the seals in a Wankel engine are more severe than most piston engines.

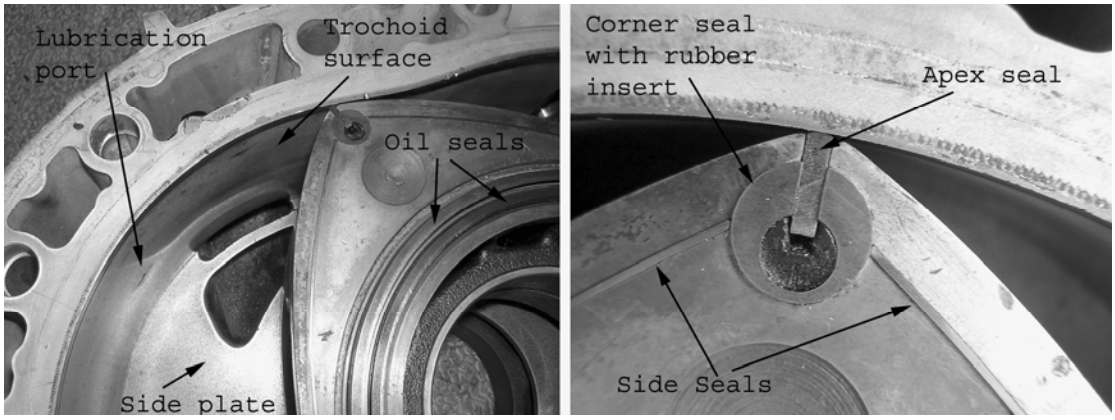

Figure 7. Mazda 13B bridge port turbo engine, showing seal arrangement .

The most common failure mode of the seals in the Mazda 13BT is abrasive wear, while premature failures are typically due to detonation causing the apex seals to fracture. Detonation is generally caused by fuel or ignition problems on turbo charged engines. The early Mazda Wankel engines have a reputation for being unreliable, a reputation gained when the apex seals were manufactured from a carbon compound and wore very quickly.

II.C. Non-Metallic Seal Materials.

The straight seals in the Pivotal Engine™ mean that non-traditional piston ring materials can be considered, notably ceramics. Ceramics are generally not suitable for use as piston rings because of the ring dynamics, and the elastic deformation required to produce a gas tight seal. The compression seals in the Pivotal Engine™ do not require elastic deformation to provide a normal force (required for sealing), this force is provided through the use of springs. The straight seals also mean that thin film coatings can be easily applied without specialised tooling. Presently, thin film coatings are applied to piston rings for specialised applications such as motor racing, but are not common in mass produced engines.

II.C.1. Ceramic Tribology.

A significant body of research has been carried out in the field of un-lubricated wear of ceramics for use in internal combustion engines, most concerned with the development of low heat rejection or adiabatic engines. The elevated operating temperatures of these engines make the use of conventional lubricants impossible. It is now generally accepted that ceramics do not offer sufficient wear resistance to be used without lubrication [6].

A sizeable portion of research published on the lubricated wear of ceramics is concerned with silicon nitride. This material has the potential to be used in engineering applications that have traditionally used metals, because of its relatively high fracture toughness (see Table 1) and better wear resistance than most metals.

Winn, Dowson and Bell [7, 8] conducted long term lubricated tri-pin-on-disc type experiments using silicon nitride, alumina and 52100 steel pins against 52100 steel discs under various speed and loading conditions. In addition, the wear response of two types of oil was investigated, a refined mineral oil and an ester oil. Both base oils have the same ZDDP and detergent additives.

The alumina pins performed poorly due to chipping of the wear surface, while the 52100 and silicon nitride pins had relatively low long term wear rates in the mineral oil, 5 x 10^{-11} $mm^3N^{-1}m^{-1}$ and 1 x10^{-11} $mm^3N^{-1}m^{-1}$ respectively. The steel pins had a high initial wear rate that decreased during the test, whereas the wear rate of the

silicon nitride pins increased proportionally with the increase in contact area. This indicates tribochemical wear, in contrast to the abrasive wear experienced by the 52100 pins.

When the silicon nitride pins were tested in the ester oil, the initial wear rates were approximately five times higher than those recorded in the mineral oil. As the test conditions became less severe (lower contact pressure due to a larger contact area), the ester based oil provided better protection than the mineral oil.

An important aspect of these experiments is the lack of evidence of the formation of a protective film on the silicon nitride pins or the 52100 disc. Oil additives such as ZDDP are reactive on ferrous surfaces, especially in tribological contacts where the oxide surface layers are removed. These types of additives reduce wear by forming protective/sacrificial films on the contact surfaces. This work, conducted by Winn et al. indicates that ZDDP additives are of little or no use in the lubrication of ceramics.

Silicon nitride components can be manufactured in a number of ways resulting in different material properties. Properties of sintered and reaction bonded materials are compared in Table 1.

Table 1 Silicon nitride properties [9]

	Compressive strength	Hardness	Fracture toughness
Sintered	2000 MPa	1500 H_v	8 $MPa^{1/2}$
Reaction bonded	550 MPa	1100 H_v	3 $MPa^{1/2}$

Silicon nitride is now being used in production engines for components such as cam followers and other components with high contact stresses. Nevertheless it would be problematic to use silicon nitride as a piston ring material. It is likely that the deformation required to install a silicon nitride ring on a conventional piston would cause the ring to fracture. The use of silicon nitride for piston rings would require a complete redesign of the piston and piston ring system, and compromises in the design may outweigh any benefits. However, silicon nitride seals have the potential to perform better than metallic seals where seal deformation is not a required characteristic of the sealing system. This has been demonstrated by the successful use of silicon nitride apex seals in Mazda's 1992 Le Mans winning 787B. It was reported

by Shimizu, R., et al. [10] that when the engine was torn down after the race there was minimal wear on the apex seals or the trochoid surface. A result of this is that silicon nitride apex seals are now readily available for use in the 13B engines. The only aspect preventing the widespread use of silicon nitride in this type of application is cost (a set of six seals costing approximately $2000 NZD).

II.C.2. Thin Film Tribology.

Thin films allow the surface properties of a component to be optimised for a specific application while maintaining the bulk material properties. This has two significant consequences. First, the usefulness of a component can be increased dramatically without having to resort to a bulk material that may have other less desirable properties or an increase in expense. Secondly, the bulk material and the thin film properties can be optimised independently of each other, typically not possible with most materials.

Thin films are deposited onto a surface using one of two methods (or variations of these), chemical or physical vapour deposition (CVD and PVD respectively). For the application of thin films onto piston rings, the PVD process is the more appropriate method due to the lower deposition temperatures, 50°C to 500°C compared to 800+°C for CVD processes. High temperatures can cause the long slender section of a piston ring to warp, leaving it unusable after the coating process.

Desirable mechanical properties of a thin film for piston ring applications include a high hardness to minimise abrasive wear and adequate adhesion with the substrate. To meet these requirements, films such as titanium nitride (TiN), chromium nitride (CrN), tungsten-carbide carbon (WC-C) and diamond like carbon (DLC) are employed.

One limitation to the use of thin films on piston rings is the maximum thickness that the film can be grown to, restricting the life of the film in a wear environment. The internal stresses of the film increase as a function of the coating thickness, thus limiting thickness is reached when the internal stress is high enough to cause the film to fail without any external influence. This problem can be overcome by depositing discrete functional layers. For example, TiN has a maximum film thickness of approximately 5μm before the film will fail. Yet it is relatively easy to deposit a TiN

layer followed by a Ti layer (by eliminating the nitrogen gas flow in the process chamber). This system can be repeated many times until a coating of the required thickness is achieved. For example, Lyubimov et al. [11] developed and tested two multi layer titanium-titanium nitride coatings for use on piston rings. The first coating system utilised four layers. The first 0.5μm thick titanium layer is a conformal interface between the cast iron ring material and the subsequent 3μm titanium nitride layer. These two layers are followed by a 1μm titanium layer and a 3μm titanium nitride layer. The intermediate titanium layer is a buffer between the hard TiN layers, reducing internal stresses in the titanium nitride layers while preventing crack propagation through the coating system.

The second coating consisted of 5 layers, being the same as the four layer coating with the addition of a 2μm titanium layer on the outermost titanium nitride layer. The purpose of this layer is to accelerate the running-in of the engine, by removing asperities and high points on the cylinder liner. Accelerating the break-in period allows loads to be distributed evenly over the ring surface earlier, which in turn reduces the wear that is experienced by the ring and cylinder liner system. Lyubimov et al. showed that when tested in a two-cycle scooter (Muaravey) the five layer titanium-titanium nitride PVD coating increased the piston ring life by 3 times compared to an uncoated ring, and 1.7 times compared to an electroplated chromium ring.

In addition to the mechanical properties attainable through the use of PVD coatings, the manufacturing process is considerably more environmentally friendly than electroplating processes. The only waste products released from the PVD process are nitrogen and argon (and methane for DLC coatings). Electroplating processes employ large volumes of toxic chemicals that need to be replaced periodically and therefore disposed of.

II.D. Tribological Testing.

Testing of wear and friction properties of materials can be conducted on several different levels with respect to the final application. Holmberg [12] divided tribological tests into six levels as shown in Figure 8. Essentially, the closer the test conditions are to the intended environment the more relevant the test results. However, the repeatability and statistical significance decrease. Whittaker and Matthews [13] reported that laboratory wear tests generally help eliminate poorly performing materials, but it is unlikely that these tests will be able to identify an optimum material combination for a specific application.

For the example of piston rings, simple tests could be conducted with a pin manufactured from the piston ring material and tested in a standard pin on disc tribometer against a hardened steel disc. This test will provide some data on the wear rate of the ring material, but it is not likely to be indicative of the performance of the piston ring material in an actual engine due to the significant difference in environmental conditions. For these reasons, most tribological testing of the piston ring cylinder liner system is conducted with a combination of miniature, component, rig and field tests.

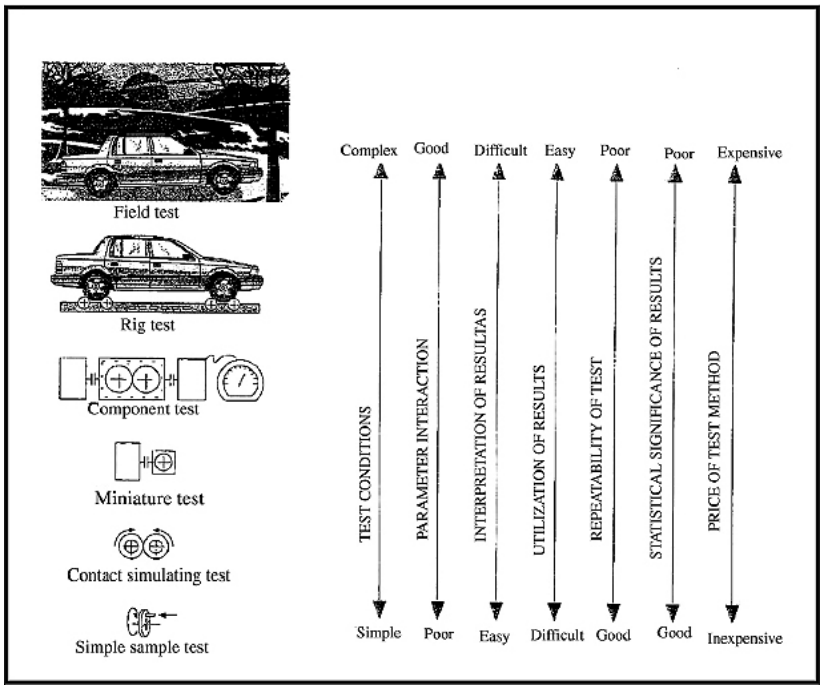

Figure 8. the six levels of simulation in tribological testing [13].

Various tests have been implemented for analysis of the piston, piston ring pack and cylinder liner system of the internal combustion engine. In this system, research is generally conducted in friction and wear of the piston ring-cylinder liner system and/or investigation of oil films formed between the piston ring and the cylinder liner. These tests can be classified into three groups: (1) fired engine tests, (2) motored engine tests and (3) tribometer tests. In regard to Holmberg's six levels of simulation, a fired engine test could be considered either a field test or a rig test, a motored engine would be a component test and a tribometer test could be a miniature test, a contact simulation test or a simple sample test depending on the type of tribometer used.

II.D.1. Fired Engine Tests.

Ma et al. [14] studied the break-in liner wear and piston ring assembly friction in a spark ignited engine (fired engine test). A surface layer activation method was used to measure the wear of the liner. Friction forces were calculated by relating engine pressures (combustion and crankcase) to the measured torque (IMEP method). During the test the engine load was controlled by a dynamometer. The engine speed and load were increased through the test to simulate a driving cycle. Ma et al. reported that the friction and wear measurements had no direct correlation to each other, although the surface roughness and friction showed a linear relationship.

In addition to instrumented and controlled experiments as outlined above, it is common for studies of piston ring-cylinder liner wear and oil consumption to be carried out in engines on test beds under simulated driving conditions and fleet tests. These tests are frequently used to validate model tests or theoretical analysis.

II.D.2. Motored Engine Tests.

Motored tests are simpler than fired engine tests. Without combustion it is much easier to control selected variables and, as a consequence of this, results are more easily interpreted although not as representative. For example, Cho, Choi and Bae [4] investigated the frictional modes of a barrel shaped piston ring under fully flooded conditions by measuring friction using a floating liner in a motored engine. These data were then used to produce modified Stribeck diagrams (Figure 6) for the lubrication regimes present near the dead centres and in the mid-stroke of the engine. The Stribeck diagram plots the friction coefficient against the bearing parameter $\mu\omega p^{-1}$,

were μ is the lubricant viscosity, ω is rotational velocity and p is the applied load. The Stribeck diagram can then be used to predict whether the piston rings are operating in a boundary, mixed or hydrodynamic lubrication regime from measured coefficients of friction with the assumption of fully flooded inlet conditions.

II.D.3. Tribometer Tests.

Most experiments that are concerned with the wear rates and friction of piston ring-cylinder liner systems have been conducted on reciprocating tribometers. Hill, Hartfield-Wunsch and Tung [15] tested three common cylinder bore materials (cast iron, Nikasil and 390 Al) against three piston ring materials (chromium plated cast iron, molybdenum coated cast iron and gas nitrided stainless steel) using a modified Cameron Plint (C-P) tribometer and an Electro-Mechanical LS9 tribometer. The C-P tribometer was operated with a load of 80N, 10mm stroke at 10Hz for 40 hours at 120ºC while the LS9 tribometer was operated with a load of 72N, 25mm stroke at 8.5Hz for 30 hours at 165ºC. The wear of the piston rings on the C-P tribometer was quantified using a mass loss technique while bore wear was measured from a surface trace. Both the bore and ring wear from the LS9 tribometer was measured using a profile trace. The lowest combined wear was with gas nitrided stainless steel rings on cast iron liners. Hill et al. also found that the results from the LS9 and C-P tribometers did not concur since the 390 Al had much higher wear rates on the LS9 tribometer. It was hypothesised that this was due to the 390 Al being more sensitive to oil and temperature than the Nikasil and cast iron bore materials.

Akalin and Newaz [16, 17] developed an analytical model to calculate friction force for the ring-liner contact in a mixed lubrication regime. Their model implemented a modified Reynolds equation, which included surface roughness and flow factors as well as a statistical representation of the surface asperities. To verify this model, a reciprocating test system was designed and built with a stroke of 84mm, maximum speed of 750rpm, maximum ring contact force of 360N and a maximum temperature of 100ºC. Their results showed that running speed, temperature and surface roughness were important parameters for defining the lubrication regime. They also found that the normal applied load only had a minor affect in the friction force in the mixed lubrication regime. Their model was a good representation of the results obtained from the test system.

II.E. Wear Measurement.

A challenge in the field of tribology is the interpretation and application of published wear rates. This is a problem because there is no specified quantity for describing the wear rate of a material or system and different wear rate measurements cannot always be converted to a more useful measure. Some measures of wear described by Ravikiran [18] include:

Wear	V	m^3
Wear rate	W	m^3m^{-1}
Specific wear rate	W_{sp}	$m^3N^{-1}m^{-1}$
Wear coefficient	K	Dimensionless
Normalised wear rate	W_n	Dimensionless

Of these measures, the wear rate W is most commonly used, being the volume loss per unit sliding distance. The specific wear rate W_{sp} is the wear rate normalised to the applied normal load and is also a commonly used measure. The wear coefficient K is W_{sp} multiplied by the room temperature hardness and W_n is W divided by the contact area. In addition to the above measures, in some instances wear is reported as a linear measurement or a mass loss.

In all cases (shown above), wear contains a volume term. In most cases the worn volume is calculated using the mass loss of the worn component in conjunction with the material density or by measuring the change in worn and unworn surface profiles relative to a known datum.

III. Procedure.

III.A. Equipment.

III.A.1. Rotational Tribometer.

The bulk of the testing was carried out on a rotational tribometer. This tribometer had been designed and built as part of an undergraduate course at the University of Canterbury. The tribometer rotates a 200mm diameter disc at 2850rpm, equating to a relative velocity of 27ms^{-1} between the seal sample and the disc surface. This is equivalent to the instantaneous velocity of the front compression seal in the engine at mid-stroke when running at 5000 rpm. The force applied to the seal sample was calculated from the combustion pressure acting on the back surface of the compression seal, shown schematically in Figure 3. Based on a combustion pressure of 5.65 MPa, for a 15mm x 1.24mm seal sample the force was calculated to be 105N. This value does not take into account the load applied by the wave spring, which is unknown (not shown in Figure 3) or any centripetal forces.

To increase the usefulness of the rotational tribometer, strain gauges were added to the vertical support. Allowing measurements of the friction between the seal and disc, which are then periodically logged to a data file. The software used to log the friction data also controls the oil delivery rate, utilising a plunger type metering device. Oil is delivered as a mist that is forced onto the disc surface by compressed air. The modified rotational tribometer is shown in Figure 9.

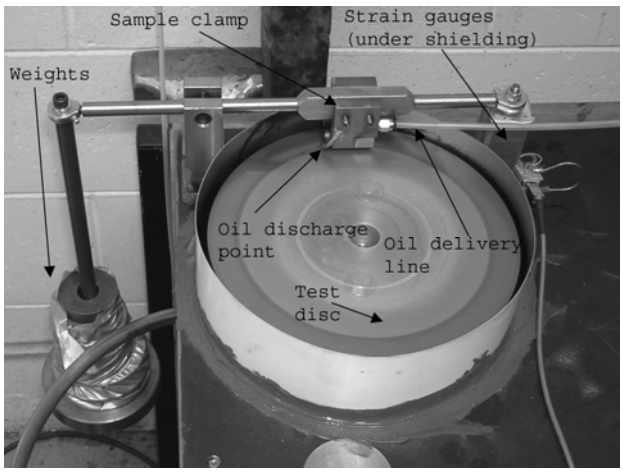

Figure 9 Rotational tribometer.

The design of the rotational tribometer was limiting in several ways, in terms of both possible analysis techniques and relevance of results to the Pivotal Engine™. The geometry of the rotational tribometer limited the analysis that could be performed on the test disc, the disc was too large to fit into the scanning electron microscope (SEM) or the atomic force microscope (AFM), preventing analysis of the wear surface. Mass loss measurements were not possible due to maximum mass limitations of the balance that had sufficient resolution. As a consequence of this, it was not possible to quantify the wear of the test disc.

The test parameters used for the compression seal samples do not occur at any point during the actual engine cycle. The parameters were selected to provide the most severe conditions while still remaining in the bounds of engine operation. The high pressures and forces due to combustion occur near TDC while the maximum velocity is in the mid-stroke region where gas pressure has little effect on the seal forces. Most importantly the rotational motion of the tribometer did not simulate the lubrication regimes present in the actual engine due to the reciprocating motion.

As a result of these differences, the wear rates recorded in a fired engine showed little correlation with results from the rotational tribometer. The test conditions were so different that a material eliminated due to poor performance (catastrophic failure) on the rotational tribometer performed adequately in the engine. In addition to this result, the seal wear rates in the engine were significantly higher (although not quantified) than those from the rotational tribometer. Ultimately, the tribological conditions in the engine were not adequately replicated on the rotational tribometer. Thus the results obtained from the rotational tribometer are not applicable to the fired engine. The need to eliminate these inadequacies led to the development of a reciprocating tribometer.

III.A.2. Reciprocating Tribometer.

To overcome the limitations of the current tribometer and better simulate the environmental conditions encountered in the engine, a completely new tribometer was designed. The reciprocating tribometer is shown in Figure 10 (with the safety guard removed for clarity) and the operating parameters of the reciprocating tribometer are summarised in Table 2. A complete parts list is shown in Table 3. The two most important design specifications were that the relative motion between the seal sample and the test block should be reciprocating and that the test block should be small enough to fit into an SEM for analysis of the wear surface. In addition to these requirements, considerations were made for the ability to heat the test block and to measure lubricating oil film thickness measurements via an electrical resistance method. Because of time and cost considerations, these features were not implemented (but could be in the future).

Table 2 Reciprocating tribometer operational parameters.

Reciprocating Tribometer Specifications	
Operating speed	400 rpm to 1400 rpm
Contact force	50N minimum 250N maximum
Lubrication	Continual Drip Feed or Fixed Volume Bath
Friction force measurement range	± 100N
Data acquisition	USB 1000H_z
Seal sample dimensions (T x L x H)	1.24 – 2.50 x 15.00 x 3.0 – 5.00 mm
Test block nominal size (W x L x H)	30mm x 90mm x 15mm
Motor power	0.275 kW
Tribometer mass	55 kg

Figure 10 Reciprocating tribometer.

Two methods for achieving a reciprocating motion were considered: (1) a linear reciprocating motion such as that of a piston in a conventional engine or (2) a rotational reciprocating motion. The latter was chosen as it negates the need for expensive linear bearings and better simulates the motion of the piston in the Pivotal Engine™.

An important design consideration is the ability to balance the tribometer. To achieve this, two test stations are driven off a common crank shaft with a 180˚ phase offset. Because the vertical crank shaft has two journals at 180˚, the centre of mass of each test station is on a different horizontal plane, inducing a moment. The use of offset connecting rods allows the horizontal planes of the test stations to be as close as possible, minimising any dynamic balance problems. Because the connecting rods are offset they will experience a bending moment. For this reason the connecting rods feature triangulated webbing to maximise strength while maintaining a low mass, the connecting rod is shown in Figure 11. The webbing on the bottom of the connecting rod is opposite that on the top to further increase strength. The surface at the bottom of the webbing (highlighted green in Figure 11) is 2mm thick and horizontal for the length of the connecting rod. A larger offset could have been used if this surface was not horizontal but that would have complicated the manufacture of the connecting rod.

The connecting rods were manufactured from 7075 T6 aluminium. This material was chosen as it has a reasonably high strength to weight ratio as well as being easy to machine. All of the components which are not mass sensitive are manufactured from 1020 steel as this is a cheap material that is easy to machine.

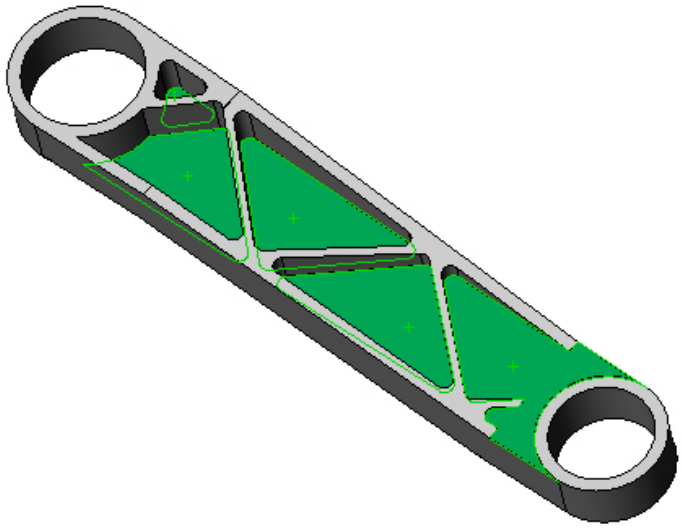

Figure 11 Offset connecting rod with triangulated webbing, the horizontal surface is highlighted in green.

Figure 12 shows an image of the crankshaft at BDC with both connecting rods fitted. The offset connecting rods mean that the centre web in the crankshaft has to be cut down to provide sufficient clearance for the connecting rods to pass. To ensure sufficient rigidity of the crank assembly the crank pins are pressed into the centre web and then welded on the back side. Welding the back side of the crank pins is required for the centre web because of the relatively small contact area between the crank pins and the web. This assembly is shown in Figure 13. The crank pins extend through the full thickness of the top and bottom crank halves so welding is not required. Not welding the outer ends of the crank pins means that the axial clearance of the big end bearing can be adjusted by pressing the crank apart and changing the thrust washers. Separate thrust washers were used so further simplify the manufacture of the crank webs (as opposed to having raised bearing surfaces on each web). The crankshaft has a throw of 40mm, which moves the seal holder through an arc of 40°. The maximum force in the tribometer occurs at the crankshaft end of the connecting rod, where a maximum force of 1597N is experienced at a crankshaft speed of 4000rpm. At the anticipated operating speed of 1000rpm, this force drops to 100N. Both of these forces will be safe for material strength and bearing life.

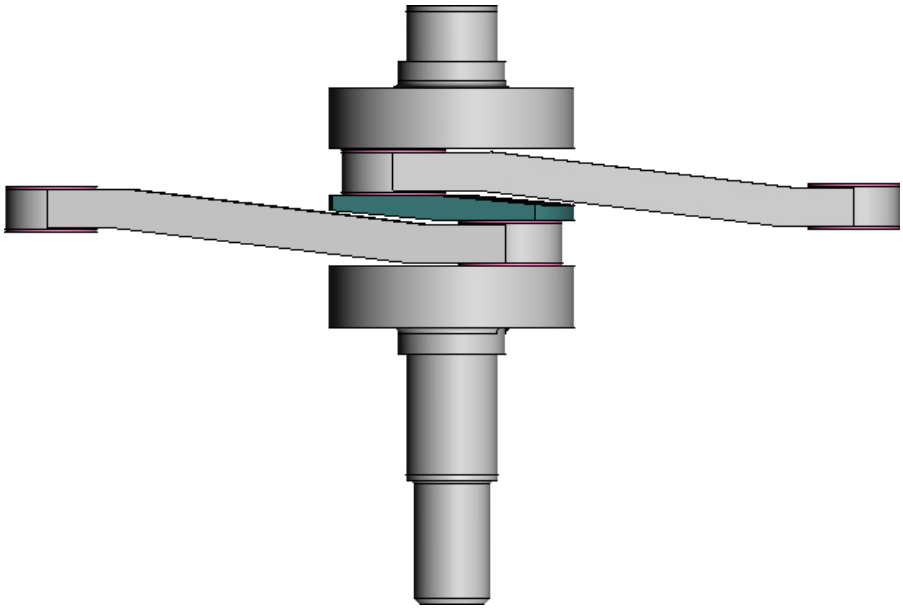

Figure 12. Tribometer crankshaft with offset connecting rods.

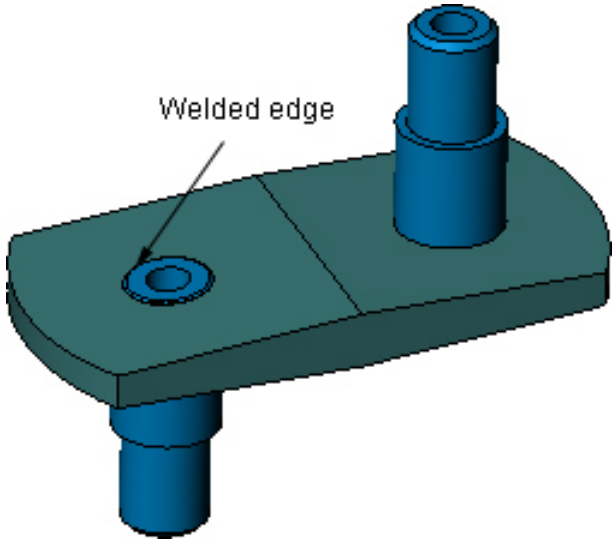

Figure 13. Crankshaft center web with crank pins welded in place.

The arm in which the seal sample is mounted (seal holder in Figure 14) is also manufactured from 7075 T6 aluminium in an effort to minimise reciprocating mass. The bearings in the seal holder assembly have a running fit on the main pivot to allow the application of a vertical load to be applied through the inner shell of the top taper roller bearing (the load path is shown in Figure 15). The applied load will prevent the inner race of the bearings spinning on the main pivot. It is for this reason that there is a minimum required applied load of 50N. The gudgeon pin has a light press fit into the seal holder and is retained by the gudgeon pin cap, which also has a light press fit on the gudgeon pin. To allow the disassembly of the connecting rod and seal holder

the gudgeon pin cap is drilled and tapped in the centre so a bolt can be threaded in to lift the cap off the gudgeon pin. The gudgeon pin has a 6mm hole drilled through its centre which can be filled with grease. A 6mm pin can be pressed into the hole forcing the gudgeon pin out of the seal holder to disassemble the connecting rod from the seal holder. Although clumsy, this procedure is required for the initial setup of the tribometer and is the only part of the tribometer that requires disassembly.

The chamber coating is applied to a 30mm x 90mm x 15mm aluminium block, the test block is held in a floating fixture with the tangential friction force constrained and measured with a load cell. Radial forces are constrained using a deep groove ball bearing on a common axis with the seal holder. The test block holder bears on an adjustable plate to allow for variances in the combined seal and test block height and flatness. Figure 14 shows an exploded view of one test station and the crankshaft (It is the levelling of this plate that requires the seal holder to be disconnected from the connecting rod).

To level the base plate, the test block and seal sample are first fitted to the tribometer. The base plate is then adjusted so that, with the combined height of the seal sample and test block, the connecting rod is not being forced up or down. At this stage, the seal holder and connecting rod are disconnected to allow room for a dial gauge and magnetic base to be moved around the base plate. The dial gauge is used to set the base plate to horizontal (or parallel relative to the main base plate), by adjusting the eight socket head cap screws on the corners of the base plate. The inner cap screws pass through the base plate and are threaded into the main base plate, while the outer cap screws are threaded into the base plate and bear against the main base plate. This allows the height and angle of the base plate to be adjusted independently.

The tribometer is built on a 20mm thick steel base, which is mounted on a fabricated steel frame using rubber mounts, providing rigidity as well as mass to dampen vibrations. To allow the speed of the tribometer to be controlled a 0.275 kW three phase electric motor is used in conjunction with an inverter. Power is transmitted from the motor to the crank shaft through an A section V-belt drive. The use of the V-belt drive will allow the tribometer speed range to be easily changed at a later date.

To ensure the safety of the tribometer operators an enclosure was constructed to completely cover the tribometer. In addition to operator safety, the enclosure also helps prevent contamination of the wear system by foreign bodies that could affect the measured wear rates.

One major deviation of the reciprocating tribometer from the actual engine is that, on the tribometer, the seal sample is rigidly clamped while in the engine there is a clearance between the seal and the piston to allow gas pressure to act on the back of the seal. This was not considered to be a significant compromise since analysis of worn seals from the engine revealed the wear surface is almost perfectly flat, indicating that the seal does not move in the seal groove.

The addition of combustion products and un-burnt fuel in the engine will affect the wear rates of the material couples, however to incorporate these aspects into the tribometer would troublesome. The addition of fuel would require the tribometer to be located in a fume hood or similar, and would create a significant fire risk due to the elevated temperatures. When testing piston rings for four-cycle engines, [19] more realistic results are obtained when testing is performed with used lubricating oil, contaminated with wear particles, fuel and combustion by-products. The nature of a two-cycle engine means that used/contaminated oil is replaced by clean oil, thus removing contaminants from the contact area. For this reason the drip feed system was deemed suitable, with used oil draining from the bottom of the tray. It is also possible to run a test with a fixed volume of oil around the test block by blocking the drain tube. The drip feed system can be seen in Figure 10. Oil is delivered through silicone tubes which are supported by copper tubes. The flexible silicone tube allows the oil delivery point to be very close or even in contact with the seal holder, ensuring that the oil is delivered to the contact zone.

Table 3 Parts list for reciprocating tribometer

Component		Material	Quantity
1	Frame	1020	1
2	Rubber mounts	N/A	4
3	Main base Plate	1020	1
4	Motor frame	1020	1
5	Motor	N/A	1
6	Motor pulley A-section 110mm	CI	1
7	Crank pulley A-section 90mm	CI	1
8	Crank bottom	1020	1
9	Crank pin	1020	2
10	Crank web	1020	1
11	Crank thrust washer	1020	4
12	Main bearing 6006 deep groove ball	N/A	2
13	Big end bearing NA4902 needle roller	N/A	2
14	Housing base	1020	1
15	Housing end	1020	2
16	Housing top	1020	1
17	Bearing retainer	1020	1
18	Top brace	1020	1
19	Top brace spacer	1020	1
20	Connecting rod	7075 T6	2
21	Small end Bearing NA4901 needle roller	N/A	2
22	Small end thrust washers	1020	4
23	Gudgeon pin	1020	2
24	Seal holder	7075 T6	2
25	Seal clamp	7075 T6	2
26	Gudgeon pin cap	7075 T6	2
27	Seal holder top bearing 30302 taper roller	N/A	2
28	Seal holder bottom bearing 6302 deep groove ball	N/A	2
29	Main pivot shaft	1020	2
30	Oil tray	1020	2
31	Sample carrier	7075 T6	2
32	Sample carrier main bearing 6202 deep groove ball	N/A	2
33	Sample carrier end bearing 626 deep groove ball	N/A	4
34	Load cell	7075 T6	2
35	Sample carrier spacer	1020	2
36	base plate	1020	2
37	Upright	1020	2
38	Upright cap	Al bar stock	2
39	Load arm A	1020	2
40	Load arm B	1020	2
41	Load collar	Al bar stock	2
42	A 38 V-belt	N/A	1
43	M10 x 40mm SHCS	N/A	4
44	M8 x 35mm SHCS	N/A	12
45	M6 x 35mm SHCS	N/A	26
46	Oil drip feed	N/A	1

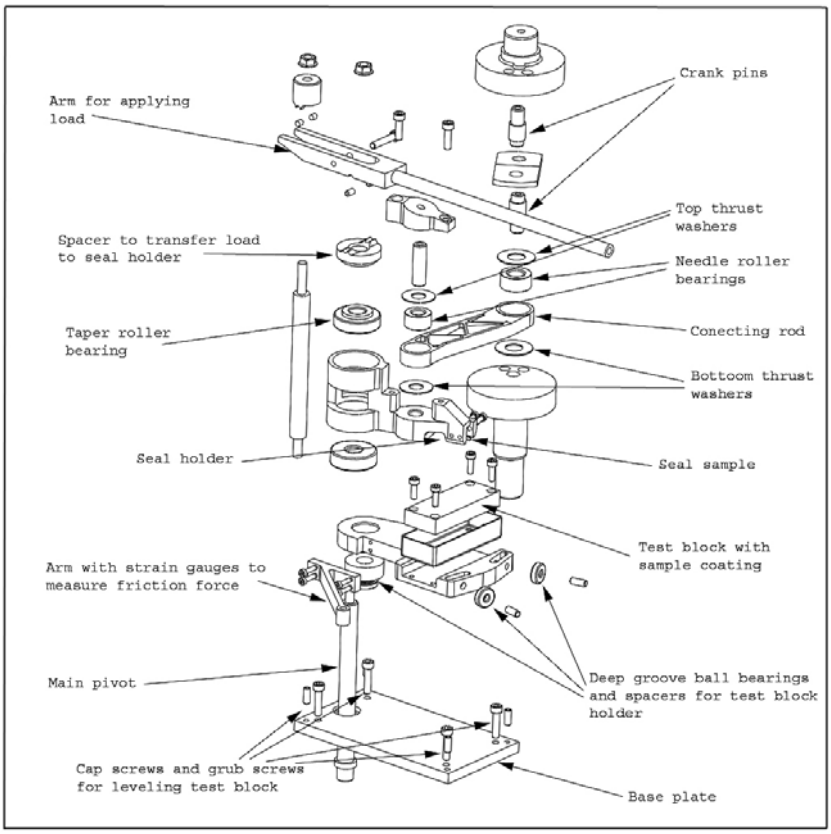

Figure 14 Exploded view of test station and crank of reciprocating tribometer.

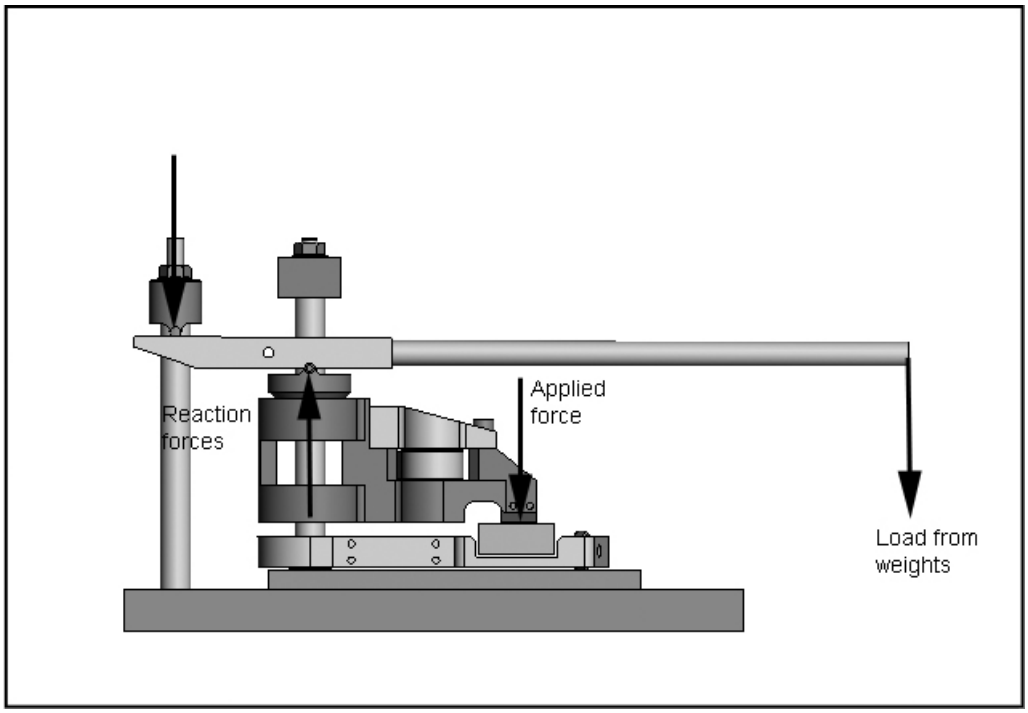

Figure 15. Reciprocating tribometer indicating the load path.

III.A.3. Other Equipment.

A Taylor-Hobson 'Tally surf' surface profile measurement system was used to measure R_a values of the chamber coatings as well as the actual surface profiles of the worn coatings. Optical images were taken using a Leica DM IRM inverted research microscope in with a Zeiss Axiocam digital camera. The images used to quantify seal wear rates were taken in dark field mode while most of the optical images used to examine microstructures used differential interference contrast. The use of differential interference contrast also allowed high magnification images to be taken of wear surfaces. Finally a JEOL JSM 6100 scanning electron microscope fitted with an Oxford eXL energy dispersive X-ray analyser system was used to take high magnification images of wear surfaces and produce EDS maps and spectra of some of the tested materials.

III.B. Material Test Procedure.

Material test procedures were implemented to standardise the experimental procedure and ensure repeatability. A range of test procedures were developed to accommodate the large differences in system wear rates as well as the two different tribometers.

III.B.1. Rotational Tribometer Test Procedure.

The first test procedure was developed for material combinations that gave wear rates that could be measured using mass loss techniques.

Four-hour Rotational Test Procedure.

1. Seal cut, de-burred, cleaned and weighed
2. Test disc dressed (600 grit wet and dry sandpaper) and cleaned
3. Surface roughness values of test disc measured (R_a)
4. Strain gauges on test rig calibrated using dead weights
5. Test run
    - continual lubrication, Morris race 2 oil
    - seal normal load of 105N
    - rotational speed of 2850 rpm
    - four hour test duration
6. Seal cleaned and weighed
7. Wear rate determined
8. Seal cut and mounted
9. Optical images taken of seal
10. Surface roughness values of test disc measured (R_a)
11. Test data entered into data base

This procedure was repeated three times for each seal – disc combination, using a new seal sample for each test. Step 2 was only applied to the first of the three tests to remove any surface damage from previous tests, and to give a consistent initial surface. The test duration of four hours was chosen arbitrarily, but provided sufficient seal wear to allow accurate mass loss measurements. Steps 8 and 9 provided little information so were omitted from most of the tests. Initially steps 3 and 10 were

implemented but because the R_a values were constant (0.54μm R_a) between different discs (before and after testing) this was deemed unnecessary for further tests.

A second, more severe procedure was implemented. This procedure was intended to simulate a starved lubrication condition, which may be present in the engine (little is known about the distribution of oil in the engine). This procedure was the same as above, except that there was no continual lubrication over the duration of the test. The disc had a layer of oil applied over the surface before the start of the test, and the test was then run for twenty minutes instead of the four hours of the first procedure.

Twenty-minute Starved Lubrication Rotational Test Procedure.

1. Seal cut, de-burred, cleaned and weighed
2. Test disc dressed (600 grit wet and dry sandpaper) and cleaned
3. Strain gauges on test rig calibrated using dead weights
4. Test run
    - initial lubrication, Morris race 2 oil
    - seal normal load of 105N
    - rotational speed of 2850 rpm
    - twenty minute test duration
5. Seal cleaned and weighed
6. Wear rate determined
7. Seal cut and mounted
8. Optical images taken of seal
9. Test data entered into data base

The testing of the arc seal samples involves the same procedure as the four-hour test, with the addition of a setup procedure prior to the start of the test. Because of the geometry of the arc seal, a different seal clamp is used. The setup procedure requires the seal clamp be adjusted so that the seal sample sits flat against the test disc. It is also necessary to clamp the weight arm to prevent the seal from tilting during the test.

In both of these rotational test procedures, the seal wear rates were determined by the total mass loss over the course of the test. It was originally intended that the disc coating wear would be measured using a Taylor-Hobson ‘Tally surf’ surface profile measurement system, however the surface topography was dominated by porosity

from the coating application process. If the test disc had been smaller, it would have been possible to quantify wear using mass loss or atomic force microscopy. Finally, the only way to assess the wear of the coating was to subjectively rank the discs based on the appearance of the surface. Even with this method, it was only possible to identify coatings that performed very badly.

III.B.2. Rotational Tribometer Test Procedure for Low Wear Material Systems.

A third test method was required because some of the compression seal materials had wear rates that were so low no mass loss (less than 0.0001 gm) could be measured over extended periods on the tribometer.

Extended Rotational Test Procedure.

1. Seal cut, de-burred, cleaned and weighed
2. Test disc dressed (600 grit wet and dry sandpaper) and cleaned
3. Strain gauges on test rig calibrated using dead weights
4. Test run
    - continual lubrication, Morris race 2 oil
    - seal normal load of 105N
    - rotational speed of 2850 rpm
    - test run for six to nine hours
5. Seal cleaned and optical images taken
6. Seal remounted in tribometer and test restarted

After a period of time (between six and nine hours) the seal sample was removed from the tribometer, cleaned in acetone and mounted in a clamp. A second used seal sample was permanently mounted in the clamp for reference measurements. Images were taken along the length of the wear surface the reference seal using a Leica DM IRM inverted research microscope in dark field mode with a Zeiss digital camera. The images were joined in Adobe Photoshop to form a montage image of the seal surface, which was then cropped to contain just the flat area of the seal surface. The reference images were processed by adjusting threshold and contrast values until they had the same black and white pixel count. The threshold and contrast values for each reference image were then applied to the corresponding montage seal image. The processing of a sample is shown graphically in Figure 16. The change in worn surface area over a period of time is then used to compare wear resistance of the various seal

materials. It should be noted that even when 100% of the seal surface had been worn there was still no measurable mass loss.

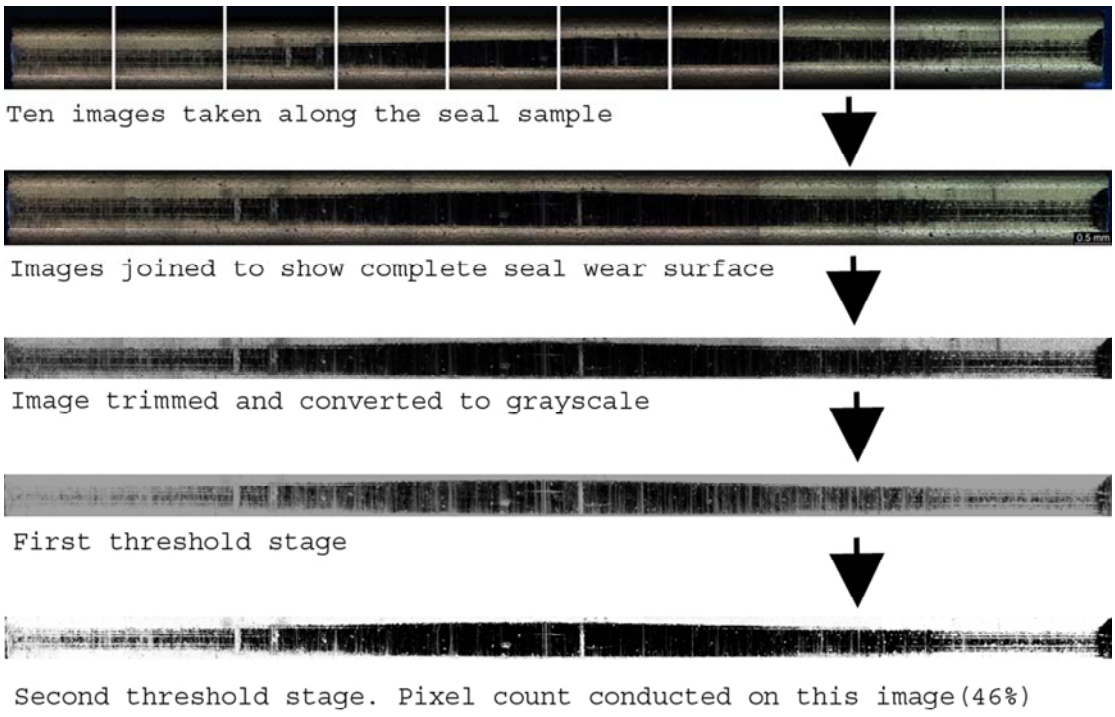

Figure 16 Seal wear surface image processing

III.B.3. Reciprocating Tribometer Test Procedure.

A fourth test method was implemented for the reciprocating tribometer. Further details of this procedure of the are given in section III.A.2.

Reciprocating Test Procedure.

1. Tribometer set up for each test block
2. Seal cut, de-burred, cleaned and weighed
3. Test block dressed (600 grit wet and dry sandpaper), cleaned and weighed
4. Test run
    - continual lubrication, Morris race 2 oil (drip feed)
    - seal normal load of 105N
    - test frequency 21 Hz (1275 rpm)
    - 40° arc at 105mm radius
    - twenty hour test duration
5. Seal cleaned and weighed
6. Test block cleaned and weighed
7. Wear rates determined
8. Test data entered into data base

IV. Results and Discussion.

IV.A. Material Selection.

Chamber and compression seal materials were selected for testing based on successful use in environments similar to those expected in the Pivotal Engine™, notably conventional two and four-cycle piston engines and the Mazda Wankel engine. In addition to this criterion, component cost had a strong influence on the selection of potential materials.

IV.A.1. Compression Seal Materials.

The primary selection criterion for compression seals was high hardness. The dominant compression seal wear mechanism is abrasive wear. Increasing the hardness of the seal material will generally increase its resistance to abrasive wear. Other parameters such as surface free energy have been shown to be related to system wear [20] but were not expressly considered in this work. The materials selected for testing are shown in Table 4.

IV.A.2. Chamber Materials.

A range of common cylinder liner materials were rejected early in the material selection process for various reasons. Cast iron, the most common cylinder liner material, has graphite flakes that provide solid lubrication and act as reservoirs for lubricant. However cast iron was not considered purely on the basis of mass. The increase in mass associated with manufacturing the engine from cast iron instead of aluminium is unacceptable. In addition to cast iron, all of the electroplated material systems were eliminated. Electroplated materials were eliminated because of the high costs involved in producing tooling that would promote an even deposition on the flat surfaces of the engine components. This includes materials such as hard chromium and Nikasil. These coating systems or variations of them are used in most motor bike engines and some automotive engines. Nikasil consists of silicon carbide particles (approximately 4μm in size) that are dispersed in a nickel matrix. The nickel acts as a binder while the dispersed silicon carbide particles minimise the wear of the system. Variations of this system are available with different binders and different ceramic particles.

The elimination of these materials left thermal spray coatings as the only option. Thermal sprayed coatings can be applied by a number of methods such as flame spraying, arc spraying, detonation gun and plasma spraying. In most of these processes, the deposited coating material is processed from a powder, although some systems use wire. The properties of the applied coating depend on the composition of the powder or wire in conjunction with deposition parameters such as power and substrate temperature. If the coating is deposited from a powder, the coating structure is also dependent on the original particle size. The chamber coating materials selected for testing are shown in Table 4.

Table 4. Test Materials.

Compression seal materials	**Chamber coatings**
Nitrided stainless steel (N-SS)	Pivotal Engineering 75B-90MXC
Mazda 13BT Apex Seal (Cast Iron)	Pivotal Engineering tungsten
Silicon nitride	Sulzer Metco XPT512
Titanium nitride coated N-SS (TiN)	Sulzer Metco F2056
Chromium nitride coated N-SS (CrN)	Sulzer Metco F4301
Tungsten carbide carbon coated N-SS (WC-C)	NASA PS304
Diamond like carbon coated N-SS (DLC)	
Silicon nitride coated N-SS (SiN)	
Plasma nitrided titanium	

IV.B. Material Characterisation.

The majority of materials selected for testing were proprietary. Because of this, there was little or no information on the material properties. In this work, the material microstructure and properties are important for two reasons. Firstly, some of the chamber coatings were not applied by the company that developed and produces the coating system. This means that the tested coating may not have the mechanical and microstructual properties intended by the developer. Secondly it is necessary to know what types of materials are being tested so results can be compared with other research.

IV.B.1. Nitrided Stainless Steel.

The composition of the stainless steel seal material is similar to AISI type 446 stainless steel. The EDS spectrum and composition is shown in Figure 17. The seal is nitrided to provide a hard wear resistant surface ($750H_v$) while the bulk material is a fine martensitic structure with a micro hardness of $400H_v$. A cross section of the nitrided stainless steel seal is shown in Figure 18 A and B. A nitrided layer can be clearly seen in both images.

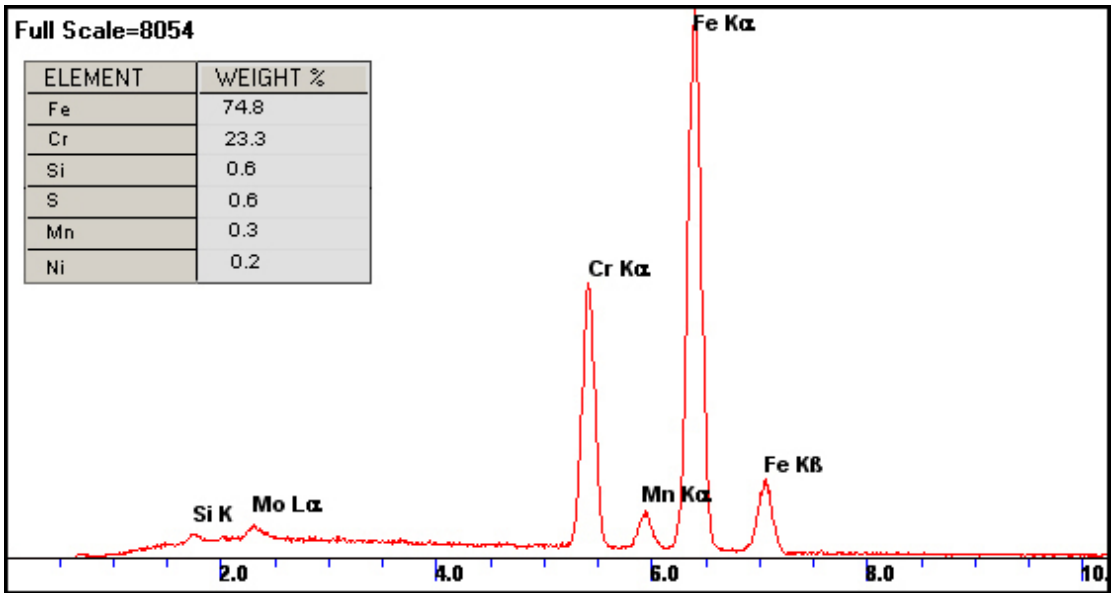

Figure 17. EDS spectrum of nitrided stainless steel seal.

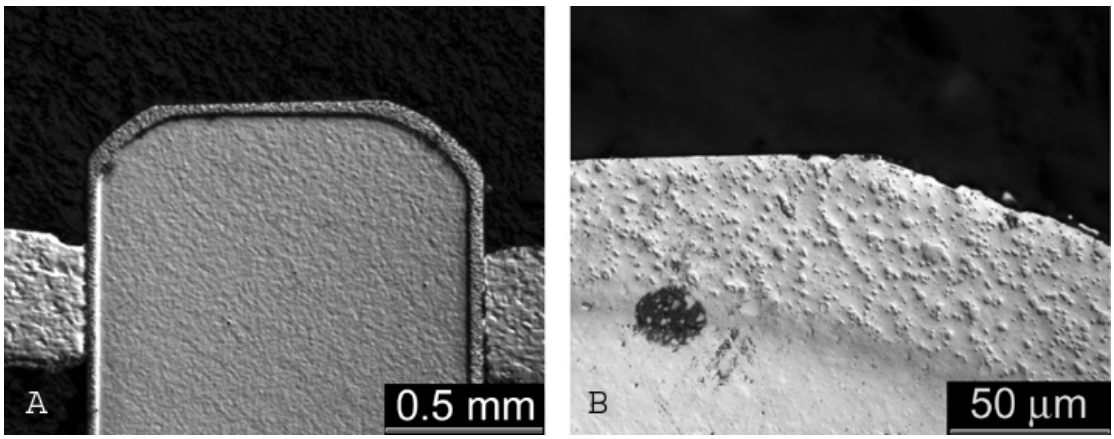

Figure 18 differential interference contrast micrographs of nitrided stainless steel seal, showing the nitrided layer.

A problem with stainless steel piston rings is that they are prone to micro welding to the aluminium ring lands under certain conditions. This can be even more detrimental to engine performance than piston ring wear. Some aluminium alloys are more susceptible to micro welding than others, making it possible to lessen this problem through material selection. Other solutions include surface treatments of both the ring and ring groove, and most importantly ensuring that there is sufficient lubrication in the piston ring groove.

IV.B.2. Mazda 13BT Apex Seal (Cast Iron).

In terms of cost and performance, cast iron is still one of the best materials available for the manufacture of piston rings. The graphite phase in cast iron provides limited solid lubrication in the form of a graphite film, as well as acting as a lubricant reservoir. This property helps prevent scuffing and high wear during periods of interrupted lubrication. The only significant disadvantage of cast iron is that it generally has low tensile strength and fracture toughness. The graphite phase acts as pre-existing cracks. This requires piston rings be made thicker than may be desirable to retain sufficient strength, which in turn increases the inertial loadings on the piston ring lands.

Since there was not a readily available supply of straight cast iron piston ring material, a Mazda 13B three piece apex seal was used for testing purposes (both rotational and reciprocating tribometers require straight seal samples). The composition of the cast iron is specific to this application. The EDS spectrum is shown in Figure 19.

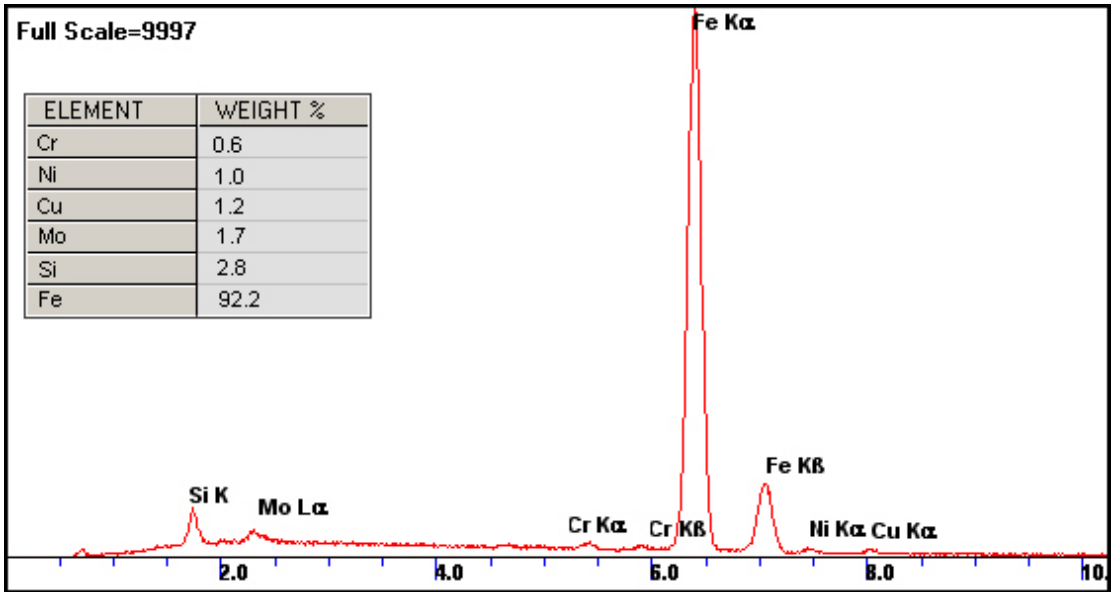

Figure 19 EDS spectrum and composition of Mazda apex seal

The Mazda apex seal is electron beam chilled [5] along the wear surface giving a hard columnar bainite structure (Figure 20 A). The back edge of the seal is softer, having a microstructure with a large volume of free graphite (Figure 20 B). The seal is manufactured in this manner to give a hard wear surface while minimising the wear on the apex seal groove. The hardness of the wear surface of the seal was 680 H_v while the back edge ranged from 370 H_v to 650 H_v depending on the proximity of the indentation to graphite.

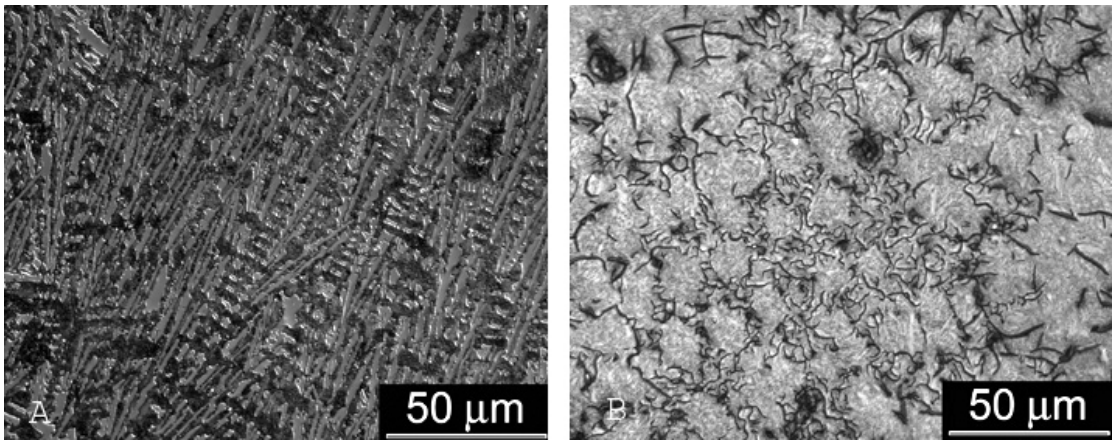

Figure 20 Optical micrographs of a Mazda apex seal (A) hard bainite structure. (B) graphite rich martensitic structure.

IV.B.3. Silicon Nitride.

Due to the budget constraints of this project, the silicon nitride seal samples tested were cut from a 'reject' reaction bonded component donated by Dynamic-Ceramic (Figure 21). The high hardness and abrasion resistance of silicon nitride necessitates the use of diamond tooling to cut and shape components. This meant the seal samples had to be hand made, and because of this the profiles were not the same as those of the stainless steel seal material. The microstructure of the silicon nitride was not investigated because of the dangerous chemicals required to etch samples.

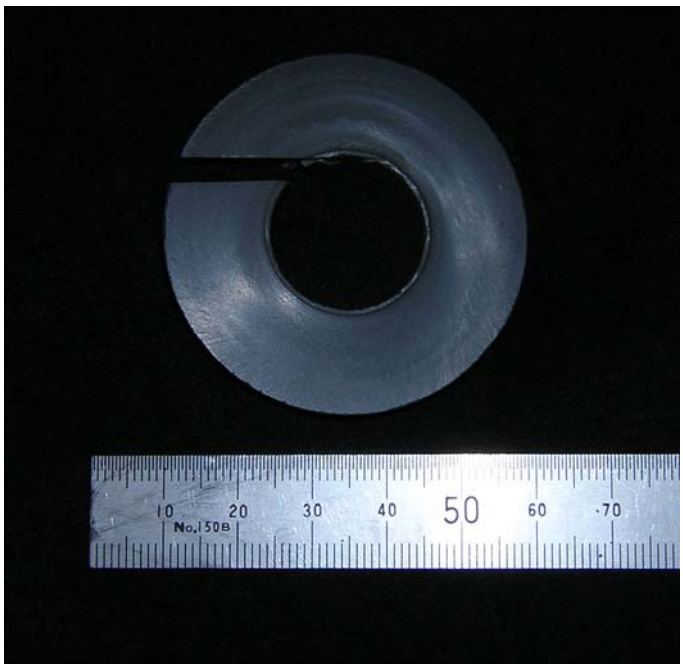

Figure 21. Reaction bonded silicon nitride sample

IV.B.4. Titanium Nitride Coated N-SS.

Titanium nitride was selected as a potential material due to its high hardness and reasonably good toughness, both of these properties being favourable in minimising abrasive wear. TiN can have hardness values of up to 2300 Hv and film thickness of up to 5μm (limited by internal stress).

TiN is deposited in one of two ways using the PVD process. A TiN target can be used in an argon atmosphere or a Ti target can be used in a nitrogen and argon atmosphere. The latter is the more common method and is known as reactive sputtering. In this process, the nitrogen in the chamber reacts with the Ti atoms deposited on the substrate surface to form TiN. The film properties are dependent on the substrate temperature, DC current bias, power and the nitrogen concentration. These variables control the amount of nitrogen in the film from $TiN_{<0.8}$ to $TiN_{>1.2}$ as well as the favoured crystallographic growth direction, either <111> or <200> directions normal to the film surface.

Because of the costs involved in acquiring a commercial titanium nitride coated sample, the Electrical Engineering department's magnetron sputtering (PVD) machine was used to deposit a TiN film on a nitrided stainless steel sample. The seal samples were cleaned in petroleum spirits followed by acetone to remove any oils on the seal material. Once mounted in the sputtering machine and a sufficient vacuum reached, the substrate was sputter etched in a high argon flow rate to remove any surface contaminants. A titanium film was deposited to act as a conformal interface between the nitrided stainless steel and the TiN film. For this layer, an argon flow rate of 9.97 sccm (standard cubic centre metre per minute) was used in conjunction with a power of 300W and a temperature of 57°. Sputtering commenced for 16 minutes using a titanium target of 99.999% purity, producing a film approximately 0.8 μm thick. The TiN layer had the same deposition parameters as the Ti layer with the addition of nitrogen at a flow rate of 2.23 sccm. The machine was run for 57 minutes, producing a film thickness of 1.7 μm. These flow rates were used as they are known to work in this particular machine (the gas flow rates affect the plasma stability), not for the specific properties that they would produce. It is likely that these deposition parameters favoured the formation of a $TiN_{>1.2}$ film, having a much lower hardness than the desired $TiN_{0.9\text{-}1}$ film. The composition of the film is indicated by the brown-

black colour as opposed to the desirable gold colour [21]. A higher nitrogen flow rate would have given a film with better properties for this application but would have slowed the deposition rate (assuming plasma stability was maintained). Figure 22 shows a cross section of the seal sample with the titanium and titanium nitride layers. The electroless nickel coating was applied to retain the integrity of the Ti/TiN film during the sectioning and polishing process.

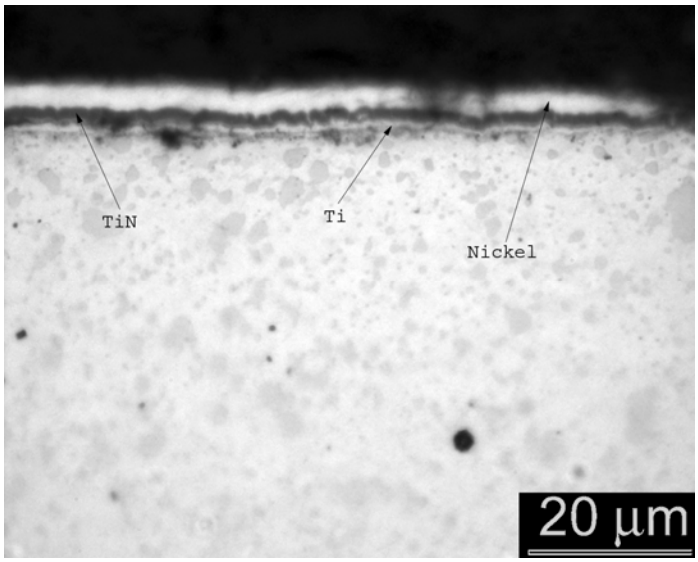

Figure 22 A optical micrograph of a layered Ti/TiN film on N-SS. The nickel layer was applied to aid in metallographic preparation.

Due to the small thickness of the film it is not possible to measure an accurate hardness value without influence from the substrate material (with the available equipment). To avoid the influence of substrate properties the criterion of $h < 0.1d$ must be met, where h is the indentation depth and d is the film thickness [22]. It is likely that the hardness of this TiN film is around 800 Hv (estimated from the film colour), which is not significantly harder than the nitrided layer on the stainless steel seal (750 Hv) and subsequently not expected to provide a significant change in wear resistance. Because of the time and cost involved in setting up the sputtering machine, it was decided not to follow this route for the acquisition of TiN samples.

TiN coated seals were provided by Total Seal. Nothing is known about the deposition parameters (except that a reactive sputtering method was used) and therefore the mechanical properties of this coating. The coating was deposited to a thickness of 4

μm (Figure 23 B) and has the characteristic gold colour of TiN_x with x in the range of 0.8 to 1.0.

IV.B.5. Chromium Nitride Coated N-SS.

CrN PVD coatings are being developed as alternatives to electroplated chromium and hard chromium coatings. The driving force for this change is the toxic chemicals involved in the electroplating of chromium. In a similar fashion to TiN, CrN can be deposited using PVD or CVD processes. The CrN coatings can be deposited to a greater thickness (approximately 10μm) than the TiN coatings, but generally have a lower hardness ($2000H_v$).

The mechanical characteristics of CrN coatings are more sensitive to the deposition parameters than TiN coatings. The chosen parameters will influence the composition and structure of the coating as well as the relative amount of each present (Cr, CrN and Cr_2N). In turn, the composition and structure determine the properties of the film [23].

CrN coated seal samples were also provided by Total Seal. Like the TiN coating, little is known about the CrN coating except that it was deposited using a reactive sputtering technique and has a thickness of 4 μm (Figure 23 A).

IV.B.6. Tungsten Carbide-Carbon Coated N-SS.

Total Seal also supplied a WC-C coating. This coating consists of two layers, a WC layer and a C layer shown in Figure 23 C. The composite thickness of the coating is 4 μm.

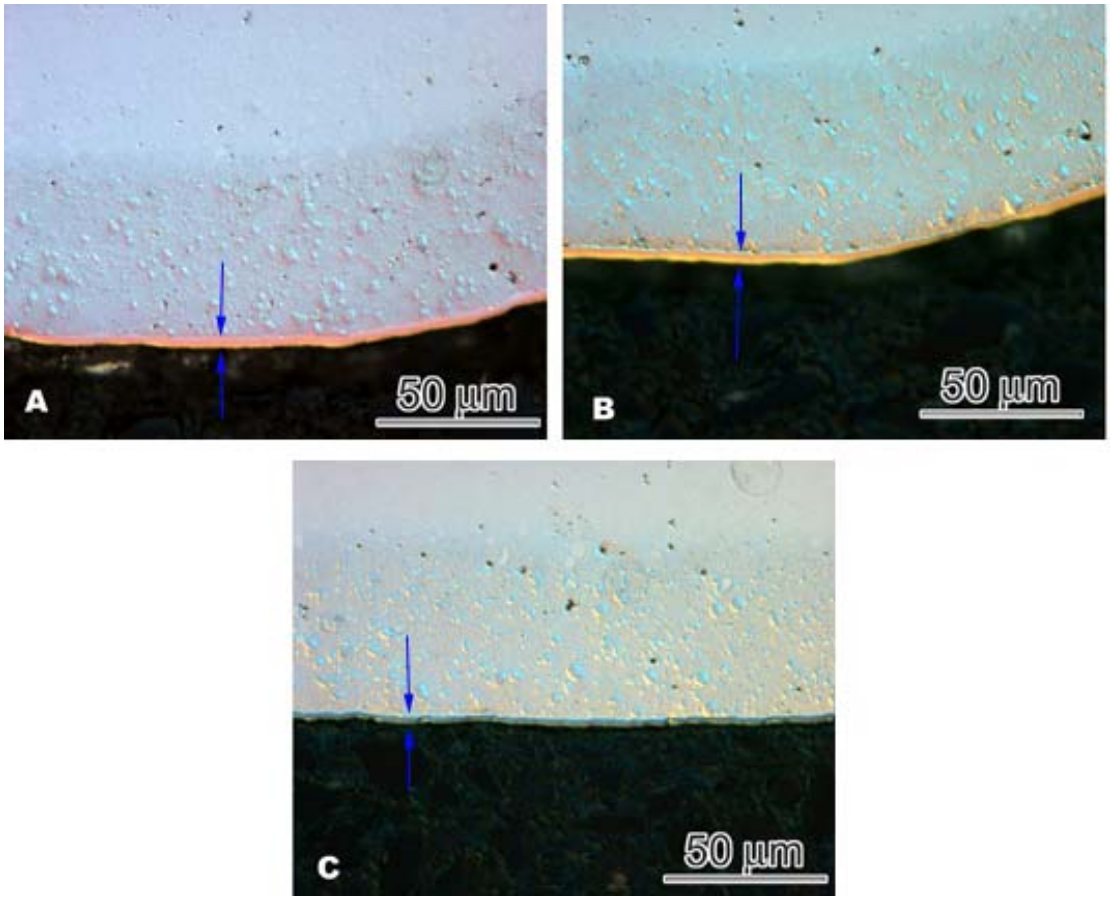

Figure 23 Differential interference contrast micrographs of Total Seal PVD coatings applied to a N-SS substrate, (A) CrN, (B) TiN, (C) WC-C.

IV.B.7. Diamond like Carbon Coated N-SS.

The term DLC covers a very wide range of coatings and subsequently a wide range of properties. DLC coatings contain carbon with different atomic bond types such as tetrahedral amorphous carbon (ta-C), amorphous hydrogenated carbon (a-C:H) and graphite. These phases are responsible for the low measured friction values and low wear rates that are characteristic of DLC coatings. The relative amounts of each of these phases determine the coating properties, particularly hardness (over 2000 H_v) and friction coefficients. In addition to the carbon phases present, DLC coatings can be deposited both simultaneously and in layered composite structures with metals, metal carbides and metal nitrides to further alter the coating properties.

Diameter Systems Ltd applied a DLC coating to the nitrided stainless steel seal substrate. Unfortunately, like the Total Seal coatings, little is known about the mechanical properties or structure of this particular DLC coating.

IV.B.8. Other PVD Coated Seals.

In addition to the CrN coated seals supplied by Total Seal. Beamalloy Technologies, LLC (Plain City, OH 43064 USA) supplied CrN and Si_3N_4 coated seals. However this company is no longer trading. The Beamalloy coatings were less the half the thickness (approx 1.2μ to 2.0μ) of the Total Seal coatings.

IV.B.9. Plasma Nitrided Titanium.

In addition to PVD and CVD processes, TiN can be formed by plasma nitriding titanium. Titanium can be nitrided to a depth of approximately 70 μm, providing a significantly longer life than the PVD TiN coatings. The use of titanium would have the benefit of reducing the weight of the seals by 43% (compared to steel), therefore reducing the forces on the seal groove. Compression seals were EDM (electro discharge machining) wire cut from a Ti-6Al-4V block and dressed with a diamond lap. Heat Treatments Ltd, (Auckland, New Zealand) carried out the plasma nitrided process. Unfortunately the seals did not have the required hardness when returned due to inadequate processing. The seals were not tested as they would have caused significant damage to the chamber surface.

IV.B.10. Pivotal Engineering 75B-90MXC Coating.

Pivotal Engineering had previously developed a coating that was used during the early stages of engine development. This coating was applied using a TAFA twin wire arc spray system with one roll of 90MXC hard facing wire and one roll of 75B bond coat wire. The TAFA twin wire arc system uses each wire as an electrode forming an arc between them. Normally both wires would be the same material. However in this case the use of two different wires allows the deposition of a material that performs better than an ‘off the shelf’ material. The 75B wire has a composition of 95% Ni and 5% Al. When used as a bond coat an exothermic reaction occurs between the nickel and aluminium, which enhances the bonding between the substrate and the coating. The 90MXC wire contains Fe, Ni and has a Cr core. This coating has relatively large splat-like phases as seen in Figure 24. There is very little optical contrast between the phases in this coating but the distribution of the metals present is shown in the EDS map (Figure 26), while the composition is shown in Figure 25. From the EDS map, it can be deduced that there are four distinct phases (1) Al, (2) Ni, (3) Ni-Cr-Fe-Mo and (4) Cr-Fe-Mo.

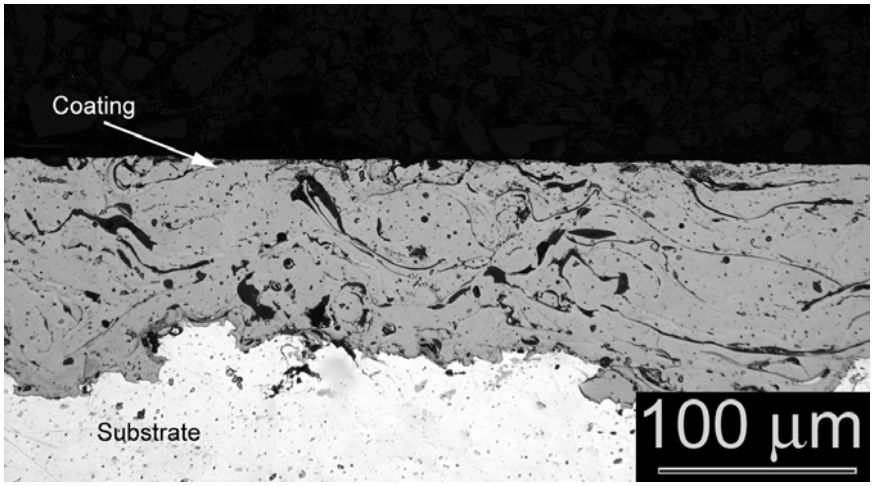

Figure 24. Pivotal Engineering 75B-90MXC coating

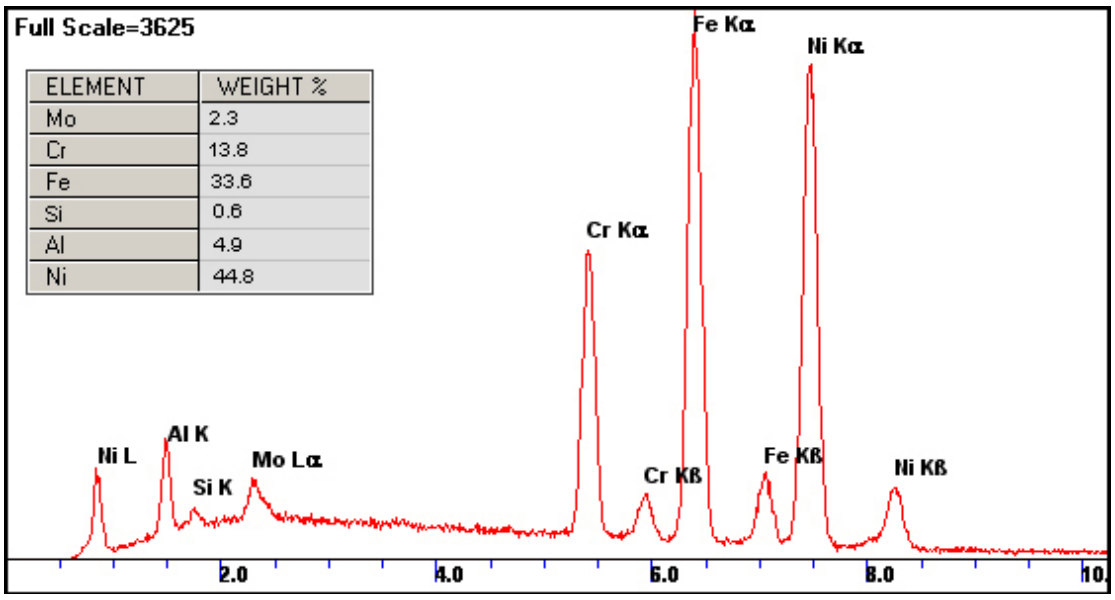

Figure 25. EDS spectrum and composition of Pivotal Engineering 75B-90MXC coating

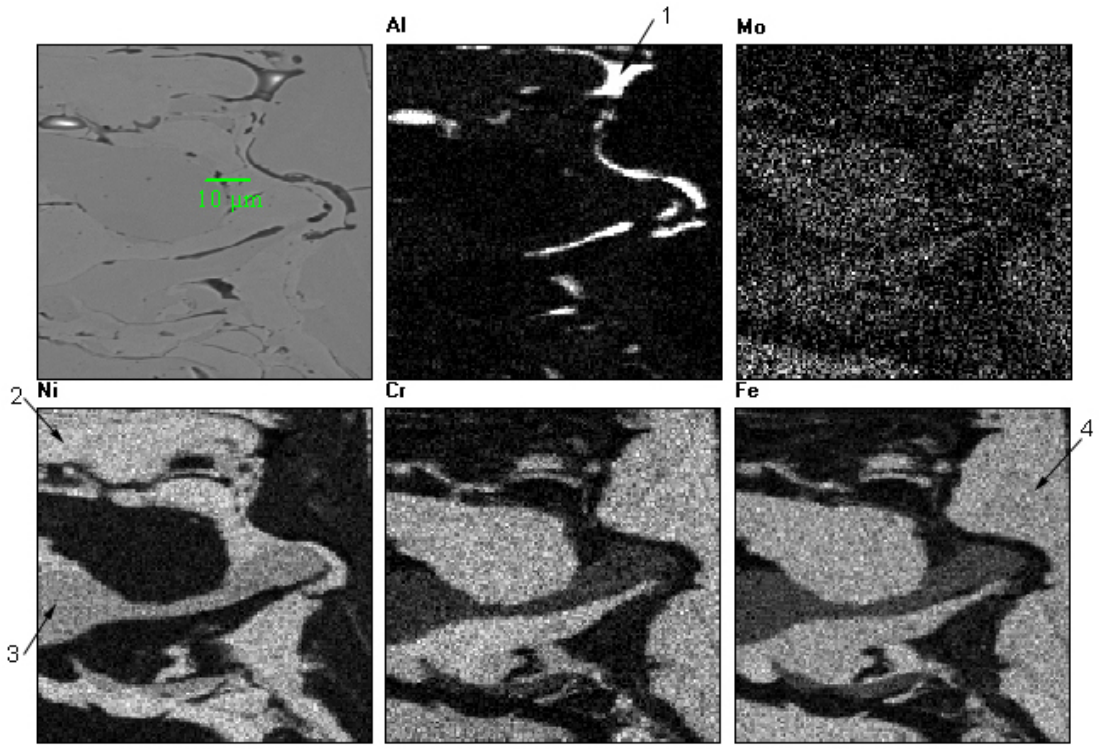

Figure 26 EDS map of Pivotal Engineering coating. The four distinct phases in this coating are (1) Al, (2) Ni, (3) Ni-Cr-Fe-Mo and (4) Cr-Fe-Mo.

IV.B.11. Sulzer Metco F4301.

The F4301 coating was originally developed by Sulzer Metco (Winterthur Switzerland) as a cylinder liner coating for use in automotive applications. The coating is predominantly iron, but contains molybdenum as an anti-scuffing agent. Cross sections of the coating are shown in Figure 27. Because the phases in the coating have different mechanical properties, material is removed at different rates during the polishing process (the polishing process is essentially three body abrasive wear). Consequently, the material removal rate of the harder phases is slower, leaving them proud of the surface. It is possible to detect this surface topography in an optical microscope using differential interference contrast (DIC). Using EDS, the hard phase indicated in Figure 27 A and B has been identified as molybdenum rich. Figure 28 shows the EDS map and Figure 29 shows the EDS spectrums. The remaining phases visible in Figure 27 C are predominantly iron, the light phase (that is not molybdenum) being an iron alloy which is attacked with a 2% nital etch while the bulk of the dark phase is likely to be an iron oxide, carbide or nitride (not attacked with a 2% nital etch). The EDS map also shows the presence of a phase containing

aluminium. It is likely that the aluminium is present in the form of an inter metallic iron-aluminium compound as the aluminium rich areas coincide with iron rich areas.

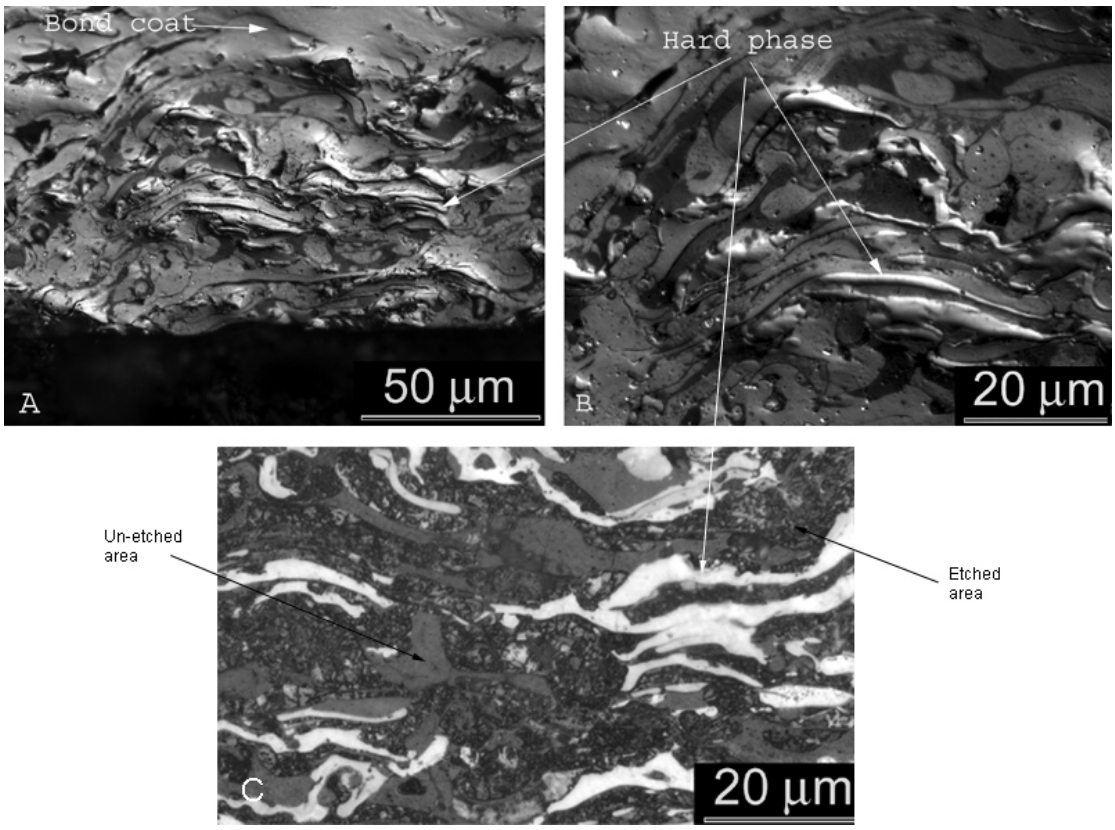

Figure 27. Optical micrographs of Sulzer Metco F4301 cross-section. (A) low magnification un-etched (DIC) (B) high magnification un-etched (DIC). (C) etched with 2% nital

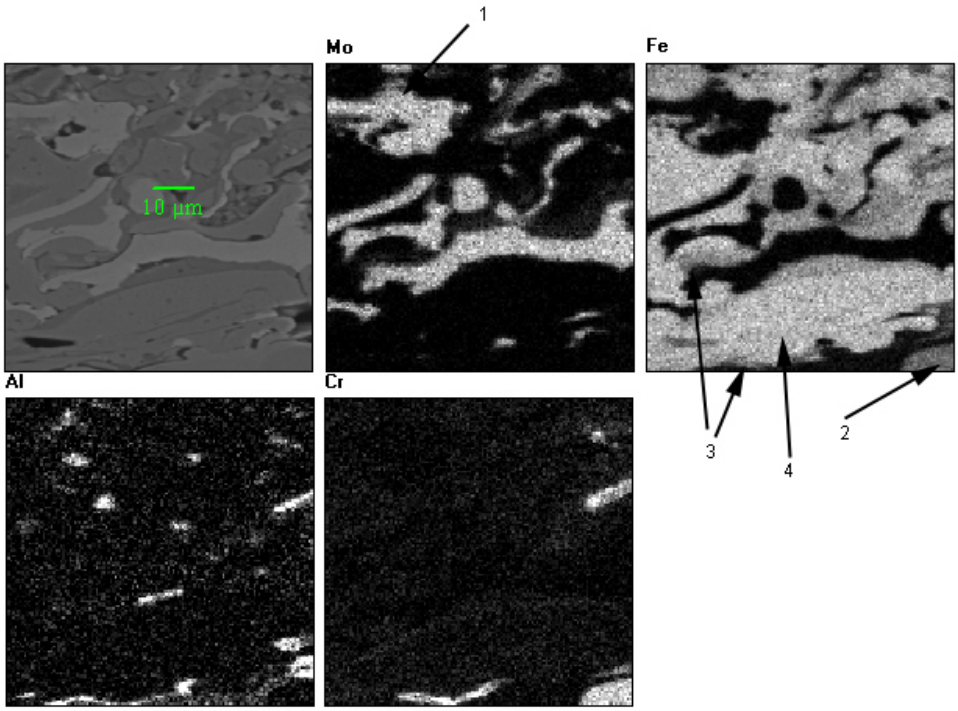

Figure 28 EDS map of Sulzer Metco F4301, showing the phases (1) Mo, (2) Fe-Cr, (3) Fe-Al, (4) Fe.

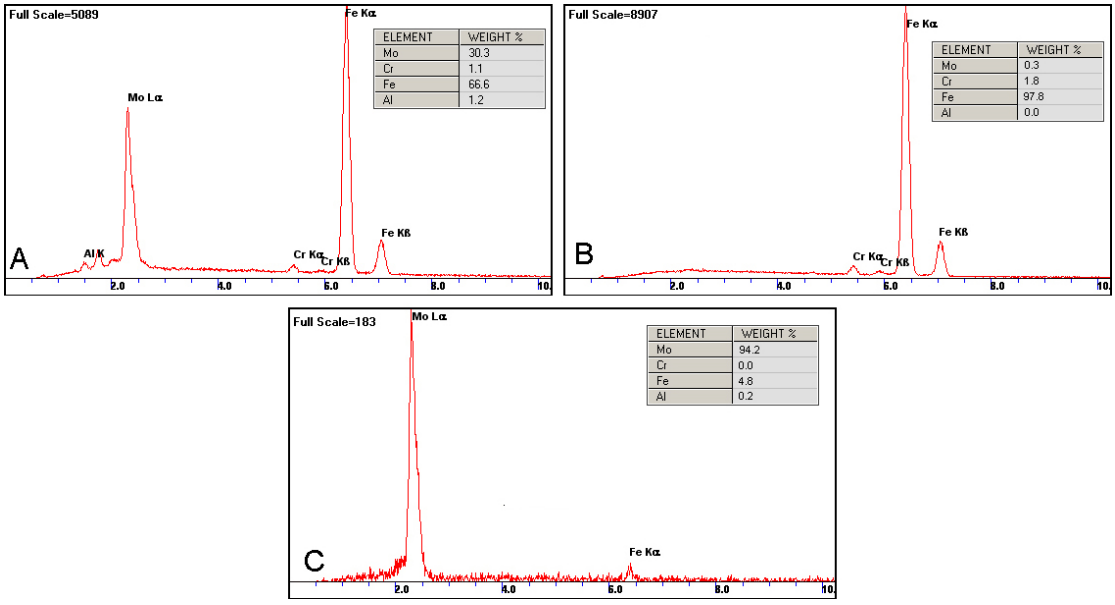

Figure 29 EDS spectrum of Sulzer Metco F4301 coating: (A) etched area, (B) un-etched area, (C) hard phase (Figure 27 (C)).

IV.B.12. Sulzer Metco XPT512 and F2056.

Both the XPT512 and F2056 coatings were developed for use in diesel engines and as such are harder than the F4301 coating (F2056 being the hardest). Both coatings have similar structures (XPT512 Figure 31 and F2056 Figure 32) and contain similar

elements, as shown in the EDS spectra (Figure 30). The only difference is the F2056 coating contains 20% aluminium compared to 2% in the XPT512 coating. Like the F4301 coating, when etched with 2% nital only the light phase in either of these coatings is attacked (Figure 32 C). The EDS maps of these two coatings are similar (Figure 33 and Figure 34), although it appears that the area used for the map of the F2056 coating is not representative of the coating composition (less aluminium than would be expected).

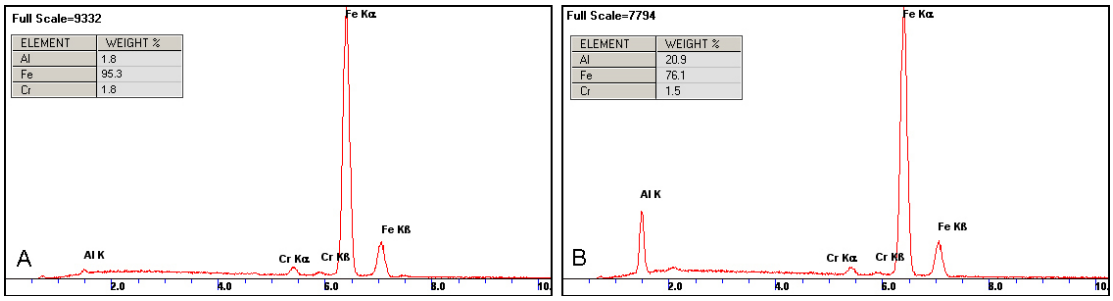

Figure 30 EDS spectra of Sulzer Metco, (A) XPT512, (B) F2056

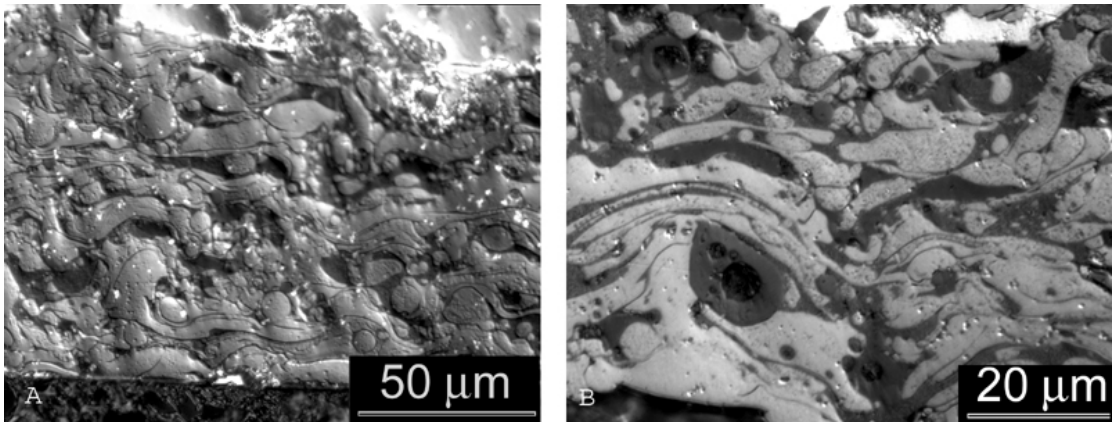

Figure 31 Optical micrographs of Sulzer Metco XPT512 cross-section un-etched (DIC) (A) low magnification (B) high magnification.

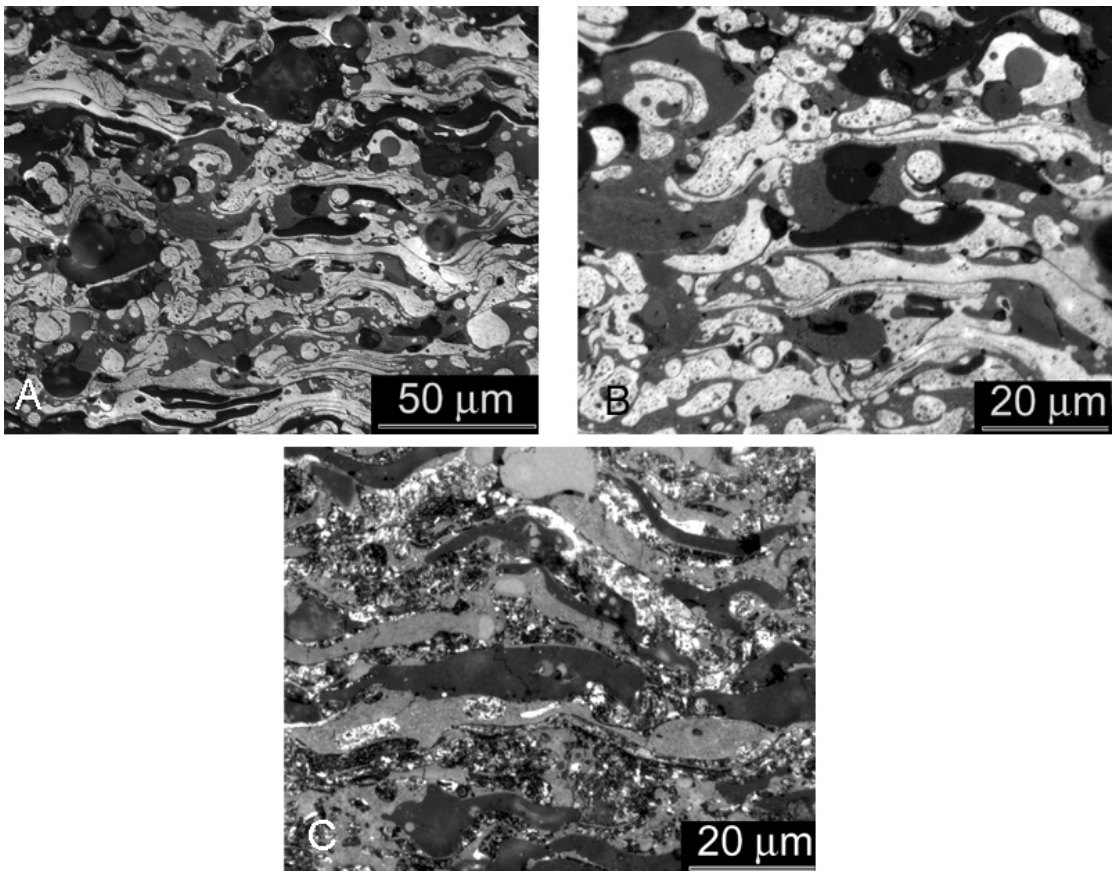

Figure 32 Optical micrographs of Sulzer Metco F2056 cross-section, (A) low magnification un-etched (DIC) (B) high magnification un-etched (DIC), (C) etched with 2% nital

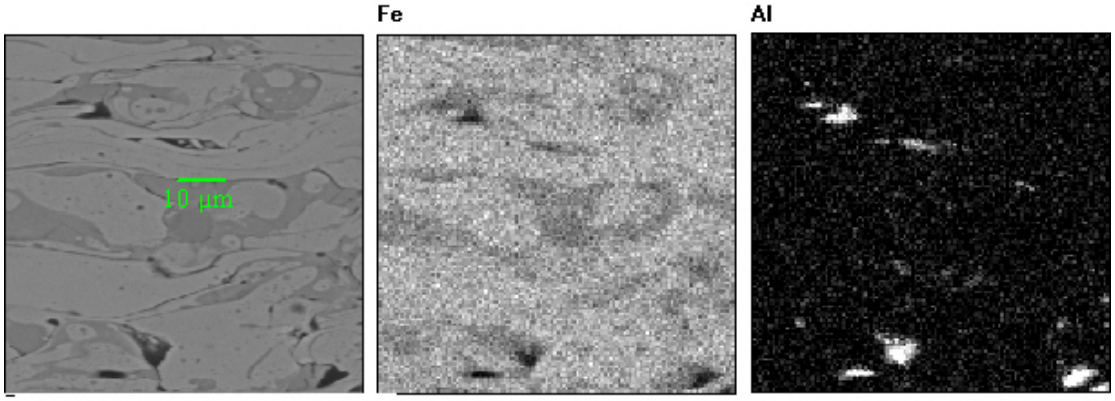

Figure 33 EDS map of Sulzer Metco XPT512 showing the distinct Fe and Al phases.

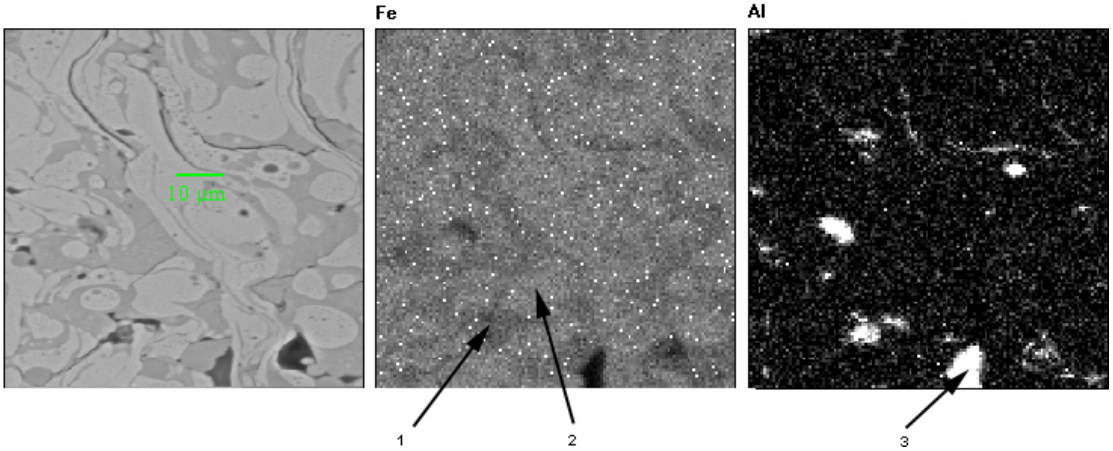

Figure 34 EDS map of Sulzer Metco F2056 showing the phases (1) Fe-Al, (2) Fe, (3) Al.

IV.B.13. NASA PS304.

The PS304 samples were supplied by Hohman Plating and Manufacturing, Inc. Dayton, Ohio USA. PS304 is a nickel-based, solid-lubricating, plasma-sprayed coating developed by NASA for use in gas bearings in large turbines to eliminate the need for lubrication systems. The composition of the powder used to deposit this coating is shown in Table 5.

Table 5 PS304 powder composition

NiCr	Cr_2O_3	BaF_2/CaF_2	Ag
60% weight	20%	10%	10%

Each of the compounds in the coating has a specific function. The nickel-chromium is the matrix material through which the other components are dispersed. The chromium oxide is a hard material to provide wear resistance during periods of metal to metal contact. The chromium oxide phase is indicated by arrows in Figure 37. The remaining compounds provide solid lubrication. Silver is a low temperature solid lubricant, while the barium and calcium fluoride compounds are high temperature solid lubricants. In Figure 37 B, silver is visible as a white phase. The distribution of calcium and barium fluoride can be seen in the EDS map (Figure 36). There are two chromium-containing phases visible in the EDS map, the largest a NiCr phase and a Cr-rich phase that does not overlap any of the other elements, which is to be Cr_2O_3.

DellaCorte et al. have reported on the unique running-in properties of this material [24]. High wear rates of counter surfaces are experienced while a solid lubricating layer is formed on the surface. Once the coating has run-in, the wear rates of the counter surface are very low. At present this coating is relatively new and has not been successfully applied to a specific application on a large scale. It is however readily available and has been used successfully by individuals in various applications, such as the wear surfaces in air cooled versions of the Norton rotary engine. An earlier incarnation of this coating was used in the Moller International/Freedom Motors rotary engine.

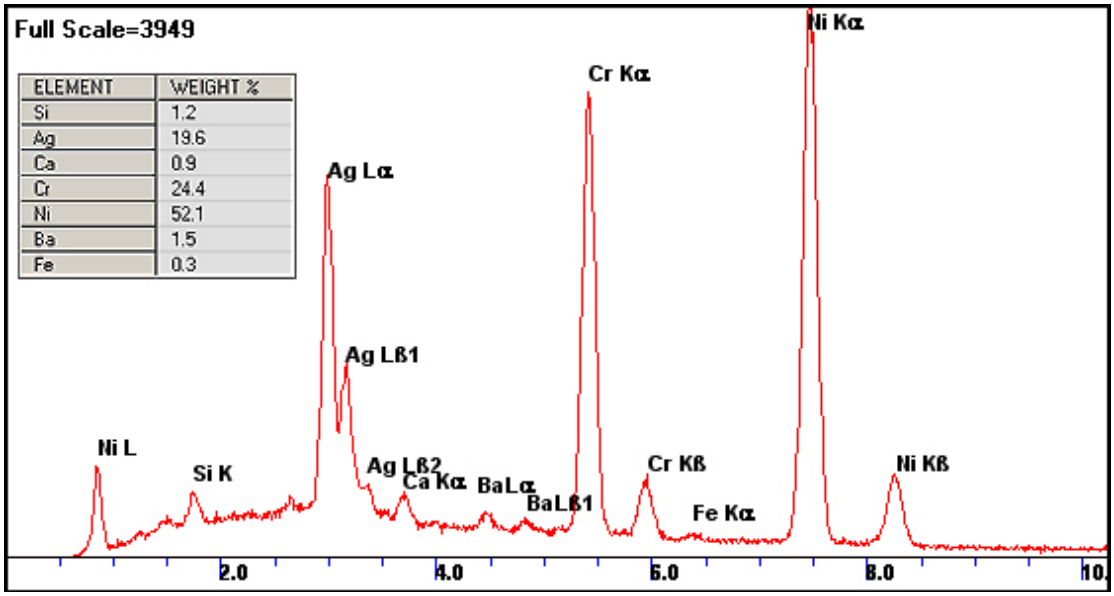

Figure 35 PS304 EDS spectrum and composition

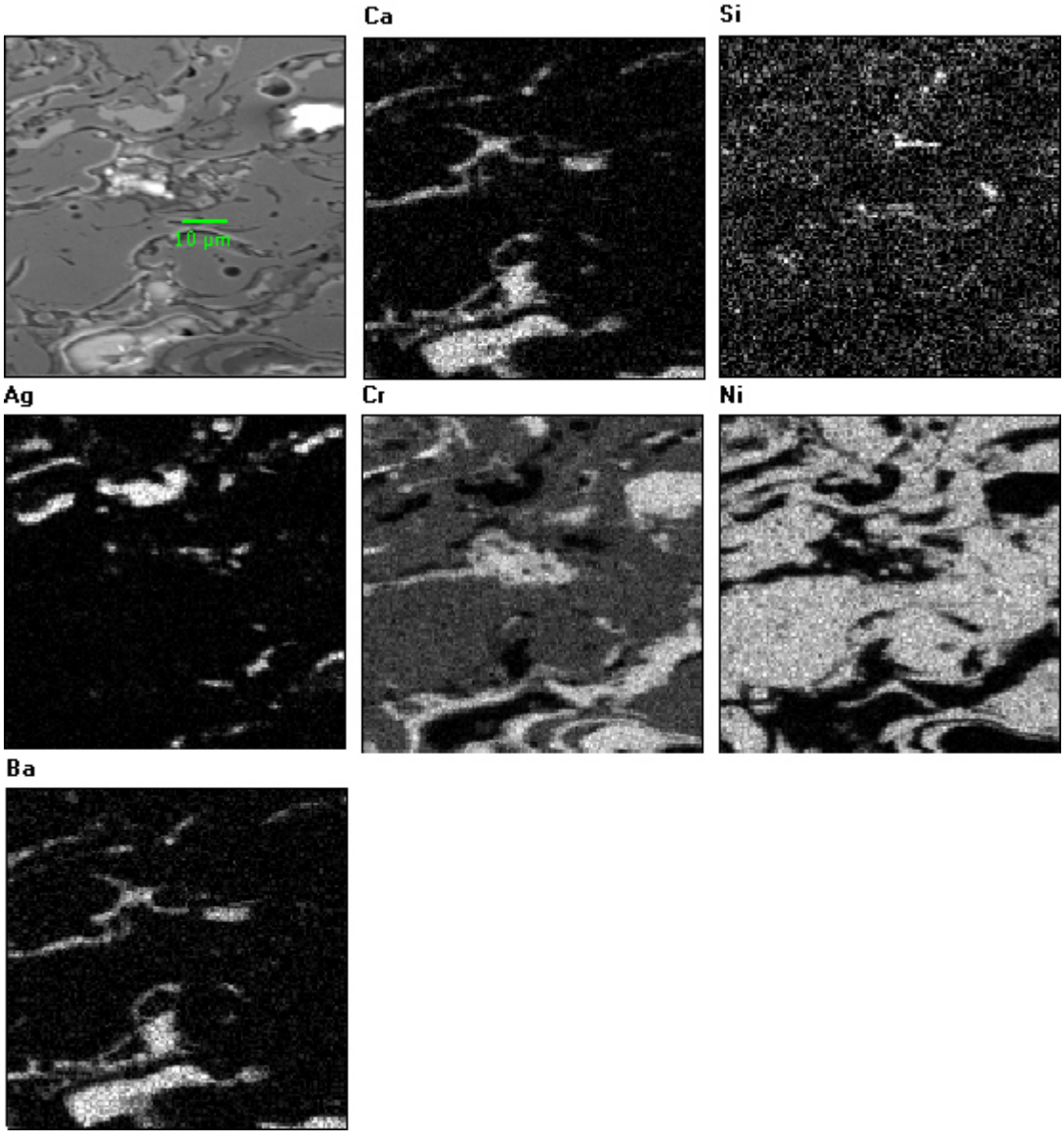

Figure 36 PS304 EDS map

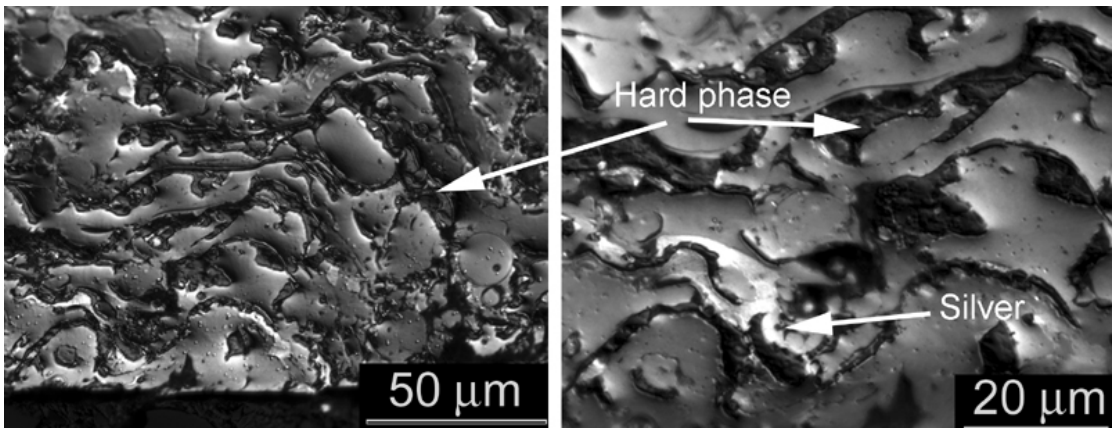

Figure 37 PS304 solid lubricating coating

IV.C. Rotational Tribometer Mass Loss Wear Results.

In this section, seal wear was sufficiently high to enable wear rates to be quantified through mass loss (>0.0001gm). For this work, the seal wear has been quantified as a wear W, with the units m^3m^{-1}, volume of seal material loss per metre of sliding distance. These units were chosen to encompass the measured and calculated variables in these experiments (sliding distance and volume loss). An equally appropriate unit would be the specific wear rate W_{sp}, which also includes the contact load, but as the load was not varied it was not considered necessary to use this unit.

All of the seal materials tested (with the exception of silicon nitride) displayed wear rates that were high enough to be measured using the mass loss technique on at least one of the chamber coatings. The results of these experiments are summarised in Table 6. To ensure statistically relevant results, the wear rates and average coefficients of friction are averages of three or more tests. The first significant inference of these results is that there is no relation between the wear rate and the coefficient of friction. It is a common misconception that high coefficients of friction are related to with high wear rates.

Nevertheless, instantaneous friction values can be used to predict the lubrication regime, and in this case average friction values can be used as there is very little variation in the friction force over the duration of a rotational test. By plotting typical friction coefficients (0.025 to 0.05) on the modified Stribeck diagram produced by Cho et al. [4] (Figure 38) it is predicted that the rotational tribometer is operating in a mixed lubrication regime, but very close to the hydrodynamic boundary.

Table 6 Results from Rotational Tribometer Tests

Seal Material	Liner Coating	Average Wear Rate m^3m^{-1} x10^{-13}	Average Friction Coefficient
Four Hour Rotational Tests			
Si_3N_4 (Beamalloy)	75B-90MXC	0.000652	0.039
Total Seal TiN	PS304	0.000659	0.050
DLC	F4301	0.00124	0.041
N-SS	PS304	0.00221	0.041
CrN (Beamalloy)	75B-90MXC	0.00262	0.042
N-SS	F4301	0.00266	0.064
N-SS	75B-90MXC	0.00348	0.061
Si_3N_4 (Beamalloy)	F4301	0.00404	0.047
Si_3N_4 (Beamalloy)	PS304	0.00487	0.055
CrN (Beamalloy)	F4301	0.00494	0.027
Mazda Cast Iron	F4301	0.00638	0.054
Total Seal CrN	PS304	0.00694	0.046
Total Seal WC-C	PS304	0.00850	0.051
CrN (Beamalloy)	PS304	0.00862	0.049
N-SS	XPT512	0.826	0.094
N-SS	Tungsten	2.84	0.058
Twenty Minute Starved Lubrication Rotational Tests			
N-SS	PS304	0.0155	0.055
N-SS	75B-90MXC	0.103	0.034
N-SS	F4301	0.248	0.093

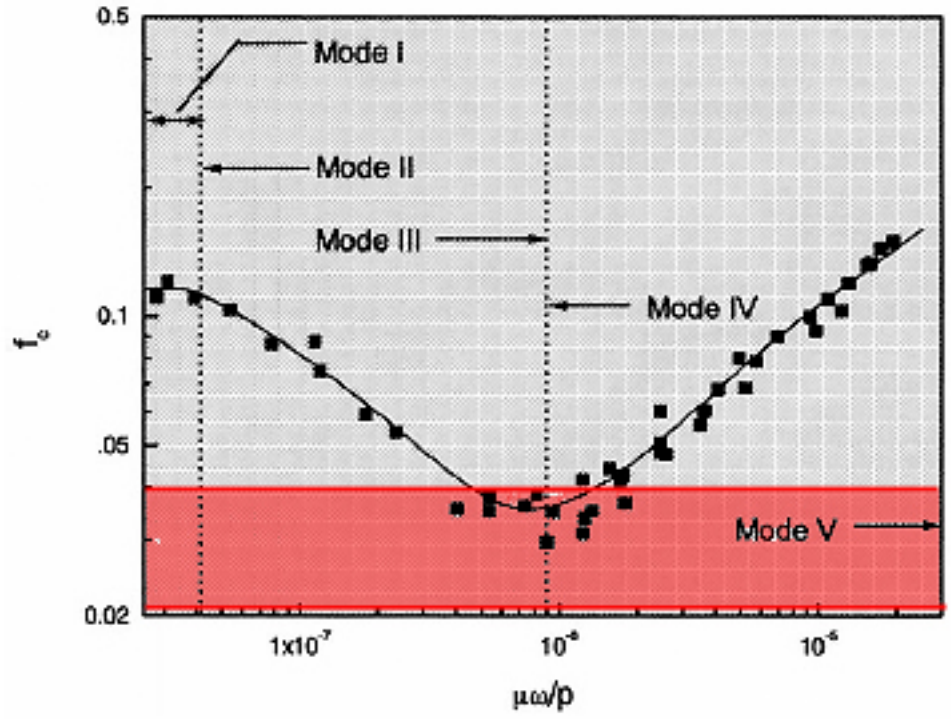

Figure 38. Modified Stribeck (f_c coefficient of friction vs. μω/P dimensionless bearing parameter) diagram representing a piston ring near mid stroke. Mode I to II is boundary lubrication, mode II to III is mixed lubrication and mode IV to V is hydrodynamic lubrication[4]. The highlighted area indicates the range of friction coefficients from the rotational tribometer.

IV.C.1. Nitrided Stainless Steel Seals Rotational Wear Test Results.

In the four-hour test the lowest average wear rate of the N-SS seal is on the PS304 liner coating, followed by the F4301 and 75B-90MXC coatings. The PS304 liner coating also had the lowest coefficient of friction, followed by the 75B-90MXC and F4301 coatings. The low average wear rate of the N-SS seal on the PS304 coating appears to be an anomaly when compared to the wear rates of the other seals on this coating. In all other tests with the PS304 liner coating it was observed that the first seal sample had a very high wear rate which then reduced with consequent tests. For example, the wear rates for the PS304 PVD Si_3N_4 tests were $1.29x10^{-15}$ m^3m^{-1}, $1.33x10^{-16}$ m^3m^{-1} and $3.29x10^{-17}$ m^3m^{-1}, while the results for the N-SS tests were $2.64E^{-16}$ m^3m^{-1}, $2.58E^{-16}$ m^3m^{-1}, $1.99E^{-16}$ m^3m^{-1} and $1.65E^{-16}$ m^3m^{-1}. PS304 is a solid lubricating coating so it is likely that the high wear during the initial tests is due to a running in process, which leads to the development of a lubricating film on the surface of the disc. The PS304 coating was the only material that exhibited a detectable break-in process.

A tungsten arc sprayed liner coating and XPT512 liner coating both produced very high seal wear rates with N-SS seal samples. After 40 minutes, the N-SS seal had worn down to the seal holder when run against the tungsten coating. For this reason only one test was conducted. Interestingly, the friction coefficient for this material system was not significantly higher than that of any of the other tests, further highlighting the independence of friction and wear.

The wear process associated with the N-SS vs. XPT512 system exhibited significant differences compared to other tests. The XPT512 coating consistently scuffed, causing damage to the disc surface and high seal wear. The wear rate and friction coefficient values shown in Table 6 are only an average of two tests because the disc was too badly damaged to conduct a third test. Scuffing occurs when the primary wear mechanism changes from abrasive to adhesive. Scuffing is characterised by a sharp increase in friction and temperature. The increase in friction is shown in Figure 39. In both of these tests scuffing occurred after approximately 11 minutes. Because scuffing is associated with a different wear mechanism, the wear and friction values cannot be compared with the remainder of the results reported here. However,

because of the high wear rates and surface damage associated with scuffing this particular system can be rejected as a potential candidate.

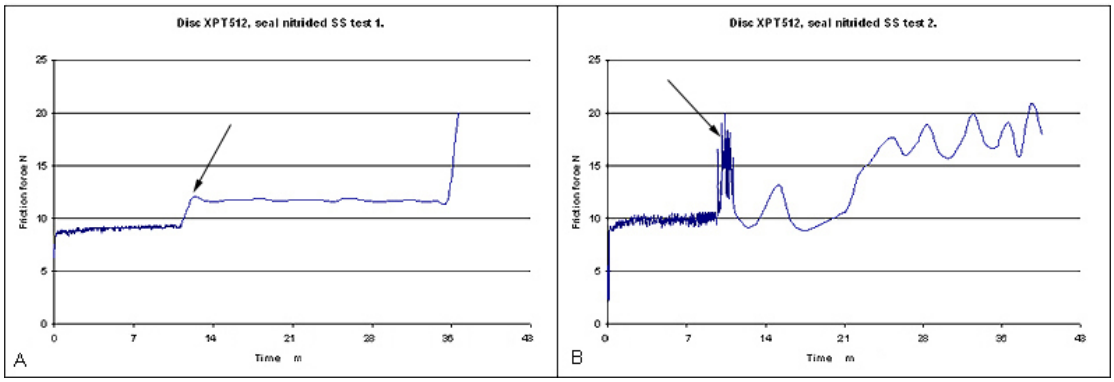

Figure 39. Friction plots for N-SS seals on XPT512 coating showing the onset of scuffing, (A) test one, (B) test two.

Under more severe, starved lubrication conditions the N-SS vs. 75B-90MXC system gave the lowest wear rate and showed a lower coefficient of friction than the F4301 coating. Because of the limited lubricant supply, the friction response is influenced more by the material couple properties than the lubricant. During the starved lubrication tests the temperature of the disc climbs rapidly to a higher temperature than the four hour tests. The limited supply of oil and the increased temperature have several consequences. The oil will become contaminated, thus reducing its ability to provide lubrication. The oil film will thin due to a decrease in viscosity and the EP additives may become more reactive.

The average wear rate of the N-SS seals on the PS304 coating was in between the 75B-90MXC and F4301 coatings, and the coefficient of friction was the lowest of the three. Again, the PS304 coating gave very high initial wear rates which then dropped significantly: $3.08E^{-14}$ m^3m^{-1} to $1.24E^{-14}$ $m^3m^{-1}$and finally $3.32E^{-15}$ m^3m^{-1}. The last value is an order of magnitude lower than the lowest wear rate on the 75B-90MXC disc of $1.68E^{-14}$ m^3m^{-1}. The starved lubrication tests may have allowed the PS304 coating to form a solid lubricating film earlier, leading an increased dependency on the solid film than the oil film. The PS304 coating by itself may not be of great use in the actual engine because the initial running in process causes too much wear on the seal or seal coatings. In spite of this, it may be possible to implement a functionally graded PVD coating that incorporates a sacrificial 'running in' layer. Another possibility is the addition of a solid lubricant such as MoS_4 to the coating surface to

reduce wear during the running in process. Either of these approaches may sufficiently reduce the 'running in' wear, providing a system that would provide satisfactory long term compression seal wear rates.

IV.C.2. Mazda 13B Apex Seal (Cast Iron).

As there are similarities between the seal arrangement in the Pivotal Engine™ and a Wankel engine three test pieces were made from a cast iron 2mm three piece Mazda rotary apex seal from a series V 13BT engine. When these samples were tested on the F4301 coating the average wear rate was significantly higher than that of the N-SS seals. In contrast to the N-SS seals, the wear rate dropped significantly over the three tests, $1.17E^{-15}$ m^3m^{-1}, $1.08E^{-16}$ m^3m^{-1} and $2.97E^{-17}$ m^3m^{-1}. Like the PS304 coating, this reduction in wear rate may be due to a solid lubricating film forming on the disc surface. In this case, the film would have originated from the high volume of carbon in the cast iron. It should be noted that the Mazda seal sample had a barrel profile, meaning that the contact pressure is much higher (due to the small contact area) than the other seal samples which have a flat contact area with small radii on the edges. The different profile will also influence the thickness of the oil film between the seal and the disc. It would have been desirable to further test this material, with the profile modified to be more like the N-SS seal material. This would have allowed a more conclusive comparison between the two materials.

IV.C.3. PVD Coated Seals.

Several PVD coatings were tested, including: diamond like carbon (DLC) supplied by Diameter Systems, chromium nitride (CrN), titanium nitride (TiN) and tungsten carbide-carbon (WC-C) supplied by Total seal, as well as CrN and silicon nitride (Si_3N_4) supplied by Beamalloy Ltd. With the exception of the PS304 disc, the Total Seal coatings gave a significant decrease in the seal wear rate and will be discussed in section III.D.1. The average wear rates for PVD coated seals on the PS304 disc were higher than on any of the other disc coatings, and again the wear rates dropped significantly with consequent tests.

The Beamalloy coated seals did not offer a great increase in performance over an uncoated seal. These two coatings were relatively thin (approximately 1.2μm) and did not have sufficient bond strength with the nitrided stainless steel substrate. The CrN

coating wore through an abrasive mechanism, similar to the N-SS seals. Because the coating was so thin it offered little extra protection, wearing through during a four hour test. The SiN coating failed/wore through a slightly different process (Figure 42 A). In addition to abrasive wear, the coating fractured and was removed from the surface. This indicates poor adhesion to the substrate and or high internal stresses.

With the exception of the N-SS seal on the XPT512 coating and the Si_3N_4 coated seal (on all coatings tested against), the seal samples wore by two and three body abrasive wear. This is characterised by striations in the direction of motion, visible in Figure 42. Unlike the seal samples, the wear of the discs could not be quantified. The damage to the disc surfaces was minimal as can be seen in Figure 40 A and B.

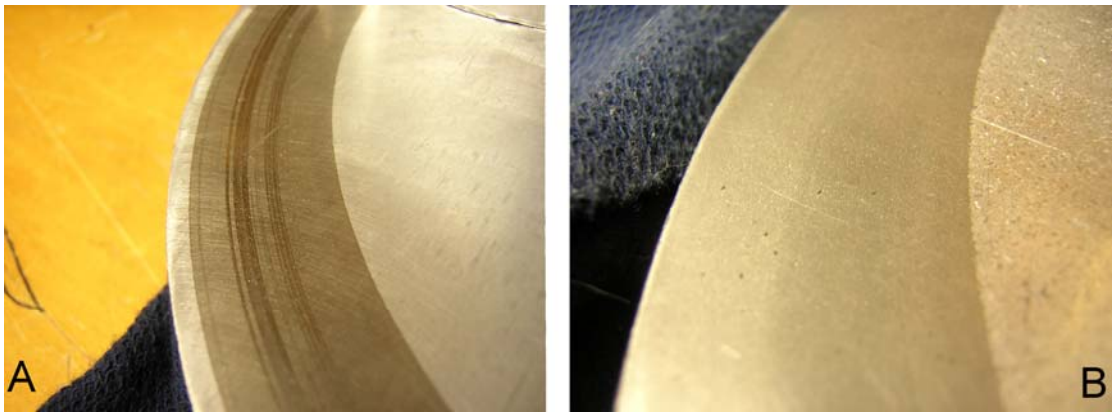

Figure 40. (A) Worn 75B-90MXC disc surface. (B) Worn F4301 disc surface.

IV.C.4. Summary of Rotational Mass Loss Tests.

From the results in Table 6 several material couples were eliminated as potential compression seal and chamber coating materials. The Pivotal Engineering arc sprayed tungsten liner coating gave highest seal wear rate recorded and for this reason was eliminated from any further testing (or microstructural analysis). The PS304 liner coating gave high initial seal wear rates and as such is not a suitable material for use in the engine so was also eliminated. The XPT512 liner coating repeatedly scuffed when tested against the N-SS seal, this should have eliminated this material couple but it was later found that this behaviour was only apparent on the rotational tribometer. The CE17 arc seal material was tested primarily to investigate the wear response of the different chamber coatings, however very little information was gained through these tests. The only compression seal materials not eliminated from

further testing were the Total Seal PVD coated seals (TiN, CrN, WC-C) and silicon nitride.

IV.D. Extended Duration Tests.

The remainder of tests conducted on the rotational tribometer were carried out over longer durations. The compression seal materials selected for testing over an extended period include, TiN, CrN, WC-C and silicon nitride. These materials were selected for further testing because they displayed minimal (immeasurable) wear during the four hour test. Because the wear rates of the seal materials and coatings in this section were so low, no change in mass could be detected even after extended test periods. To quantify the seal wear, the worn surface area was measured at approximately eight hour intervals. The results for these tests are shown in Figure 41.

IV.D.1. PVD Coated Seals.

The WC-C coated seal was tested against the F4301 disc coating for a period of approximately eight hours. At the conclusion of testing the coating had completely worn through in some areas and there was no measurable mass loss, meaning neither the mass loss nor the surface area wear quantification method was suitable. For this reason, the result from this material is not shown in either Table 4 or Figure 41. The WC-C coating displayed lower wear rates than those presented in Table 4 and higher wear rates than those in Figure 41. The worn surface of the WCC seal is shown in Figure 42 B, where it can be seen that this seal has worn through an abrasive wear mechanism and not failed like the Si_3N_4 film shown in Figure 42 A.

Of the remaining seal and chamber coating combinations, the highest wear was recorded with the CrN coated seal running on the F4301 disc coating. The higher wear rate of the CrN coated seal is likely to be due to the slight reduction in hardness over the TiN coated seals. The CrN coated seal was not tested on either the XPT512 or F2056 coatings because it was expected, based on the results with TiN coated seals, that the wear would be even higher than that on the F4301 coating.

The TiN coating provided greater wear resistance than the CrN or WC-C coatings. The lowest TiN wear rates were recorded when run against the F4301 coating, followed by the XPT512 and F2056 coatings respectively. The difference in the wear rates for the TiN coated seals can be related to the distribution and volume of hard

materials in the disc coatings. These results show that seal wear rate increases with the increasing hardness of the disc coatings. The F4301 coating is softer than the XPT512 and F2056 coatings and contains molybdenum, which acts as an anti scuffing agent. The composition of the XPT512 and F2056 coatings are similar, although the F2056 coating is harder.

The TiN coated seal was tested twice against the F4301 disc coating because the oil system failed during the first test at around twenty hours. This can be seen as the area of high friction in the friction plot (see Figure 43). This period corresponds with a jump in percentage of worn surface area in Figure 41. Although the first test was run without oil for a period of time and there was a subsequent increase in the worn surface area, both tests tended towards the same worn surface area. The duplication of this test also serves to validate the repeatability of this test method.

IV.D.2. Silicon Nitride Seals.

Of all of the materials tested, reaction bonded silicon nitride was the most wear resistant. Silicon nitride seal samples were tested on the F4301 and F2056 coated discs. Silicon nitride was not run against the PS304 coating because the fluorine in the solid lubricating component of the coating reacts with the silicon nitride, breaking down both materials. The wear rates measured in these tests were less than half that of the TiN coated seals. Unlike the TiN coated seals, the wear rate of the silicon nitride seals appears to be reasonably independent of the counter surface material. The friction plots of the silicon nitride seals on the F4301 and F2056 coatings are shown in Figure 45 and Figure 46 respectively. The friction force in Figure 46 is significantly lower than the friction force in Figure 45. This may in part be due to material properties but is more likely a result of different seal geometry (the silicon nitride seals were hand made). The seal tested on the F4301 coating had a smaller radius on the leading edge than the seal used on the F2056 coating. Because of the different geometry, the friction forces from these two tests cannot be compared to the other results. During both tests the seal did not wear evenly across its face. This was because the seal was not as flat (due to manufacturing) or conforming as the stainless steel seals. The effect of this is that the specific contact force is much higher due to the lower contact area, making the test more severe.

In addition to abrasive wear, the silicon nitride seals exhibited tribo-chemical wear in some areas. This is identified by the polished appearance of the seal surface (Figure 47). In this case the tribochemical wear is a secondary wear mechanism and as such does not significantly contribute to the overall wear of the seal.

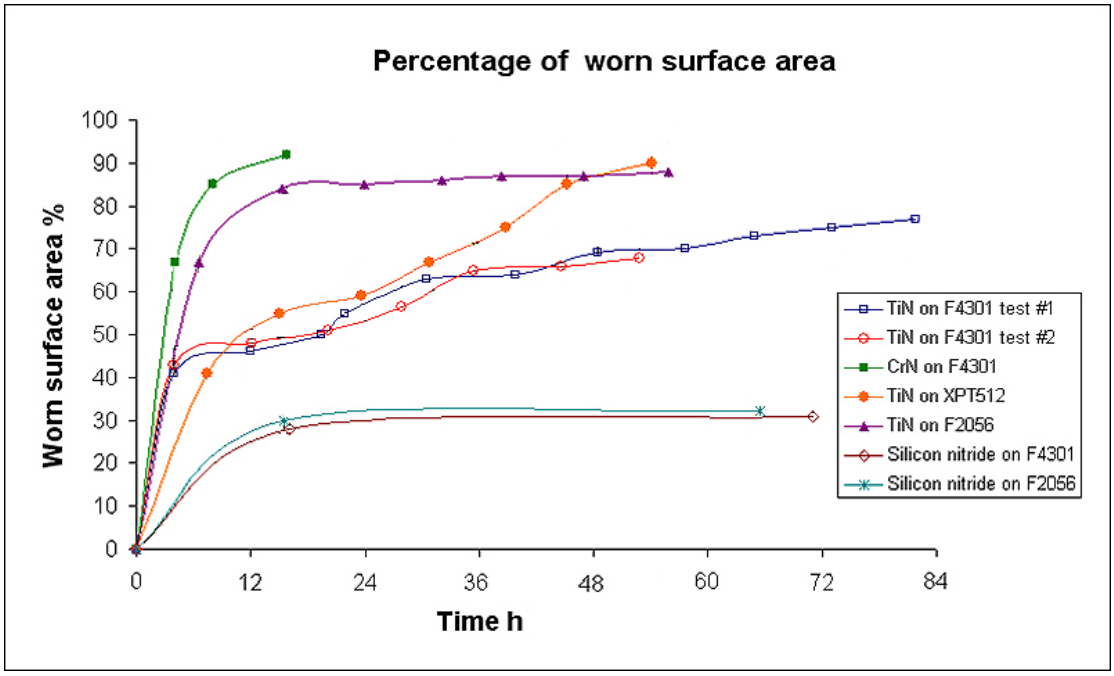

Figure 41. Percentage of surface area time plot for seal samples with low wear rates.

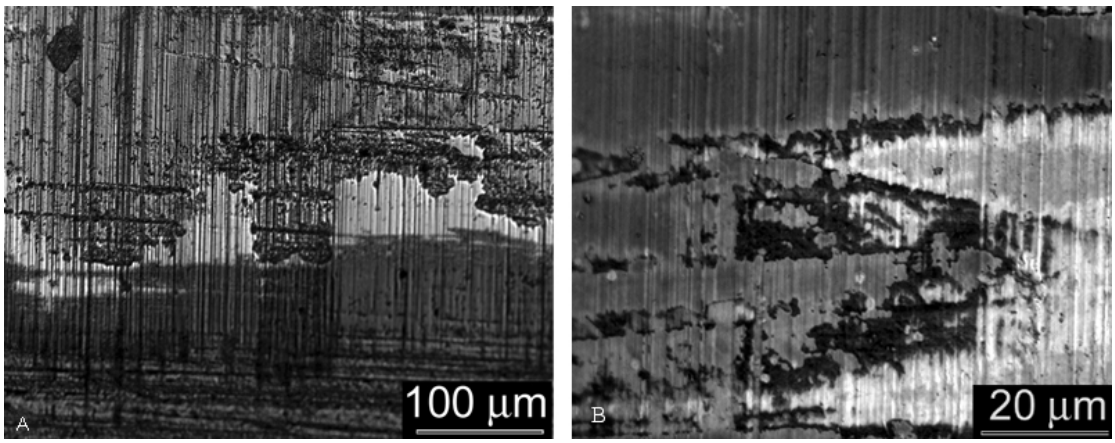

Figure 42. Optical micrographs of the wear surface of (A) Si_3N_4 coated seal tested against F4301 coating. (B) WCC coated seal tested against F4301.

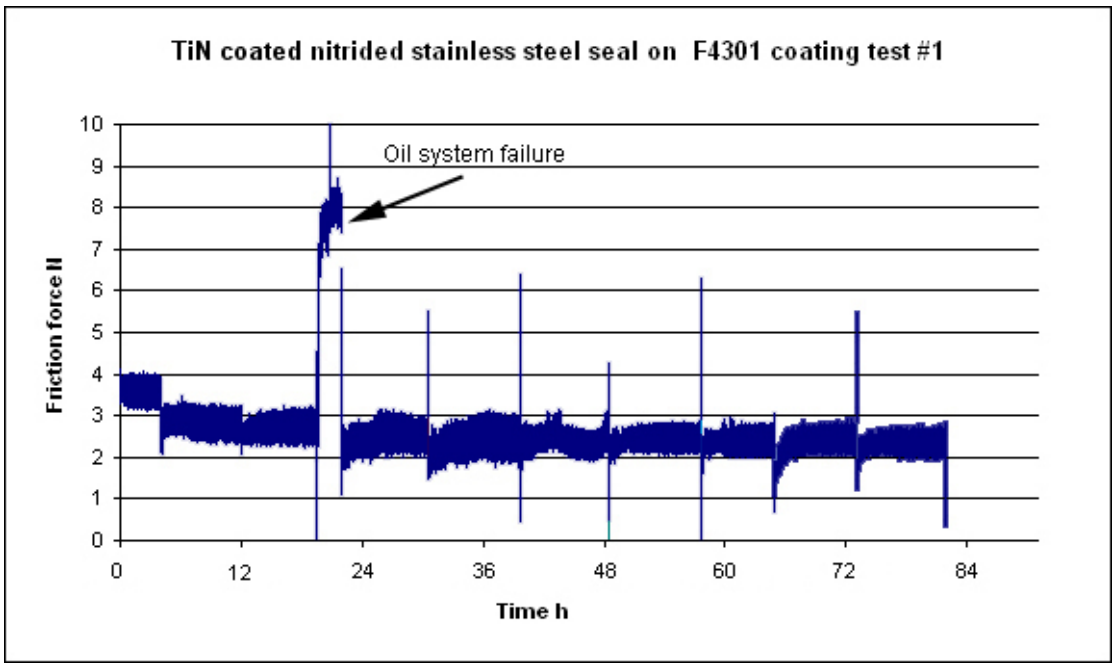

Figure 43. Friction plot for TiN coated seal on F4301 coated disc test #1

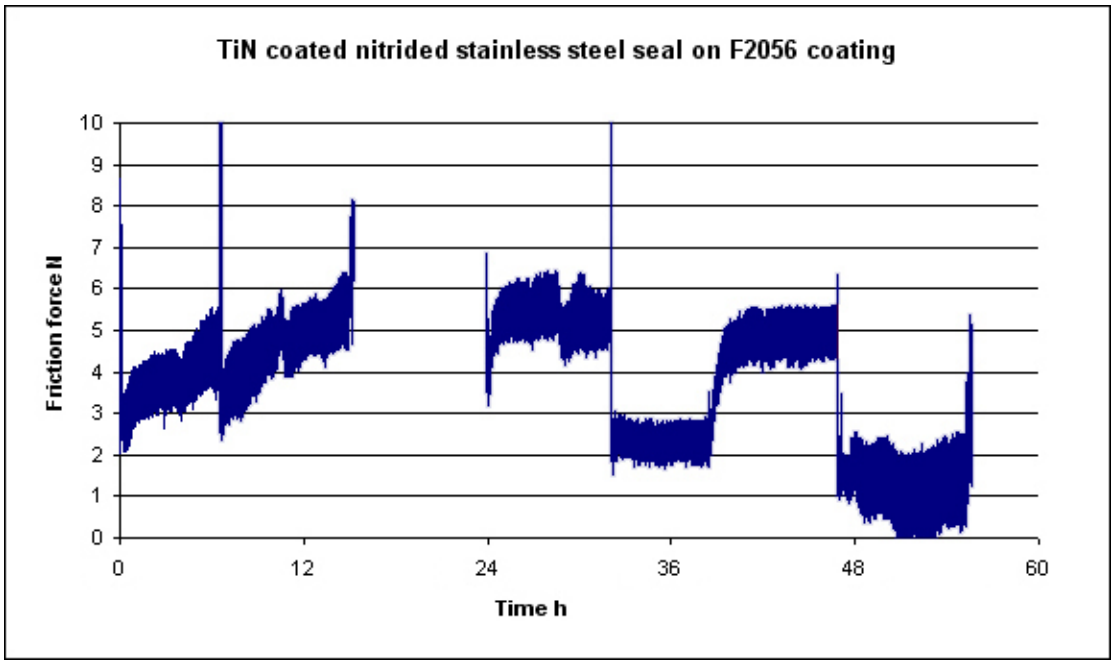

Figure 44 Friction plot for TiN coated seal on F2056 coated disc

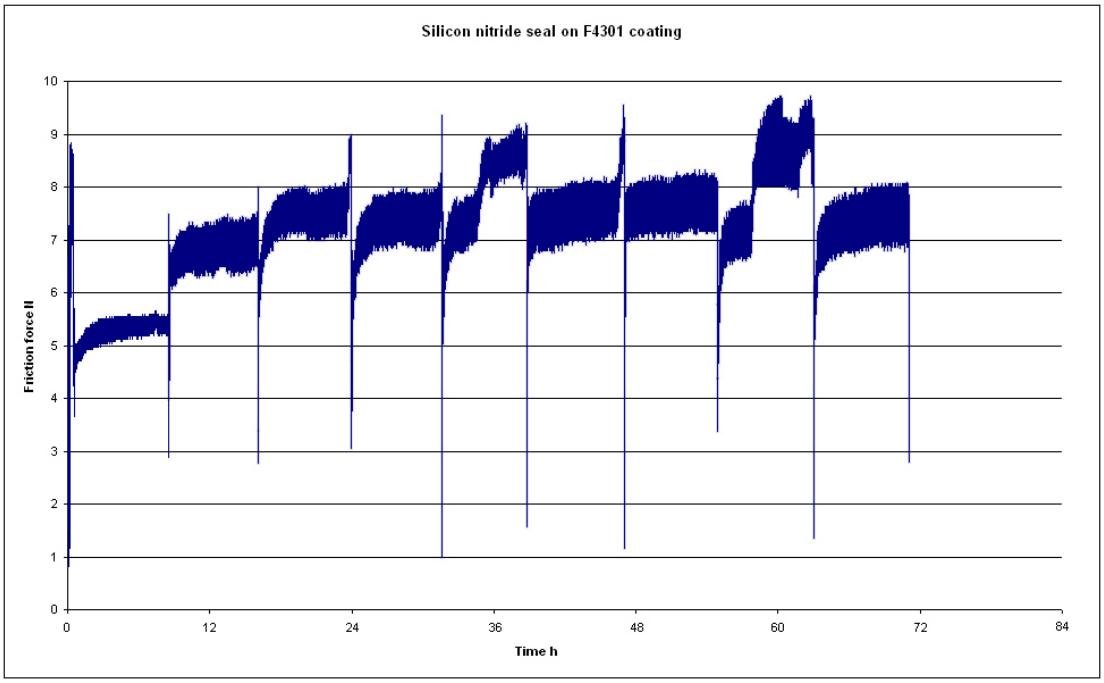

Figure 45. Friction plot for silicon nitride seal on F4301 coated disc.

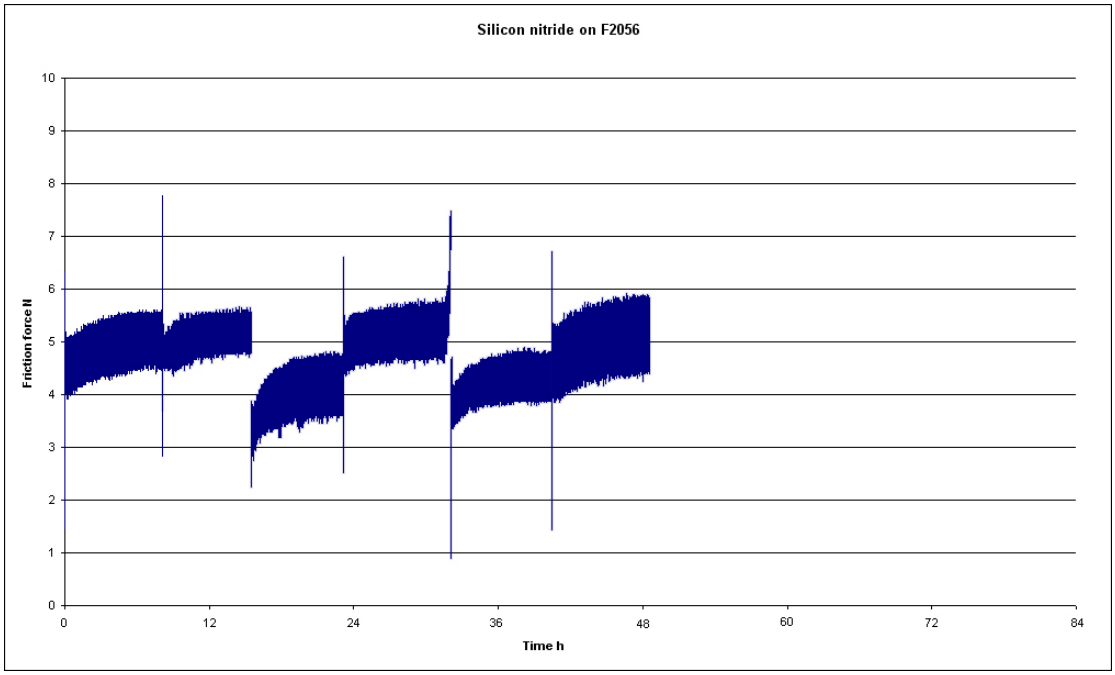

Figure 46. Friction plot for silicon nitride seal on F2056 coated disc.

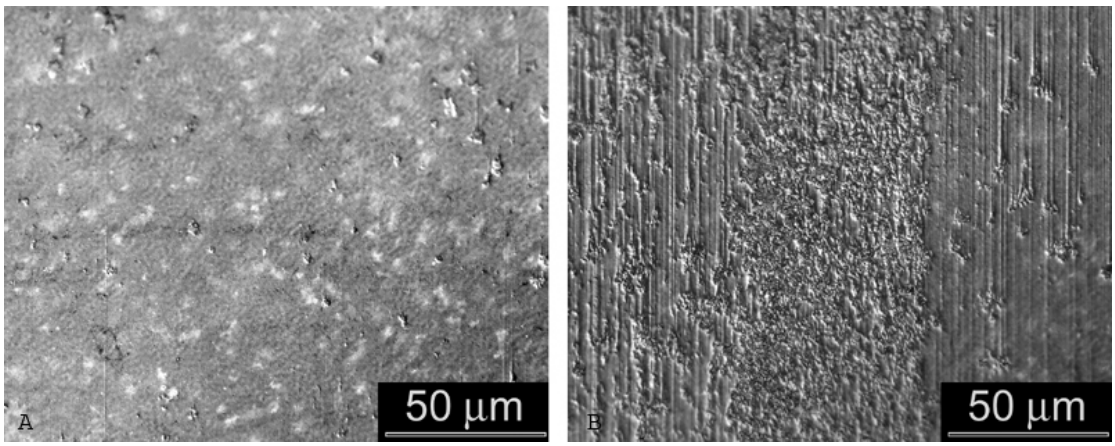

Figure 47. Optical micrograph of the wear surface of silicon nitride seal. (A) tribochemical wear. (B) abrasive wear.

IV.E. Fired Engine Test Results.

A one litre twin chamber engine was used to test the seal and chamber coatings. The initial test was conducted with one chamber having CrN coated seals and the other having TiN coated seals. Both sets of chamber surfaces were coated with F4301. Having two seal coatings tested in the same conditions allowed the wear rates of both coatings to be compared, as well as the relativity between the results from the engine and the tribometer. During the test, the engine was run at 3000 to 4000 rpm with a load of approximately 6 kW.

The first engine test was prematurely stopped because of an unrelated component failure. However after four hours of running, both sets of seals showed significant wear on the ends nearest the corner of the chamber. The coatings had been removed from the first 12mm – 15 mm of the seals (this area is indicated in Figure 48). The TiN seal had slightly less material removed than the CrN seal. Because of the damage caused by the engine failure, it was not possible to measure the mass loss of any of the seals or quantify a wear rate.

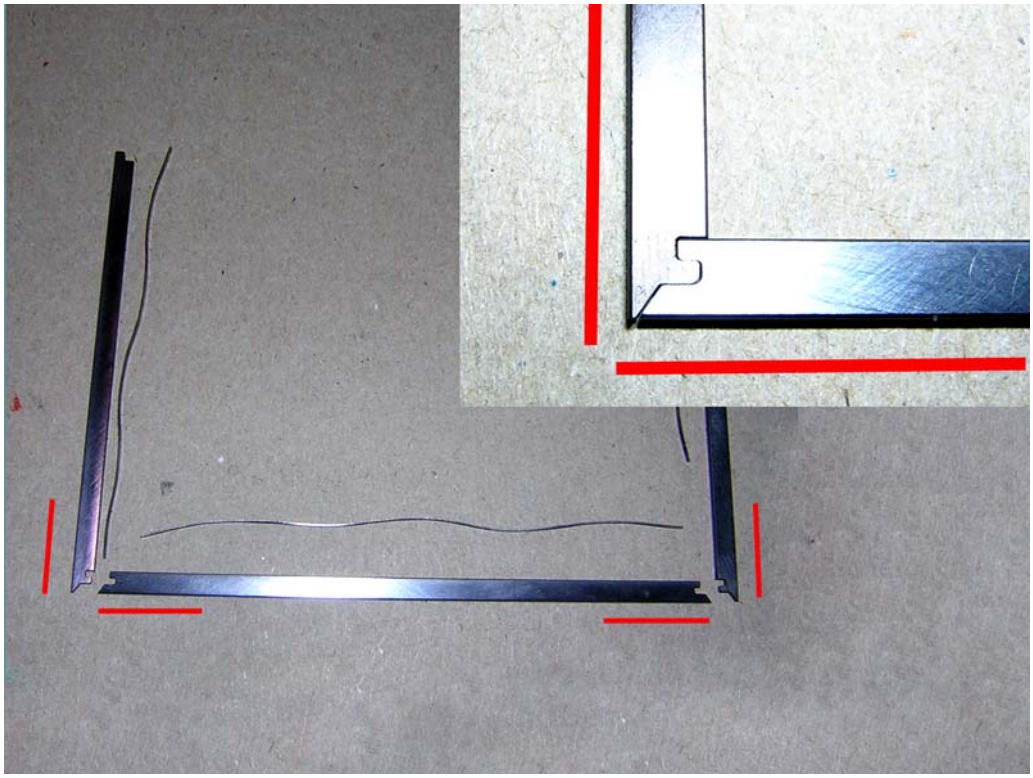

Figure 48 Compression seal configuration. Areas of high wear are indicated in red.

A second engine test was conducted using TiN coated seals against F4301 and XPT512 chamber coatings. After approximately 40 hours running the TiN coating had completely worn through along the length of all six seals. Unlike the tribometer tests, there was no scuffing from the N-SS seal running on the XPT512 coating (after the TiN had worn off). Again, the wear rates of the seals could not be quantified because of other factors.

Although the wear rates of the seals in the engine were not quantifiable, it was obvious that the wear rates in the engine were much higher than those from the tribometer. The speed and loads on the tribometer were selected to be equivalent to the engine running at 5000 rpm with a load of 70 kW. Even though the wear rates were very different, the wear mechanisms of the seals from the engine and samples from the tribometer were the same. Figure 49 A and B are optical images of a seal used on the tribometer and engine respectively. Both of these images indicate two and three body abrasive wear with similar sized wear tracks.

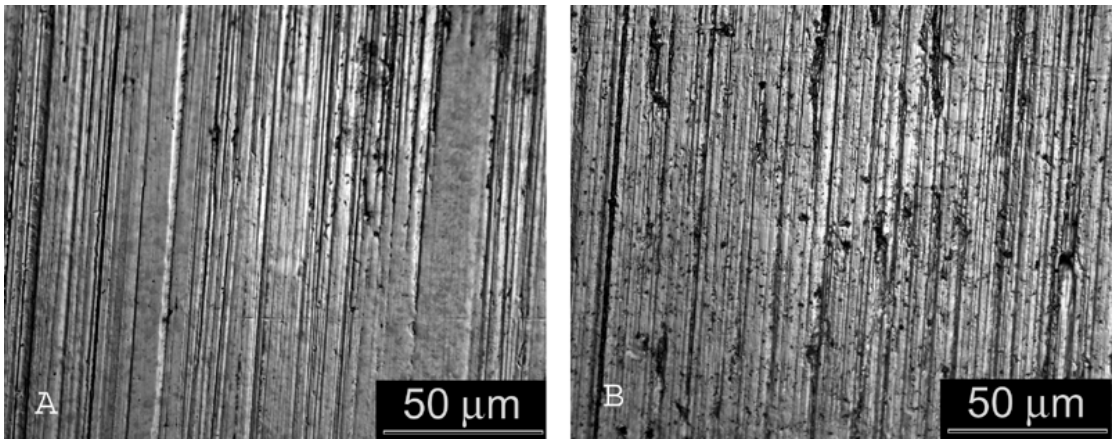

Figure 49. Optical micrographs of (A) wear surface of N-SS seal used on tribometer. (B) wear surface of CrN coated seal used in engine. Both seals were run against F4301 coating (CrN coating completely removed).

IV.E.1. Compression Seal Analysis.

To gain a better understanding of the wear system in the engine, the profile of a worn side compression seal was investigated, as shown in Figure 50. The first observation from Figure 50 is that the profile of the wear surface of the seal is almost flat and normal to the top surface of the seal. This indicates that the seal has very little movement in the seal groove. If the seal had movement in the groove it would be anticipated that a rounded wear profile would be present. The second observation is

the large difference in the volume of material removed along the length of the seal. The greatest wear occurs on the end of the seal in the corner of the chamber.

From this analysis, a compression seal with a larger radius or full barrel profile may ultimately provide a longer engine life. The barrel profile can develop thicker oil films for a longer period of time as more material would have to be removed from the seal to eliminate the radius. In addition to the longer lasting profile, the barrel face would reduce the contact force exerted on the compression seal because the combustion gas pressure is more balanced across the seal.

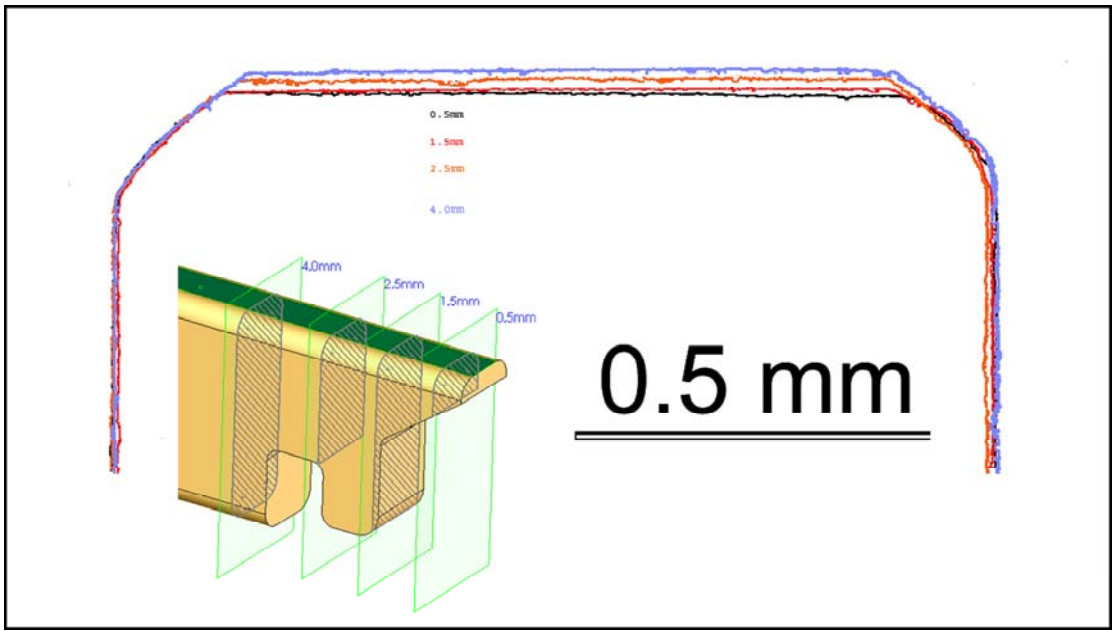

Figure 50. Side compression seal wear profiles, top of seal is on the left hand side of the image.

IV.E.2. Alternative Compression Seal Designs.

The seal wear in the Pivotal Engine™, as well as being higher than on the tribometer, was much higher than would be expected in a conventional two stroke engine producing similar power. The accelerated wear in the Pivotal Engine™ may be caused by a number of reasons, including increased temperatures, lubrication starvation and high contact forces between the seals and the chamber. Upon disassembly of an engine, there are no obvious signs of over heating or lubrication starvation. This leaves contact forces as the most likely cause of high wear.

It was hypothesised that the wear on the ends of the seals may be due to centripetal forces from the movement of the piston. This would explain the wear on the ends of the side and front seals. As the side seals are pushed forward, the bevel would force the end of the side seal onto the side plate as well as forcing the ends of the front seal against the exhaust block. To test this hypothesis, the piston motion was analysed using Solid Works and Cosmos Motion in order to determine the magnitude of the centripetal forces on the seals. Figure 51 shows the force exerted on the curved surface of the chamber (front seal) from the centripetal acceleration of the seal at 3000 and 6000 rpm against the crank angle.

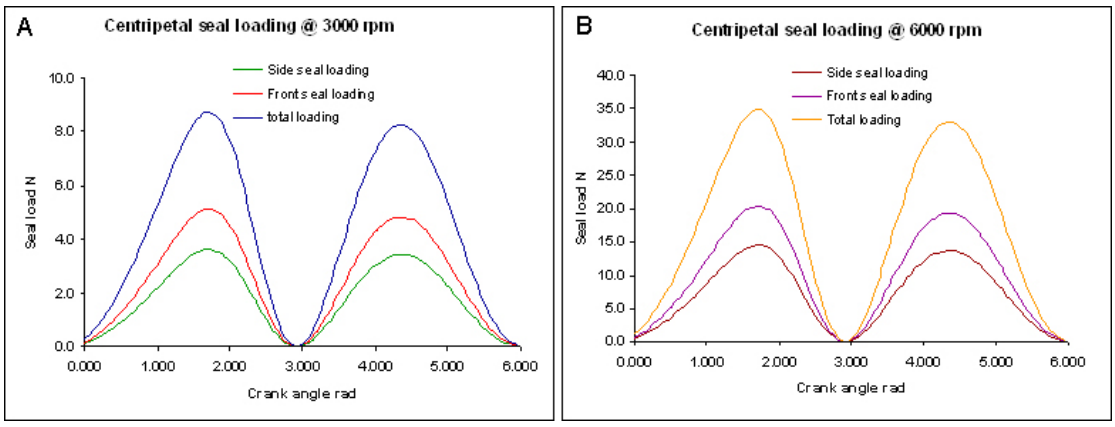

Figure 51 Analysis of centripetal compression seal loading (A) 3000rpm (B) 6000rpm.

The centripetal force exerted on the front seal will be distributed along its entire length. Even at 6000 rpm the centripetal force is small compared to that from combustion pressure (35N compared to approximately 650N). However if the centripetal force is not uniformly distributed along the front seal point loadings could become significant. Because there is no information on the clearances and distortion of the components in the Pivotal Engine™ it is impossible to estimate any point

loadings. However at the engine speed of 3000 to 4000 rpm the centripetal seal loads are minimal and should not cause the wear rate of the seals to be accelerated to the extent that was seen in the engine.

It is possible that high wear on the ends of the seals may be due to the thermal expansion of the front seal generating high loads in the corners of the chamber. To test this theory, seals were manufactured with a square detail on the corners, eliminating the bevel that would force the seals into the corner of the chamber. A CAD image of this seal design is shown in Figure 52 B. However, due to outside influences this seal configuration was never tested.

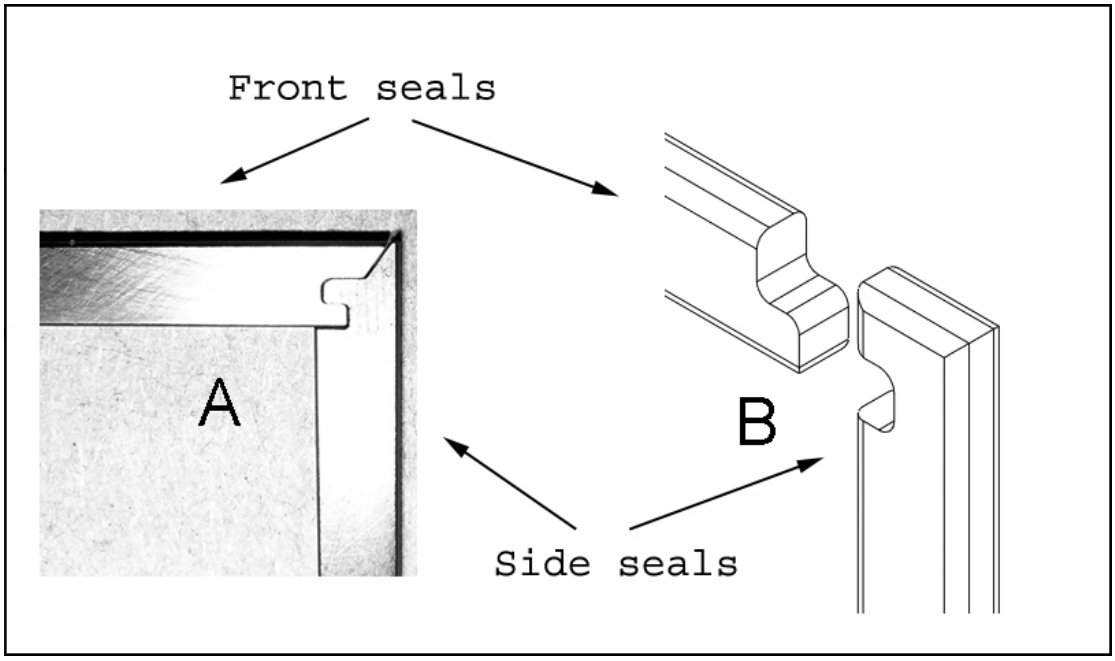

Figure 52. Alternative seal design (A) original seal corner detail (B) proposed seal corner detail.

A second alternative to the current seal design is shown in Figure 53. A piston and seal arrangement was designed in such a way that the front and side seals are isolated from each other through the use of a corner seal. Figure 53 shows the finished piston and an exploded view of the seal arrangement. The exploded view has two alternative front seal options. The two piece design is to provide better gas sealing than the one piece design. The small piece of the seal will wear faster than the long piece because the back area exposed to gas pressure is larger than the front area in contact with the chamber. If the front seal is slightly under size (length), the front edge of the small piece will wear until the end clearance is taken up. If the seal is oversize the ends of

both seal pieces will wear until the front surfaces of both seals are in contact with the chamber. This type of seal arrangement is utilised in several implementations of the Wankel rotary combustion engine and some types of pump. Unfortunately, it appears that this piston will not be tested in an engine.

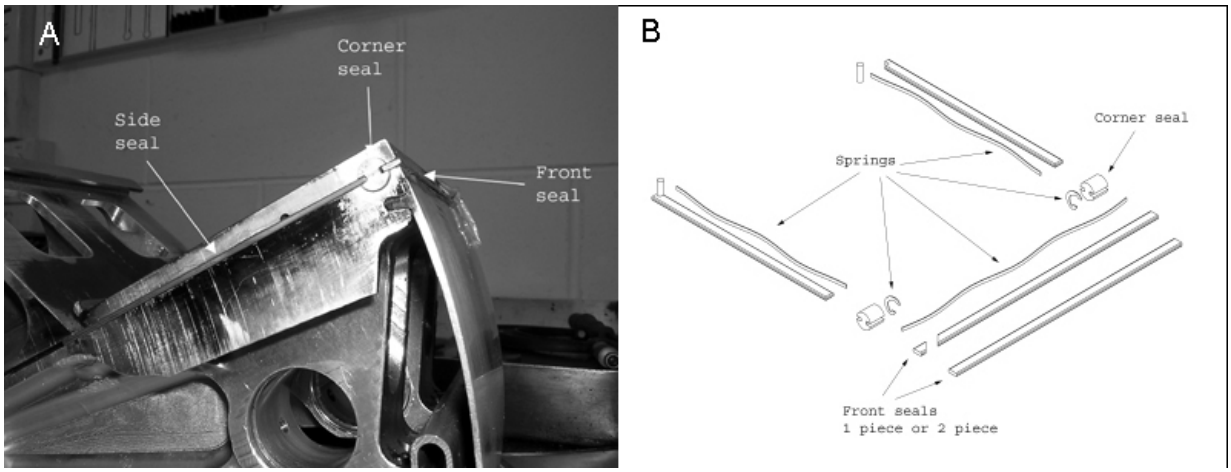

Figure 53. Piston with Mazda type corner seal arrangement (A) piston assembled with springs and seals (B) CAD image of corner seal type arrangement.

IV.E.3. Other Factors.

One aspect of the engine that little is known about is the distortion of the chamber. Distortion of the side plates, head and exhaust block can be introduced in several different ways, during both assembly and operation. When the engine is assembled there are several long bolts that extend through both chambers and shorter bolts that are fastened into the head and exhaust block. In Figure 54 A, the bolts that are threaded into the head and exhaust block are highlighted in green and the through bolt holes are highlighted in blue. The torque and the tightening order of these bolts will have a significant affect on the degree of elastic deformation that the side plates and exhaust block experience. At present there is no documented tightening torque or tightening order of these bolts.

As well as the strain induced from the bolts and studs, the sealing arrangement can affect the distortion of the chamber. The Pivotal Engine™ does not use gaskets but has grooves machined to locate o-ring cords. These grooves are highlighted red in Figure 54 B. Because the o-ring cords cannot completely enclose the areas to be

sealed a significant amount of sealant is used. The type of sealant used between the mating faces of the engine can cause significant changes in clearances and therefore strain and distortion of the chamber.

The last two mechanisms of chamber distortion occur when the engine is running. The first is due to the differing rates of thermal expansion between the aluminium chamber and the steel bolts. This problem is compounded by using bolts with large differences in length. To overcome differences in rates of thermal expansion, head bolts and through bolts in rotary engines are usually waisted to reduce rigidity so excessive strain is not applied to the aluminium components. The last mechanism of chamber distortion is from combustion pressure during the power stroke forcing the chamber walls apart. The area exposed to high pressure is highlighted in Figure 54 A. In the Pivotal Engine™ this problem is compounded due to the design of the side plates. A relatively large flat part inherently has low stiffness. Combined with the volume of material removed from the back of the side plate for coolant cavities, the stiffness is greatly reduced.

The distortion of the chamber could cause excessive seal wear in two ways: either the reduction of clearances causing high seal loadings, or the compression seals may have sufficient stiffness that the combustion pressure does not force the seal to conform to the distorted chamber. This would cause the seals to experience high point loadings. The best way to analyse these factors would be to perform a finite element analysis of the engine components.

Bore (chamber) distortion can be a problem in both conventional two and four stroke engines reducing piston ring life and increasing oil consumption. To prevent this problem, several low volume engine manufacturers are now designing and producing ‘mono block’ engines where the cylinder head and cylinder are cast as one part to increase the rigidity of the engine.

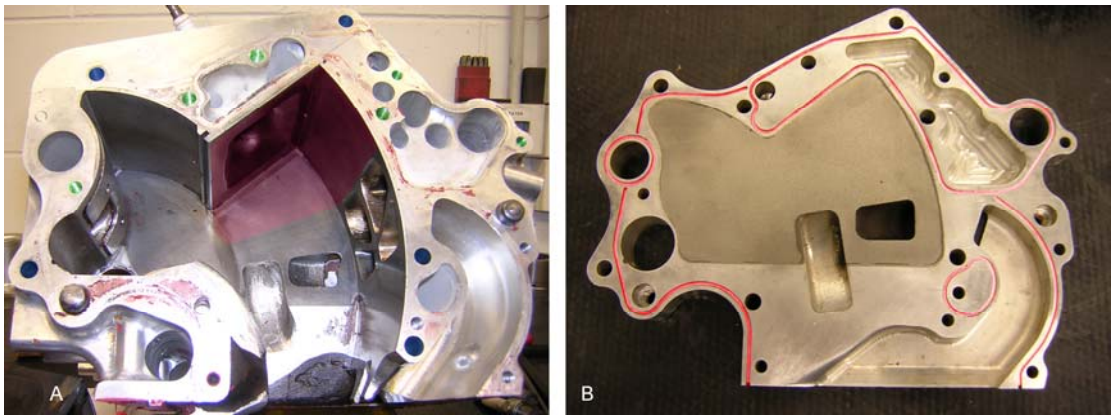

Figure 54. The Pivotal Engine™, (A) with the area of high combustion pressure highlighted in red, threaded bolt holes highlighted in green, through bolt holes highlighted in blue. (B) with the o-ring cord grooves highlighted in red.

IV.F. Reciprocating Tribometer.

Reciprocating tests were run for approximately twenty hours. The increased test duration over the rotational tribometer is because of the significantly lower speed, which gives lower sliding distance per unit time. The reciprocating tribometer must run nine times as long as the rotational tribometer for the equivalent sliding distance. However, the more severe lubrication and therefore wear conditions on the reciprocating tribometer mean that the wear of the test block is high enough to be measured using the mass loss method. The test block wear rates were quantified in the same manner as the seal samples, i.e., the mass was recorded before and after each test and the difference used to calculate the wear rate. The appearance of the test block is much more similar in appearance to the wear surfaces observed in the fired engine tests.

IV.F.1. Reciprocating Tribometer Results.

Due to time constraints, only the F4301 liner coating was tested versus several seal materials (TiN, CrN, Cast iron and N-SS) on the reciprocating tribometer. The results of these tests are summarised in Table 7. The best seal material tested on the reciprocating tribometer was Total Seal TiN. Although there was no measurable mass loss at the conclusion of a twenty hour test a significant area of the 4µm thick coating had been removed from the seal surface. This wear rate is much closer to what was observed in a fired engine. Similarly, the 4µm thick CrN coating had worn through at the conclusion of a twenty hour test (with no measurable mass loss). In these tests the CrN coating is ranked second to the TiN coating due to the fact that a greater area had been removed from the CrN coating. Also of note is that the wear rate of the F4301 test block was significantly lower against the TiN coated seal than the other three seal materials.

When tested on the rotational tribometer, the N-SS seal gave lower wear rates (Table 6) than the Mazda cast iron seal. This contradicts the results obtained on the reciprocating tribometer, where the cast iron seal gives lower wear rates than the N-SS seal. The most likely reason for this change in results is that the different seal profiles have a more pronounced affect on seal wear because of the changing lubrication regimes. From these tests, the TiN coated seal has been identified as having the lowest wear rate while the N-SS seal had the highest. Additionally, the

F4301 test block had the lowest wear rate against the TiN coated seal. The cast iron seal gave the highest wear rate of the F4301 test block but this is not considered to be as important as the seal wear rate, since the engine life is currently limited by the seal wear rate.

Table 7 Wear rates from reciprocating tests.

Seal Material	Oil	Average Seal Wear Rate m^3m^{-1} $x10^{-13}$	Average chamber coating Wear Rate m^3m^{-1} $x10^{-13}$
TiN	Morris race 2	0.000	0.0189
CrN	Morris race 2	0.000	0.0702
Mazda Cast Iron	Morris race 2	0.00171	0.0873
N-SS	Morris race 2	0.00225	0.0511
N-SS	Castrol A747	0.000562	0.000
N-SS	ELF HTX976	0.00111	0.0345
N-SS	Maxima 927	0.00152	0.572
N-SS	Mobil	0.438	Not measured

On the reciprocating tribometer, much more information can be gained from the friction response of the system than the rotational tribometer. Again, there is no correlation between the magnitude of the friction force and wear rates.

Friction plots from the reciprocating tribometer are shown in Figure 55 A and B. These plots contain friction force data from one complete crankshaft revolution. Because, friction force is always in the opposite direction to the relative surface velocity the sign of the friction force must change for each crankshaft revolution. At the turnaround points the relative velocity between the seal and the test block drops to zero and because the velocity is zero at this point the friction force must also be zero. Between the turnaround points the relative velocity increases to a maximum at mid-stroke.

The reversal in wear resistance between the N-SS and cast iron seals from the rotational to reciprocating tribometers may be explained by the different seal profiles influencing the lubrication regime in which the system is operating. As noted earlier, the cast iron seal has a barrel type profile, while the N-SS seal has a flat face with radii on the edges. The barrel profile appears to help the transition from a mixed to hydrodynamic lubrication regime through the mid-stroke. This is indicated by an increase in friction force with the increase in velocity (Figure 55 B). The friction force

in the mixed lubrication regime is less dependent on velocity, therefore it is probable that the system in Figure 55 A is in a mixed lubrication regime. Because the N-SS seal is operating in a mixed lubrication regime through the mid-stroke it is likely to have a higher wear rate than the Mazda cast iron seal which, is operating in a hydrodynamic lubrication regime through the mid-stroke.

Even though these two seal materials are operating in different lubrication regimes through the mid-stroke, the actual seal wear rates are not greatly different. This is because most of the seal wear (and test block wear) occurs at the turnaround points where both are operating in a boundary lubrication regime. The transition to a boundary lubrication regime is identified by the peaks in friction force at the turnaround points in Figure 55 (A), (B) and (C). As the velocity tends to zero at the turnaround point the oil film thickness decreases, allowing metal-to-metal contact between the seal and the coating with an associated increase in friction and wear.

The lower tribometer speed during the acquisition of the friction data for the Mazda cast iron seal was not intentional. The tribometer speed is reduced to acquire the friction data by lowering the driving frequency of the motor to $10H_z$ (without an actual speed feedback). The reduction in speed also reduces the torque that the motor can deliver. This means that the high friction force with the Mazda apex seal reduced the tribometer speed.

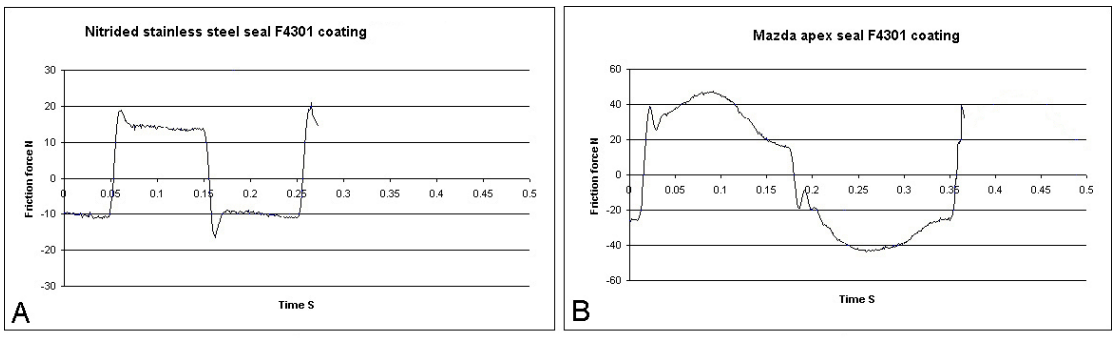

Figure 55. Friction plots from reciprocating tests, (A) Boundary lubrication at turnaround points, mixed lubrication through mid-stroke. (B) Boundary lubrication at turnaround points, hydrodynamic lubrication through mid-stroke.

In Figure 56 there are additional peaks after the turnaround point. These peaks are due to a stick-slip phenomenon. The friction force between the seal and the test block is high enough that the test block and carrier are deflected with no relative movement between the contacting surfaces. When the force is sufficiently high to overcome the

friction force the test block and carrier will try to return to an equilibrium position. However because of the sudden drop in force, the test block will tend to over-shoot the equilibrium position. The test block must then travel in the same direction as the seal sample to return to the equilibrium position, reducing the relative velocity and again allowing metal to metal contact causing the cycle to repeat. In part this is caused by the stiffness (or lack of) of the tribometer, allowing the test block to deflect. There was a general trend for this type of friction response to occur later in the test period. The most likely reason for this is that the increase in temperature reduces the oil viscosity causing more severe boundary lubrication conditions near the turnaround points.

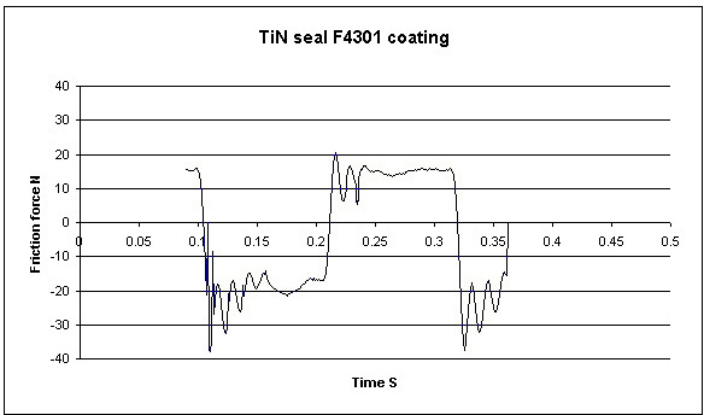

Figure 56 Friction plots from reciprocating test, boundary lubrication and stick-slip at turnaround points, mixed lubrication through mid-stroke

IV.F.2. Test Block Surface Analysis.

The reduction in size of the test block on the reciprocating tribometer over the test disc on the rotational tribometer allowed analysis of the wear surface. The first significant aspect of the surface topography of the test block is the high surface porosity as shown in Figure 57 A. A conservative estimate using a pixel count of the processed image (Figure 57 B) gives a surface porosity of 40%. The high surface porosity dominates surface roughness measurements and preclude intentional surface texturing (such as plateau honing). There is no significant deviation in surface roughness between a test block dressed with new 400 grit silicon carbide paper and a test block dressed with new 1200 grit silicon carbide paper (average Ra values of 0.52 μm and 0.54 μm respectively). Because the different silicon carbide papers do not affect the macroscopic surface topography, it would also be expected that the wear process would not alter the macroscopic surface properties, and this is in fact the case. The surface roughness vales (Ra of 0.54 μm) are not discernible from unworn and the

surface porosity is not affected by the wear test (shown in Figure 57). It is possible that the porosity will act as a lubricant reservoir, however the voids are much larger than most intentionally created surface features so may not be as beneficial.

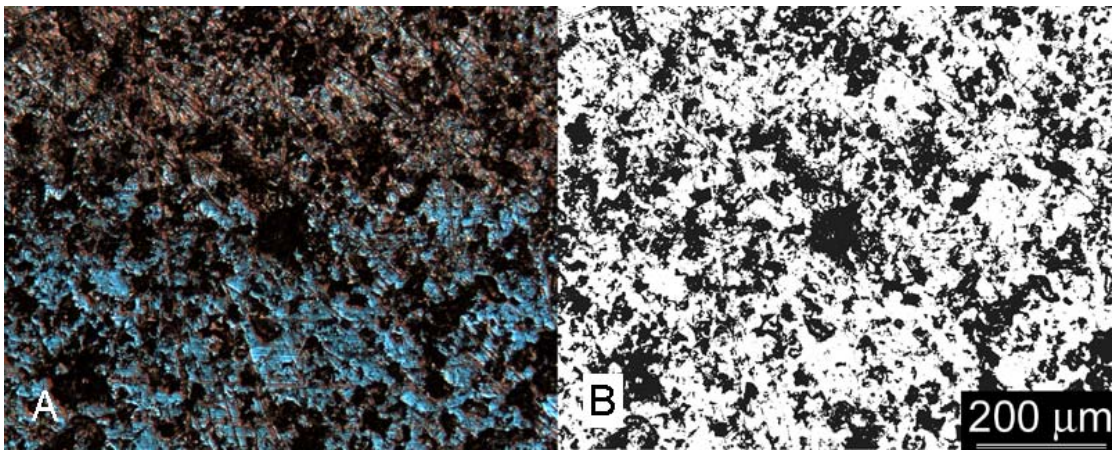

Figure 57 F4301 test block surface at turnaround point. (A) raw image, the worn area is blue. (B) processed image showing approximately 40% surface porosity.

On a microscopic level, the worn and unworn surfaces are very different. Figure 58 shows an SEM image of an unworn area of the test block surface at 1000x magnification. The visible surface texture results from the test block being dressed with 600 grit silicon carbide paper. This surface is very different from the worn surfaces shown in Figure 59 A and B, where only the deepest valleys from the original surface texture remain. Abrasive wear is responsible for the removal of most of the original surface features, as indicated by wear striations in the sliding direction. There is also a polishing type wear mechanism present although this will remove orders of magnitude less material than abrasive wear.

In addition to abrasive wear and polishing, plastic flow is evident. In plastic flow, material is 'smeared' over the edges of pre-existing surface features. The repeated plastic deformation eventually causes flakes of material to be removed from the surface in a fatigue-like process. Plastic flow is observable on the wear surface at both the mid stroke and the turnaround points (highlighted in Figure 60). There are also areas on the wear surface where entire 'splats' have been removed from the coating surface, such as shown at the top right corner of Figure 60 A.

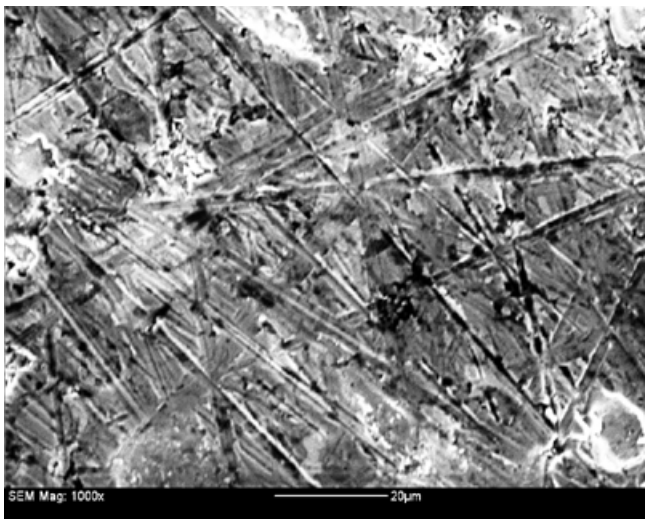

Figure 58 SEM image of un-worn area showing initial surface texture.

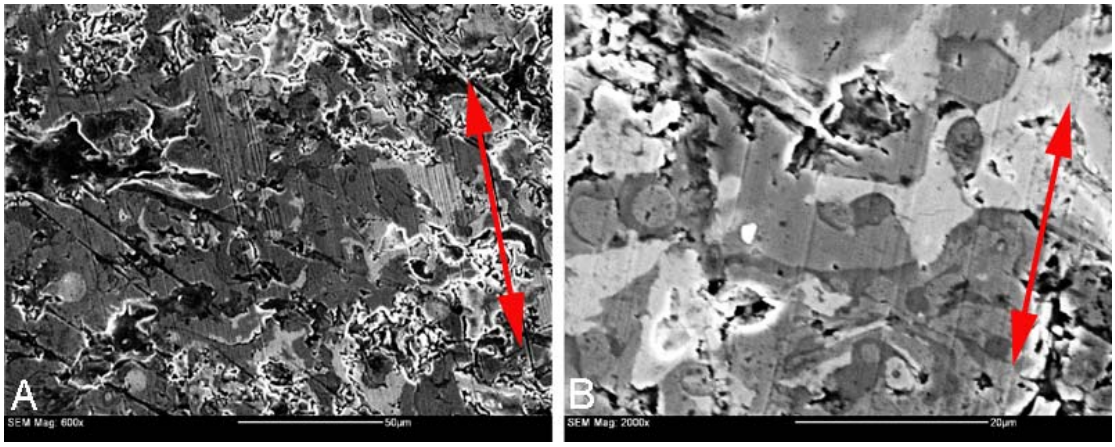

Figure 59 SEM images of worn areas (arrows indicate sliding direction) on F4301 coating, showing: (A) abrasive wear, (B) abrasive wear and polishing.

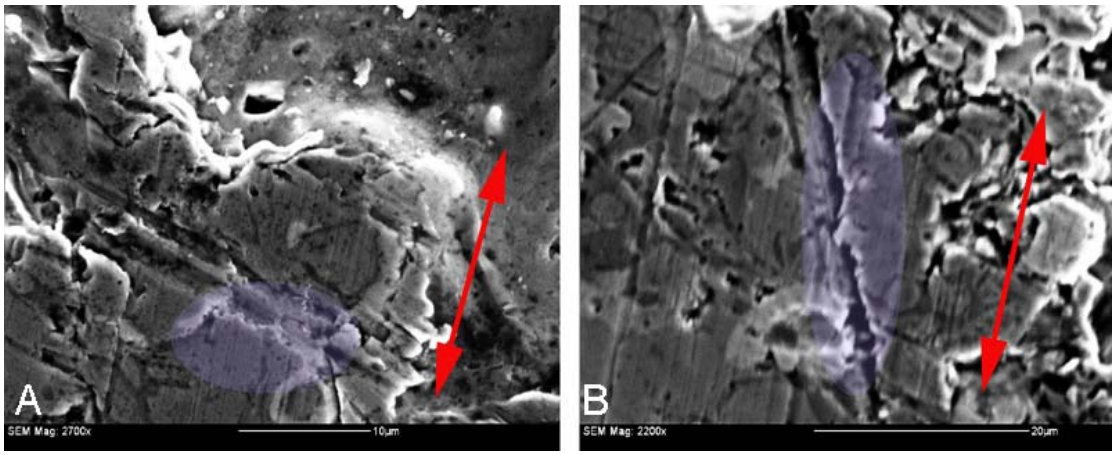

Figure 60 SEM images of worn areas (arrows indicate sliding direction) on F4301 test block. (A) turnaround point (B) mid stroke. Highlighting indicates areas of plastic flow.

IV.F.3. Lubricant Tests.

In addition to testing different material combinations, different oils were tested on the reciprocating tribometer. The oils include Morris race 2 (which was used for all other tests), Elf HTX976, Castrol A747, Maxima 927 and general purpose Mobil two-stroke oil. The Morris and Elf oils are fully synthetic race oils, while the Castrol and Maxima oils are synthetic castor blends. These oils are specifically formulated for high performance applications. For example, the Castrol oil is specified for water cooled engines that run from 12000 to 18000 rpm. Of these four oils only Morris specifies that it exceeds API TC requirements. The Mobil oil is a mineral oil, meeting TC requirements. In contrast to the other oils, the Mobil oil is recommended for use in lawnmowers, chainsaws and motorcycles.

Perhaps the biggest governing factor in the use of these oils (in the intended application of the Pivotal Engine™) is cost. The four high performance oils range from $30 NZD to $60 NZD per litre while the Mobil oil is less than $10 NZD per litre. Even if an engine is running at 200:1 fuel oil ratio the use of the high performance oils will have a significant contribution to the overall running costs.

It is interesting to note that the different oils have as much effect on the system wear rates as the different materials. To ensure consistency and relevance to other results all of the oil tests used N-SS seals and F4301 coated test blocks. The lowest test block wear rate was recorded with the Castrol A747 oil. The test block wear rate was even lower than that of the test block run against the TiN coated seal, in this case no mass loss was measured. Of all the oils tested, the Castrol oil also provided the best wear protection for the N-SS seal. The seal wear rates with the Elf, Maxima and Morris oils are reasonably close, however the Elf oil definitely offers better wear protection to the test block than the other two oils. The high test block wear rate with the Maxima oil is due to minor scuffing at the start of the test, ideally this test would have been repeated but time constraints did not allow this.

The most significant result from the oil tests is the extremely high seal wear rate recoded with the Mobil oil. Based on cost alone it would be expected that this oil would not perform as well as the high performance oils. However it highlights a danger of developing an engine using only high performance oils. If the Mobil oil (or

any other general purpose oil) was used in a Pivotal Engine™ it is likely that it would not last more than a couple of hours before the compression seals failed.

V. Conclusions.

It was found that the test results from the rotational tribometer have little relevance to how a material couple perform in a fired engine. Seal wear rates on the rotational tribometer were much lower than in the engine. There was also no detectible wear of the chamber coatings on the tribometer (in most cases). In addition to the significantly lower wear rates, one particular material couple (XPT512 and N-SS) continually scuffed when tested on the rotational tribometer while performing as well as other material combinations in a fired engine. The reason for these very different system wear responses is because the conditions on the tribometer do not represent the conditions in the fired engine. Most importantly, the rotational tribometer operates in a mixed-hydrodynamic lubrication regime, minimising wear. The engine will operate in boundary, mixed and possibly hydrodynamic lubrication regimes at different points in the cycle. Most wear occurs while the engine is operating in the boundary lubrication regime.

The reciprocating tribometer was designed and built to overcome all of the deficiencies of the rotational tribometer. Most importantly the reciprocating motion allows the transition between boundary, mixed and hydrodynamic lubrication regimes. As a result the system wear observed on the reciprocating tribometer is much more representative of the system wear in the actual engine. An indication of this is that the test blocks from the reciprocating tribometer have a similar wear pattern to the side plates of the Pivotal Engine™, areas of high wear at the turnaround points with less wear through the mid-stroke.

From the testing conducted on the reciprocating tribometer, the best wear system was found to be TiN coated seals run against F4301 coated test blocks with Morris race 2 oil. From standardised tests (N-SS seals against F4301 coated test blocks) used to compare different oils it was found that the Castrol A747 oil provided the best wear protection to both the seal and test block. It should be noted that the use of different oils had as much affect on the system wear as different material combinations. A Mobil general purpose two-cycle oil produced seal wear rates two orders of magnitude higher than the other high performance oils. Although not tested on the reciprocating tribometer, silicon nitride seals are likely to significantly increase the

service life of the Pivotal Engine™. This material has been shown to significantly increase the seal and chamber service life in the Mazda Wankel engine.

V.1. Recommended Future Work.

It is recommended that silicon nitride seals be tested on the reciprocating tribometer and in a fired engine to verify this material as having the desired wear properties to increase the service life of the Pivotal Engine™

To date, all of the fired engine tests and most of the tribometer testing has been conducted using full synthetic racing two-cycle oil. It may be anticipated that this type of oil would be used in an aircraft application but for power generation and applications where low running costs are important the use of these oils is likely to be prohibitively expensive. For this reason, it is recommended that testing should also be conducted with different oils to ensure that the Pivotal Engine™ can endure being run with cheaper oils.

Since the wear rates from the reciprocating tribometer, as well as published data from similar experiments, all show compression seal/piston ring wear rates significantly lower than those recorded in the Pivotal Engine™, further investigation should be carried out into the actual forces in the fired engine and the distribution of these forces on the compression seals.

Forces that have not been considered in this study arise primarily from the distortion of the combustion chamber. Because the compression seals have a limited ability to conform to the chamber, there will be areas of the seal that are exposed to high localised contact forces, which may be the cause of the high recorded seal wear rates. There are three areas that should be investigated with regard to chamber distortion: (1) the tightening order and tightening torque of the bolts and studs that hold the side plates against the head and exhaust block, (2) the thermal expansion and stiffness of the alloy steel studs and bolts compared to the aluminium side plates, head and exhaust block, and finally (3) the distortion of the relatively thin side plates due to combustion pressure.

At this stage of the development of the engine, it is recommended that a document is drafted containing clearances and tolerances for critical engine components, as well as an assembly guide including a procedure for the assembly and disassembly of the engine, including tightening torques and orders for all threaded fasteners. This type of document is required to eliminate uncontrolled variables between engines, ensuring that all test engines are similar, and that test results are in fact representative of any modification and not artifacts of unknown/uncontrolled factors.

References.

1. Setright, L.J.K., *Some unusual engines*. 1975, London: Mechanical Engineering Publications.
2. Andersson, P., J. Tamminen, and C.-E. Sandstrom, *Piston ring tribology. A literature survey.* VTT Tiedotteita - Valtion Teknillinen Tutkimuskeskus, 2002(2178): p. 8-105.
3. Rabute, R. and T. Tian, *Challenges involved in piston top ring designs for modern SI engines.* Journal of Engineering for Gas Turbines and Power, 2001. **123**(2): p. 448-459.
4. Cho, S.-W., S.-M. Choi, and C.-S. Bae, *Frictional modes of barrel shaped piston rings under flooded lubrication.* Tribology International, 2000. **33**(8): p. 545-551.
5. Muroki, T. and J. Miyata. *MATERIAL TECHNOLOGY DEVELOPMENT APPLIED TO ROTARY ENGINE AT MAZDA.* in *International Congress and Exposition - Society of Automotive Engineers.* 1986. Detroit, MI, Engl: SAE, Warrendale, PA, USA.
6. Woydt, M. *Materials-based concepts for an oil-free engine*. in *World Tribology Congress*. 1997. London: Mechanical Engineering Publications Limited.
7. Winn, A.J., D. Dowson, and J.C. Bell, *Lubricated wear of ceramics Part II: the wear and friction of silicon nitride and steel in the presence of mineral oil or an ester based lubricant.* Tribology International, 1995. **28**(6): p. 395-402.
8. Winn, A.J., D. Dowson, and J.C. Bell, *Lubricated wear of ceramics. Part I: The wear and friction of silicon nitride, alumina and steel in the presence of a mineral oil based lubricant.* Tribology International, 1995. **28**(6): p. 383-393.
9. Dynamic-Ceramic, *http://www.dynacer.com/:* Crewe Hall, England.
10. Shimizu, R., et al. *Mazda 4-rotor rotary engine for the Le Mans 24-hour endurance race*. in *International Congress and Exposition, Feb 24-28 1992*. 1992. Detroit, MI, USA: Publ by SAE, Warrendale, PA, USA.
11. Lyubimov, V.V., et al., *Development and testing of multilayer physically vapour deposited coatings for piston rings.* Surface & Coatings Technology, 1992. **52**(2): p. 145-151.
12. Holmberg, K., *Operational reliability &systematic maintenance*. Finnish J. ed. 1991, London: Elsevier Applied Science.
13. Whittaker, L.V. and A. Matthews, *Comparison of a simulated 'in-service' rig test with a standardised laboratory abrasion test.* Surface and Coatings Technology, 2004. **177-178**: p. 603-610.
14. Ma, Z., et al., *Break-in liner wear and piston ring assembly friction in a spark-ignited engine.* Tribology Transactions, 1998. **41**(4): p. 497-504.
15. Hill, S.H., S.E. Hartfield-Wunsch, and S.C. Tung, *Bench wear testing of common gasoline engine cylinder bore surface/piston ring combinations.* Tribology Transactions, 1996. **39**(4): p. 929-935.
16. Akalin, O. and G.M. Newaz, *Piston ring-cylinder bore friction modeling in mixed lubrication regime: Part II - Correlation with bench test data.* Journal of Tribology, 2001. **123**(1): p. 219-223.
17. Akalin, O. and G.M. Newaz, *Piston ring-cylinder bore friction modeling in mixed lubrication regime: Part I - Analytical results.* Journal of Tribology, 2001. **123**(1): p. 211-218.
18. Ravikiran, A., *Wear quantification.* Journal of Tribology, Transactions of the ASME, 2000. **122**(3): p. 650-656.

19. Truhan, J.J., J. Qu, and P.J. Blau, *The effect of lubricating oil condition on the friction and wear of piston ring and cylinder liner materials in a reciprocating bench test.* Wear15th International Conference on Wear of Materials, 2005. **259**(7-12): p. 1048-1055.
20. Kazmierczak, A., *The new ring seal of the combustion engines and its surface free energy.* Industrial Lubrication and Tribology, 2004. **56**(1): p. 6-13.
21. Lou, H.Q., et al., *Effect of deposition conditions on the characteristics of reactively sputtered titanium nitride films.* Surface & Coatings Technology, 1997. **90**(1-2): p. 123-127.
22. Friedrich, C., et al., *Measurement of the hardness of hard coatings using a force indentation function.* Thin Solid Films Proceedings of the 1996 23rd International Conference on Metallurgical Coatings and Thin Films, Apr 22-26 1996, 1996. **290-291**: p. 216-220.
23. Rebholz, C., et al., *Structure, mechanical and tribological properties of nitrogen-containing chromium coatings prepared by reactive magnetron sputtering.* Surface and Coatings Technology, 1999. **115**(2): p. 222-229.
24. DellaCorte, C., A.R. Zaldana, and K.C. Radil, *A systems approach to the solid lubrication of foil air bearings for oil-free turbomachinery.* Journal of Tribology, 2004. **126**(1): p. 200-207.